DOE/NASA/0167-82/4
NASA CR-167983
GARRETT NO. 31-3725(4)

ADVANCED GAS TURBINE (AGT) POWERTRAIN SYSTEM DEVELOPMENT FOR AUTOMOTIVE APPLICATIONS

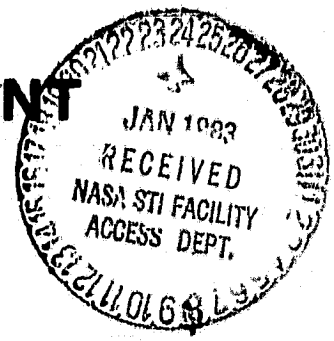

FOURTH SEMIANNUAL PROGRESS REPORT (JULY 1981 — DECEMBER 1981)

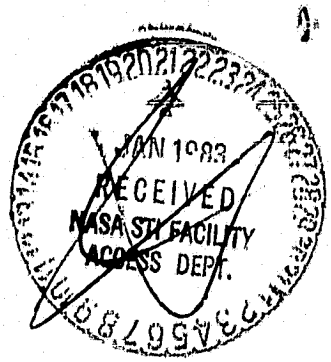

Engineering Staff of
Garrett Turbine Engine Company
A Division of The Garrett Corporation

July 1982

Prepared for

NATIONAL AERONAUTICS AND SPACE ADMINISTRATION
Lewis Research Center
Cleveland, Ohio 44135
Under Contract DEN3-167

for

U.S. DEPARTMENT OF ENERGY
Office of Vehicle and Engine Research and Development
Technology Development and Analysis Division
Washington D.C. 20585

DOE/NASA/0167-82/4
NASA CR-167983
GARRETT NO. 31-3725(4)

ADVANCED GAS TURBINE (AGT) POWERTRAIN SYSTEM DEVELOPMENT FOR AUTOMOTIVE APPLICATIONS

FOURTH SEMIANNUAL PROGRESS REPORT
(JULY 1981 — DECEMBER 1981)

Engineering Staff of
Garrett Turbine Engine Company
A Division of The Garrett Corporation

July 1982

Prepared for
NATIONAL AERONAUTICS AND SPACE ADMINISTRATION
Lewis Research Center
Cleveland, Ohio 44135
Under Contract DEN3-167

for
U.S. DEPARTMENT OF ENERGY
Office of Vehicle and Engine Research and Development
Technology Development and Analysis Division
Washington D.C. 20585

TABLE OF CONTENTS

TABLE OF CONTENTS (Cont)

LIST OF ILLUSTRATIONS

LIST OF ILLUSTRATIONS (Cont)

LIST OF TABLES

1.0 SUMMARY

This report describes progress and work performed by the Garrett/Ford team to develop an Advanced Gas Turbine (AGT) powertrain system for automotive applications, during the period July through December 1981. This work was performed for the Department of Energy under NASA Contract DEN3-167. This is the fourth in a series of semiannual reports. Work performed during the first three periods (References 1, 2 and 3) initiated design and analysis, ceramic development and component testing.

Project effort conducted under this contract is part of the DOE* Gas Turbine Highway Vehicle System Program. This program is oriented at providing the United States automotive industry the high-risk long-range technology necessary to produce gas turbine powertrains for automobiles with reduced fuel consumption and reduced environmental impact. It is intended that technology resulting from this program reach the marketplace by the early 1990s.

The advanced automotive gas turbine, when installed in a Ford vehicle (3000 pounds inertia weight), will provide:

- A CFDC fuel economy of 42.8 miles per gallon based on Environmental Protection Agency (EPA) test procedures and Diesel No. 2 fuel. The AGT-powered vehicle will substantially give the same overall vehicle driveability and performance as a comparable production vehicle powered by a conventional spark-ignition powertrain system
- Emissions less than federal standards
- Ability to use a variety of fuels

The Garrett/Ford project efforts were modified during March 1981 to accommodate imposed budget constraints. The primary changes involved reducing first generation component tests, deferral of gearbox and transmission systems development, and stopping vehicular integration activities. These changes permitted concentration of remaining resources toward continued development of higher technology components and ceramics necessary for the AGT engine. As noted herein, progress through December 1981 indicates that AGT engine performance goals will be achieved; Mod I (metal) engine tests have been initiated. The major accomplishments for this period are summarized in the following paragraphs.

1.1 Engine/Powertrain Development

Assembly of AGT101 engine S/N 001 was completed on schedule in late July 1981. Testing was initiated as planned including rollover, windmilling, cold motoring, hot motoring and hot start. Leakage tests were conducted during testing using a helium leak detection system. Minor turbine rubs and internal leakage problems were resolved and corrective hardware modifications incorporated. On December 15, 1981, the first successful self-sustaining run was achieved. The power section was operated at 50,430 rpm at a turbine inlet temperature of 1256°F for approximately two hours. Total time accumulated on S/N 001 was 23.5 hours at the end of this reporting period.

1.2 Compressor Development

The compressor stage was aerodynamically tested from 50- to 100-percent design speed. The compressor was low in flow and pressure ratio by 8 to 10 percent at 100-percent speed, and within 1 point of the Mod I efficiency goals. The compressor map was input to the Mod II cycle analysis, holding all other component technology levels as predicted. Results of this exercise showed that the AGT101 powertrain installed in a 3000-pound inertia-weight vehicle achieved this same driveability and was within 1 mpg of the contract goal.

1.3 Combustor Development

Emissions testing of the Mod I diffusion flame combustor was completed. Although this

*A list of abbreviations and acronyms is presented in Appendix D, herein.

system is not designed to meet program goals, the combustor met the CO goals at all power conditions and the HC goals at cruise and maximum power.

Fuel nozzle development was reinitiated on the Mod II combustor design.

1.4 Ceramic Component Development

Ford has successfully spin tested a ceramic-bladed turbine rotor to 115,000 rpm (proof speed) with minor blade tip failure. All subcontractors are proceeding with delivery of static structural components. Development testing of static ceramic components continued with thermal shock testing of both the Si_3N_4 and SiC stator vanes. Preparation is underway for initiation of ceramic thermal screening rig and structures rig testing.

1.5 Rotor Dynamics

Successful and repeatable operation of the rotor dynamics test rig to 100,000 rpm with and without the slave gearbox has been accomplished. The test program has developed a satisfactory Mod I rotating assembly, foil bearing, rolling element thrust bearing, hydraulic mount, and compressor ring seal.

2.0 INTRODUCTION

This report is the fourth in a series of Semiannual Technical Summary Reports for the Advanced Gas Turbine (AGT) Powertrain System Development Project, authorized under NASA Contract DEN3-167 and sponsored by the DOE. This report has been prepared by The Garrett Turbine Engine Company (hereinafter referred to as Garrett), a Division of The Garrett Corporation, and includes information provided by Ford Motor Company, The Carborundum Company, and AiResearch Casting Company. The project is administered by Mr. Roger Palmer, Project Manager, NASA-Lewis Research Center, Cleveland, Ohio. This report presents plans and progress from July 1981 through December 1981.

Project effort conducted under this contract is part of the DOE Gas Turbine Highway Vehicle System Program. This program is oriented to provide the United States automotive industry the high-risk long-range technology necessary to produce gas turbine powertrains for automobiles that will have reduced fuel consumption and reduced environmental impact. It is intended that technology resulting from this program reach the marketplace by the early 1990's.

The advanced automotive gas turbine, when installed in a Ford vehicle (3000 pounds inertia weight), would provide:

- A CFDC fuel economy of 42.8 miles per gallon based on Environmental Protection Agency (EPA) test procedures and Diesel No. 2 fuel. The AGT-powered vehicle will substantially give the same overall vehicle driveability and performance as a comparable production vehicle powered by a conventional spark-ignition powertrain system
- Emissions less than federal standards
- Ability to use a variety of fuels

The Garrett/Ford Advanced Automotive Gas Turbine has been designated the AGT101. The AGT101 includes ceramic parts in the ultimate configuration. The program was initiated in October 1979 and was to entail 68 months. Two phases were planned; Phase I was 45 months long and Phase II 23 months. Phase I was to involve most of the component/ceramic technology effort and the early engine and vehicle testing. Phase II was scheduled to include completion of the all ceramic engine effort plus the vehicle deliveries and evaluation.

Budget reductions in mid FY 1981 have resulted in a re-orientation of the program. The vehicle, transmission and engine gearbox/transmission effort have been indefinitely deferred. The program is now oriented toward developing the long-range high-risk technology of the AGT101 gas turbine such that the auto industry can carry that technology forward to production in the 1990's. Emphasis on ceramics, gas bearings, low emission combustion and improved component performance will continue. The AGT101 gas turbine is being used as a test bed to develop these technologies.

Since FY 1982 and subsequent year funding is not defined, the actual program details also are not defined. Garrett and Ford have suggested that the technology work be continued through FY 1985, culminating in the demonstration of the original goals of engine specific fuel consumption, power output, and emissions. In addition, the viability of ceramics will have been demonstrated in the AGT101 test bed and the potential of economically producing the ceramic parts in automotive production quantities will have been assessed by Ford. When these goals are achieved, Ford will be in a position to proceed, without Government support through the typical preproduction tasks which then could lead to production in the 1990's.

The primary technology challenges in the program continue to be the development of ceramic components and related high-performance gas turbine aerothermodynamic components for the AGT101. The AGT101 is nominally a 100 shp engine capable of speeds to 100,000 rpm and operation at turbine inlet temperatures to 2500°F. Specific fuel consumption is less than 0.3 over much of the operating range.

This report is structured to review the power section effort conducted to date. Mod I (metal) engine testing was started during this period. This discussion is followed by a review of the component/ceramic technology development. Appendices include progress reports from Ford, AiResearch Casting Company, and the Carborundum Company.

3.0 POWERTRAIN DEVELOPMENT

3.1 AGT101 Engine Test

Assembly of AGT101 S/N 001 was initiated June 26, 1981. This first build incorporated an external duct system as shown in Figure 1 to provide separate flowpaths for the compressor and turbine so internal leakage could be measured. The engine was coupled to a rotating carrier planetary type gearbox with an overall ratio of 37.124:1. Several trial assemblies were made to develop assembly techniques and final engine assembly was completed July 24, 1981. When test cart plumbing and instrumentation were completed, the engine was installed in the test cart as shown in Figure 2.

The engine was next installed in the test cell with supporting hydraulic start cart, lubrication cart, and controls. Initial engine rollover tests were conducted on July 30, 1981; speeds of 20,000 to 30,000 rpm were reached without incident. Additional rollover tests were conducted to resolve minor problems in the hydraulic start system, laboratory and control interfaces.

The engine and necessary support equipment then was moved to a test cell with an air supply

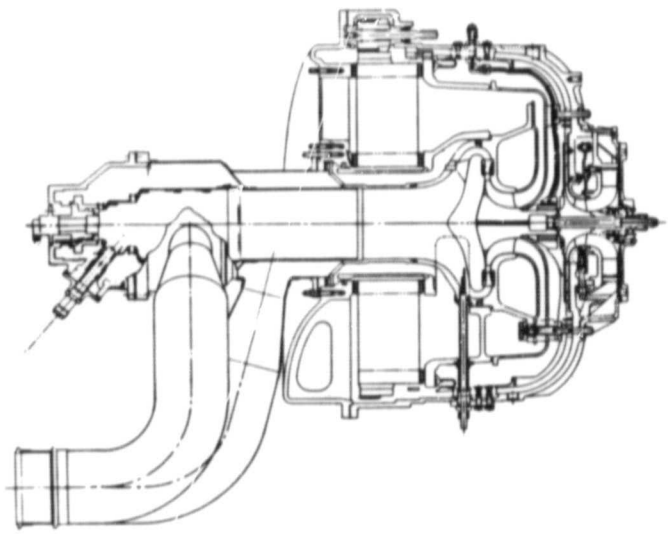

Figure 1. AGT101 Mod I Configuration with External Duct.

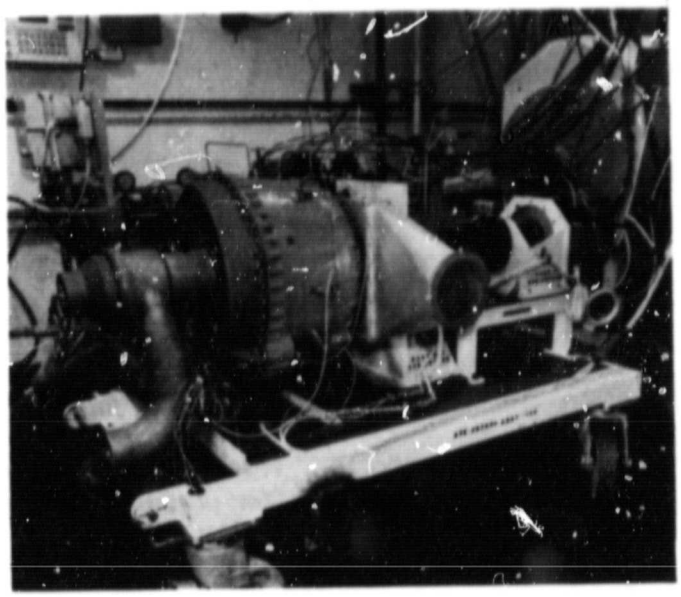

Figure 2. AGT101 Mod I Engine Installed in Test Cart.

capability for windmill testing. The engine was motored to 37,000 rpm by the hydraulic starter with open compressor and turbine flowpaths. A power match between the hydraulic motor and compressor/turbine load was attained at 37,000 rpm.

The laboratory air supply then was connected to the turbine inlet. The AGT was motored to 33,000 rpm by the hydraulic starter and the turbine air pressure was increased until the AGT speed was 51,000 rpm. This speed was maintained for 30 minutes while engine parameters were monitored. The mechanical windmilling test was completed on August 24, 1981 verifying stable operation of the rotating group as well as hydraulic system and mechanical instrumentation.

Following these tests, the engine was prepared for regenerator seal break-in and leakage evaluation using a helium flow-seeding technique, shown schematically in Figure 3. When using this helium flow-seeding technique, the compressor and/or high pressure (HP) regenerator inlet flow is seeded with helium at

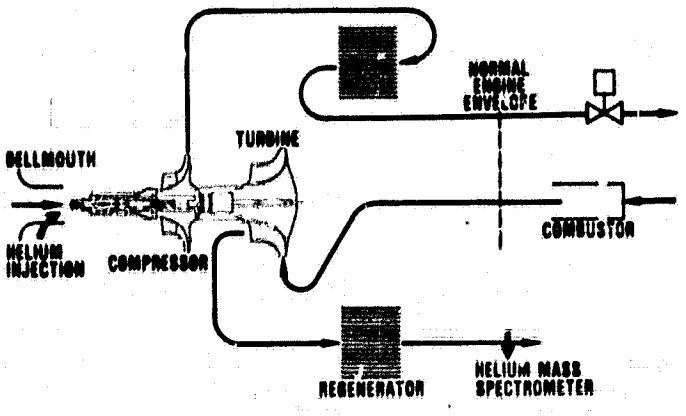

Figure 3. AGT101 Mod I Test IA, Helium Leak Detection Schematic.

selected injection ports. This seeded flow is ducted from the test cell after passing through the HP side of the regenerator core. Conditioned combustor inlet flow then is introduced to the burner. A proper compressor and turbine flow match is maintained and fuel is introduced as required to control turbine inlet temperature. Regenerator seal leakage from the HP side (seeded) to the low pressure (LP) side (unseeded) is determined by means of mass spectrometer measurements of helium concentrations in the exhaust.

When regenerator seal break-in and leakage testing was initiated, attempts to reach operating speed and temperature were terminated due to inner diffuser movement into the turbine, resulting in slight rubs. These rubs did only minor damage to the turbine rotor and it was subsequently reused. Detailed analytical and experimental investigation verified that the inner diffuser was deflecting under thermal gradients imposed during engine tests. The inner and outer diffusers were modified to add three radial slots; also, spacers were mounted between the diffusers to prevent excessive movement.

The engine was reassembled and leakage evaluation engine tests were resumed in October 1981. During these tests, the TIT was increased to a maximum of 1250°F at an engine speed of 50,000 rpm while leakage was monitored. Helium leak testing revealed that internal leakage was about 35 percent of compressor flow. Therefore, further testing was deferred until leakage could be decreased. Fuller's Earth then was introduced into the compressor inlet to provide visible indication of leakage areas. The engine was removed from the test cell for disassembly, inspection and analysis. A total of 12 hours and 13 minutes operation had been accomplished by October 26, 1981.

The engine was disassembled and progressively photographed. No evidence of damage was present. Internal leakage, as indicated by Fuller's Earth traces, was evident at the flipper seal, regenerator seals, turbine shroud piston seals, exhaust housing piston seal and numerous instrumentation penetrations. A comprehensive analysis and static leakage test of each suspected component was initiated. Twenty different potential leakage paths were identified and relative leakage values established for the points shown in Figure 4. The leakages were established using separate fixtures and adapters that permitted selective leak testing of the actual assembled AGT engine and components.

Relatively high leakages were determined for the regenerator core, regenerator seals, flipper seals, turbine shroud piston rings, and exhaust housing piston rings. The turbine shroud piston ring provided erratic sealing when

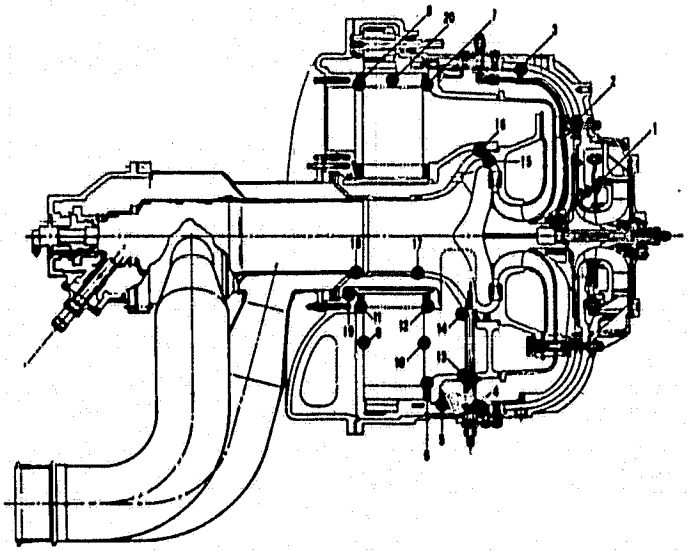

Figure 4. AGT101 Leak Path Designations.

a pressure reversal occurred during engine operation.

Springs were added to the piston rings to balance the reversed differential pressures reducing leakage by 90 percent. Similar springs were added to the exhaust housing piston rings.

The NGK manufactured Magnesium Alumina Silicate (MAS) regenerator core used in the initial engine tests was internally porous. An Alumina Silicate (AS) core manufactured by Corning was tested and had negligible internal leakage and was substituted for the NGK core.

A silicone rubber and fiberglas seal replaced the low-temperature flipper seal. A new, tight, concentric metallic flipper seal was obtained for subsequent engine tests. The engine was reassembled (Build 4) with the cited improvements and the static leakage results are presented in Table 1. Column 1 presents the measured cold leakage and Column 2 extrapolates this data to hot conditions using the indicated temperature corrections. Column 3 shows equivalent data with regenerator leakage obtained from regenerator hot rig helium leak test.

Build 4 incorporated a fixed carrier gearbox with a ratio of 38.134:1 and a reversed output shaft rotational direction. The fixed carrier

TABLE 1. MOD 1 BUILD 4 PREDICTED LEAKAGE

Leak Number	Location	(Column 1) Static Leakage (lb/min at 5 psid 75°F)	Average Operating Temp (°F)	$\sqrt{\theta}$ Correction for Engine	δ Correction for Engine	(Column 2) Engine Predicted(1) Leakage (lb/min at 5 psid)	(Column 3) Engine Predicted(2) Leakage (lb/min at 5 psid)
1	Foil bearing passage	0.233	180	0.91	0.62	0.131	0.131
2	Overboard + bolt circle	0.050	180	0.91	1.00	0.045	0.045
3	Flipper seal, outer(3)	0.000	180	0.91	1.00	0.000	0.000
4	TCs, outer case	0.068	180	0.91	1.00	0.062	0.062
5	Flipper seal, inner	0.043	180	0.91	1.00	0.039	0.039
6-12	Regenerator seals	1.780	800	0.65	1.00	1.159	0.599
13	TCs at flow sep hsg	0.115	1250	0.56	1.00	0.064	0.064
14	TCs at trans duct	—	1250	0.56	1.00		
15	Piston rings (4.0 to 5.1)	—	1250	0.56	1.00		
16	Piston rings (3.5 to 5.1)	—	1150	0.58	1.00		
17	Butt fit to trans duct(4)	1.135(4)	1150	0.58	1.00	0.658(4)	0.658(4)
18	Slip fit SAGT duct(4)	—	1150	0.58	1.00		
19	Exhaust hsg piston rings	0.135	800	0.65	1.00	0.088	0.088
20	Regenerator core porosity	0.038	800	0.65	1.00	0.025	0.025
Total leakage		3.597				2.271	1.711
Total leakage affecting performance(5)		2.462				1.613	1.053
Effective leakage, % of inlet flow						14.6	9.6

(1) Based on static cold test data
(2) Based on helium leak detection in hot rig
(3) Seal replaced with O-ring
(4) Leakage not affecting performance
(5) Based on 11 lb/min inlet flow

gearbox was substituted for the rotating carrier gearbox based on more stable rotor dynamics obtained during comparative evaluations on the rotor dynamics test rig. A baseline static engine leak test was made prior to test cell delivery.

The engine was installed in the test cell and on December 15, 1981, a smooth start and acceleration to 50,000 rpm was made. The TIT was adjusted to 1000°F and helium leak testing initiated. Compressor flow and back pressure were adjusted to approximate corresponding turbine conditions including the measured internal leakage. The TIT was increased to 1250°F while decreasing turbine pressure to maintain a steady-state speed of 50,000 rpm. A match of compressor flow and pressure ratio was obtained with the turbine by adjusting the compressor flowpath back-pressure valve. This match represented the engine self-sustaining conditions for both the turbine and compressor even though the flowpaths were separated. The engine was shut down and external ducting separating the compressor and turbine flows was removed and replaced with a duct connecting the flowpaths as schematically shown in Figure 5.

On December 15, 1981 the engine, shown in Figure 6, was started and accelerated to 50,000 rpm. Idle fuel consumption was approximately 3 lb/hr using JP-4 fuel. This test provided the first self-sustaining operation of the AGT101 as a complete unit. One hour and 58 minutes of self-sustaining operation was achieved on the first run.

Leak test data confirmed static leakage measured prior to dynamic testing. This verifies that the leakage measurement techniques employed will be a useful development tool. Results indicate that overall leakage was approximately 12 percent of compressor flow which is a significant decrease compared with the 35 percent leakage noted earlier. The leakage rates determined during the self-sustaining conditions using the helium leak detection apparatus are presented in Table 2.

During the latter part of December 1981, fuel system modifications were made to improve fuel atomization and lightoff characteristics.

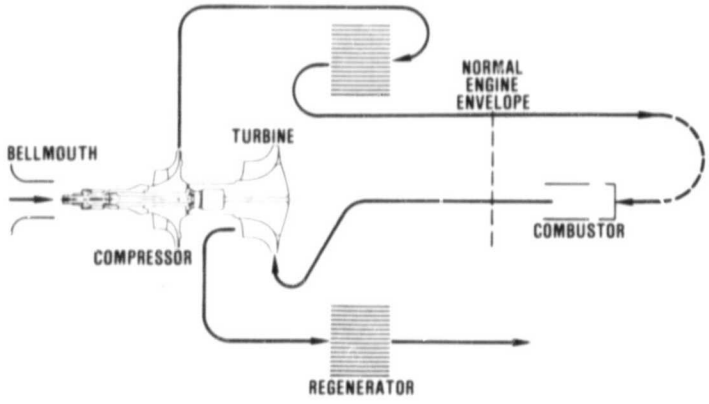

Figure 5. AGT101 Mod I Test IV, Self-Sustaining.

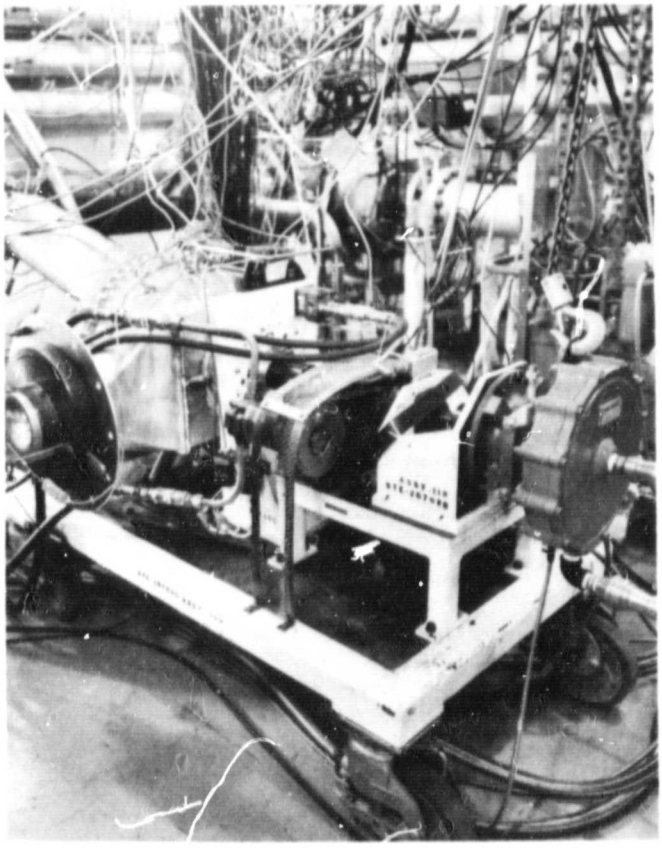

Figure 6. AGT101 Engine Test.

TABLE 2. SELF-SUSTAINING ENGINE MEASURED LEAKAGE RATES AND ENGINE CONDITIONS

	Leakage of Compressor Flow (percent)	Leakage (lb/min)
Total Interpath Leakage	12.22	1.613
Leakage Upstream of Station 3.1 (Leaks 1 through 8 plus approximately 1/2 of 20)	6.64	0.877
Leakage Downstream of Station 3.1 (Leaks 9 through 19 plus approximately 1/2 of 20)	5.58	0.736

ENGINE CONDITIONS

Compressor Inlet Temperature	=	75°F
Compressor Inlet Flow	=	12.99 lb/min
Turbine Inlet Temperature	=	1256°F
Rotor Speed	=	50,430 rpm
Combustor Inlet Pressure	=	21.35 psia

4.0 COMPONENT/SUBSYSTEM DEVELOPMENT

Component Subsystem Development activities during this reporting period entailed completion of Mod I component development testing and analysis, continuation of ceramic development activities, and reinitiation of Mod II combustor development. Figure 7 shows the performance rating stations for the engine and components.

The following sections discuss major efforts and accomplishments during the reporting period for each component/subsystem.

4.1 Compressor

The original test program established for the compressor components encompassed: aerodynamic - impeller only (vaneless diffuser) test, impeller plus diffuser vane row 1, impeller plus vane rows 1 and 2, and impeller plus vane rows 1, 2 and 3 (full stage) with and without IGVs; and mechanical-impeller strain gauge testing with full stage diffuser and IGVs. In addition to these tests, aerodynamic mapping of the IGV system on a separate rig (Reference 3) was planned. Due to budget constraints, the test program was reduced in scope to mechanical impeller strain gauge testing and aerodynamic full stage testing with IGVs. Selection was based on Mod I engine test program support with restoration of the full test program based on funding at a later point in time.

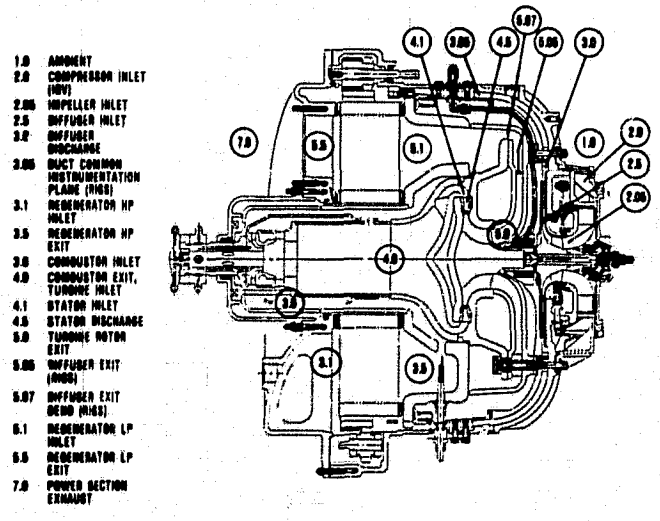

Figure 7. AGT101 Performance Rating Stations.

Activities during this reporting period encompassed impeller holography, impeller strain gauge testing and compressor aerodynamic testing.

4.1.1 Impeller Holography Test Results

An aluminum (2219-T6) and titanium (Ti-6-4) impeller were mechanically evaluated to determine vibratory blade and disk characteristics. Holography and acoustic testing was conducted, and these results then were compared with previously predicted analytical results. Table 3 summarizes these efforts. Figures 8 through 10 show the predicted vibratory mode shapes and the holography results for selected frequencies. Figure 11 presents a Campbell diagram for the titanium impeller. In general, test values agree quite well with analytical predictions.

4.1.2 Compressor Test Rig

The compressor test rig, described in reference 3 and shown in Figure 12 is a straddle-mounted bearing configuration simulating engine flowpath geometry.

Static and total pressure and total temperature instrumentation were located along the entire flowpath (Figure 13) to determine overall compressor system performance, individual

TABLE 3. SUMMARY OF VIBRATORY BLADE MODES (Aℓ, 0 RPM, 70°F)

Blade Mode	Predicted ISOVIB	Acoustic (Average)	Holography (Average)
1	4,681	4,567	4,561
2	10,340	10,427	10,411
3	12,341	13,108	13,138
4	15,172	16,858	17,127
5	17,194	18,467	18,681
6	18,201		22,256
7	22,174	24,877	25,277

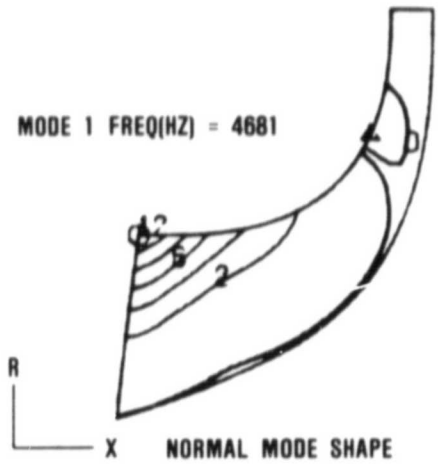

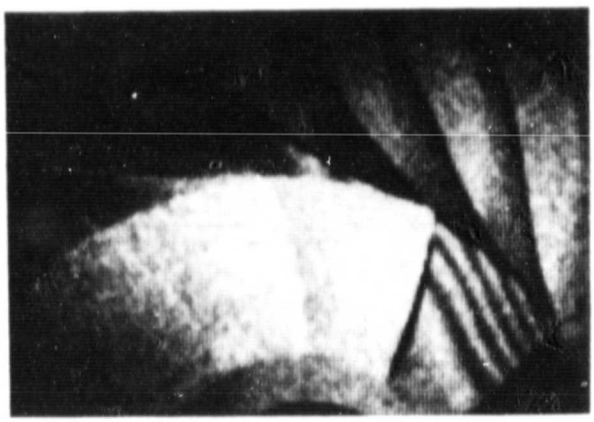

Figure 8. AGT101 Impeller Blade Vibratory Mode 1.

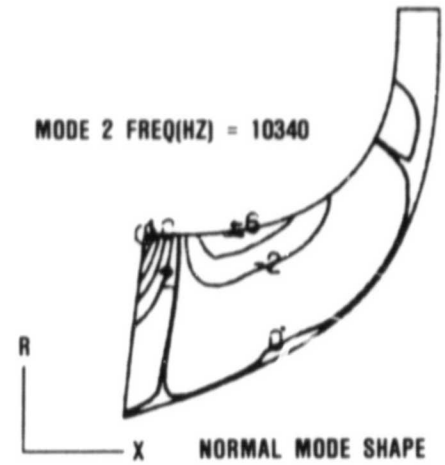

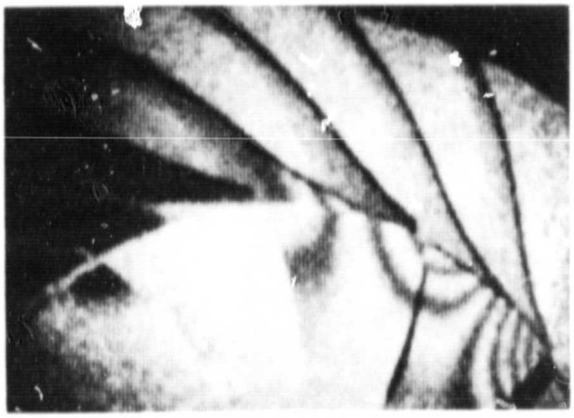

Figure 9. AGT101 Impeller Blade Vibratory Mode 2.

component performance, and salient diagnostic information. Mechanical integrity instrumentation was appropriately installed to establish vibration levels, shaft runout, bearing temperatures, and oil flow and temperature.

Impeller strain gauge instrumentation included gauges, slip ring assembly and appropriate readout equipment.

The titanium impeller was selected for initial rig testing in order to be consistent with the first engine builds.

4.1.3 Test Procedure

Following successful mechanical checkout tests, the test rig was assembled with the strain gauged titanium impeller and slip ring readout assembly. All mechanical and aerodynamic instrumentation was installed including capacitance probes to assess impeller running clearance during test.

During aerodynamic performance mapping, the test rig was accelerated to the desired corrected speed with the impeller axial clearance adjusted open (0.030-inch axial). Once the desired speed was achieved, the impeller clearance was closed to the desired condition (0.004-inch knee), and the discharge valve closed raising the pressure ratio from choke to surge for each selected speed line. Impeller clearance was adjusted, as required, to maintain approximately 0.004-inch knee clearance. A minimum of eight data points were taken for each speed line. The inlet guide vanes were

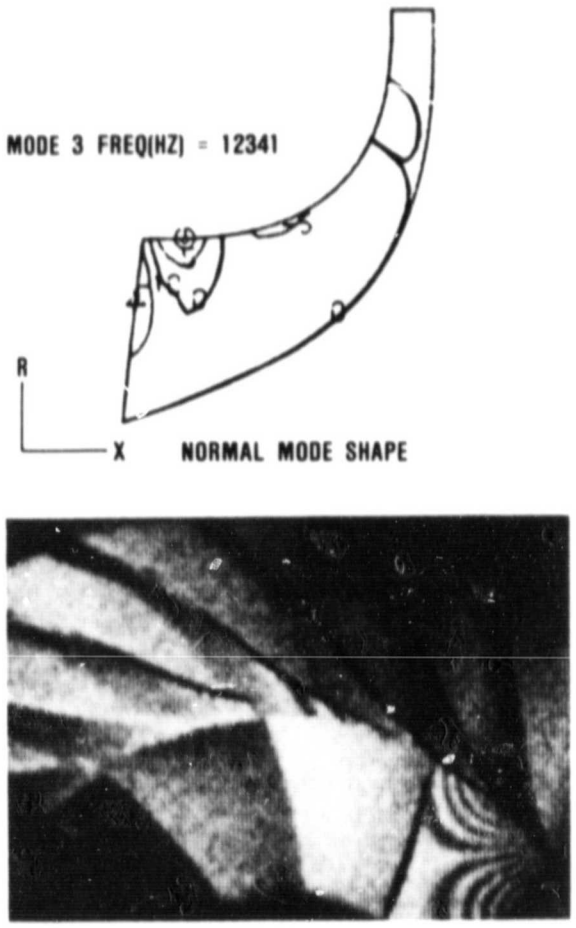

Figure 10. AGT101 Impeller Blade Vibratory Mode 3.

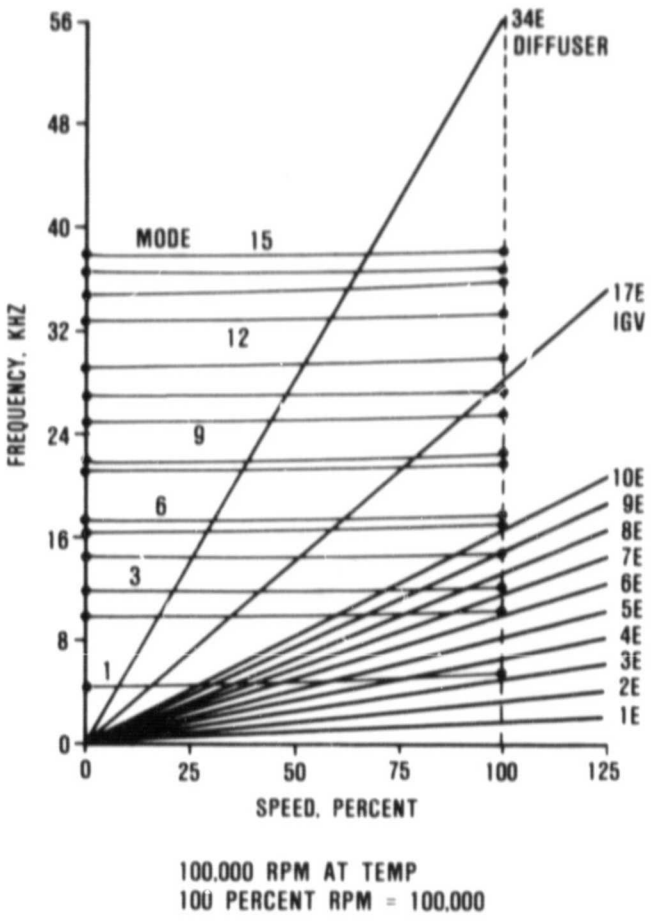

Figure 11. AGT101 Titanium Impeller Campbell Diagram.

held at a constant setting for all speeds, then the IGVs were indexed and all selected speed lines repeated. Table 4 presents the data matrix.

Compressor stage hardware had the following deviations:

- o Impeller edge-of-blade to stationary shroud contour mismatch limited axial running clearance to 0.007 inch compared to design value of 0.003 inch
- o Two of twelve inducer blades had significant undercut (0.018 and 0.012 inch) near the leading edge
- o Blade thickness approximately 0.002 to 0.004 inch over print increased blade blockage by 1 percent

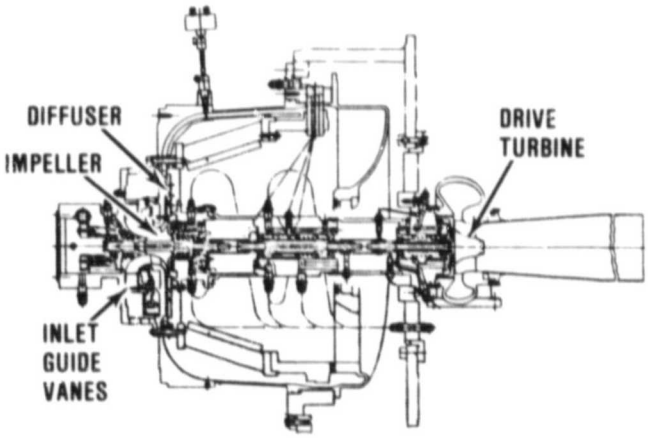

Figure 12. Compressor Test Rig.

MASS FLOW/INLET (1.0) TO (2.0)	ASME BELLMOUTH T_T — 16 THERMOCOUPLES P_S — TANK
COMPRESSOR INLET (2.0) TO (2.05)	P_S — HUB, SHROUD
IMPELLER SHROUD (2.05) TO (2.5)	P_S — SHROUD C_L — CLEARANCE PROBES
DIFFUSER (2.5) TO (3.0)	P_S — SHROUD P_T — 12 DUAL ELEMENT RAKES T_T — 12 DUAL ELEMENT RAKES
MECHANICAL INSTRUMENTATION	BEARING TEMPERATURE, SHAFT RUNOUT PROBES, VIBRATION, OIL FLOW, IMPELLER BACKFACE STATICS

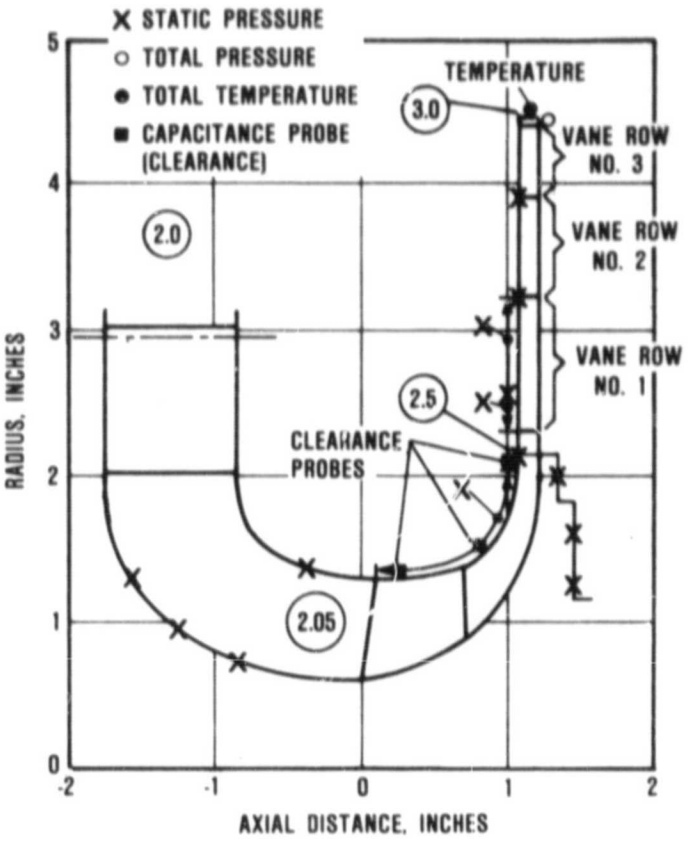

Figure 13. AGT101 Compressor Instrumentation Locations.

- Impeller exit blading over print in hub region increased blade blockage by 3.4 percent
- Diffuser vane height under print by average of 2.3 percent

4.1.4 Impeller Strain Gauge Test Results

The titanium impeller was instrumented with 10 strain gauges. Placement was based on holographic and acoustic test results. Gauges were placed on full and splitter blades with two gauges on the impeller backface. Figures 14 through 16 show the strain gauged impeller prior to test. Figure 17 shows the compressor rig in the test facility with the slip ring assembly installed.

Following initial mechanical checkout, the unit was accelerated to idle speed (50,000 rpm). The discharge valve was adjusted, raising the pressure ratio to idle conditions with the IGVs set at 0-degrees and data scans were recorded. While holding a constant discharge valve setting, the unit was accelerated in 10,000 rpm increments and held at selected speeds for approximately 1 minute. During the hold, all strain gauge and aerodynamic data was recorded. Strain gauge data was recorded on tape during all accelerations. At approximately

TABLE 4. DATA MATRIX.

Corrected Speed, %	IGV Setting, Degrees
50	-20, 0, 20, 40, 60, 70
60	0, 20, 40, 60, 70
70	-20, 0, 20, 40, 60, 70
80	0, 20, 40, 60, 70
90	-20, 0
95	0
100	-20, 0

80,000 rpm, the unit decelerated and a sharp increase in vibration was observed. All strain gauge output signals were reading zero at this time. The unit was allowed to roll down and a limited inspection was conducted.

Figure 14. Strain Gauged Impeller, Front View.

Figure 15. Strain Gauged Impeller Blade.

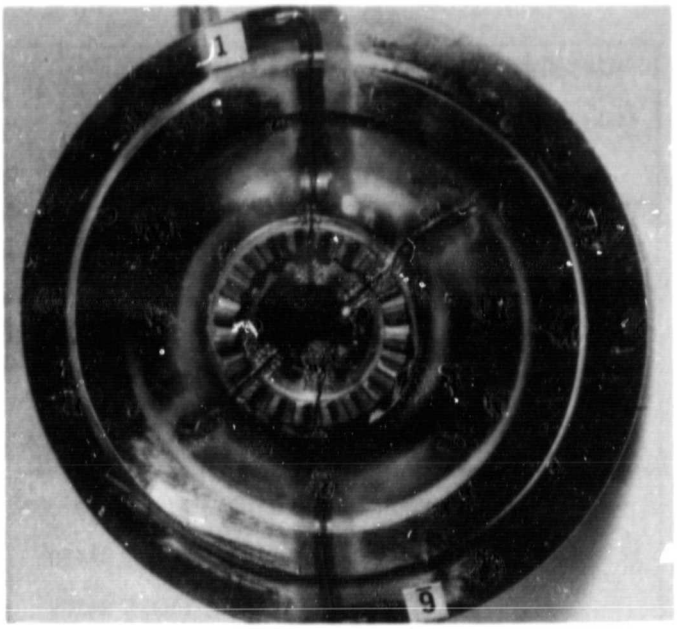

Figure 16. Strain Gauged Impeller, Backface.

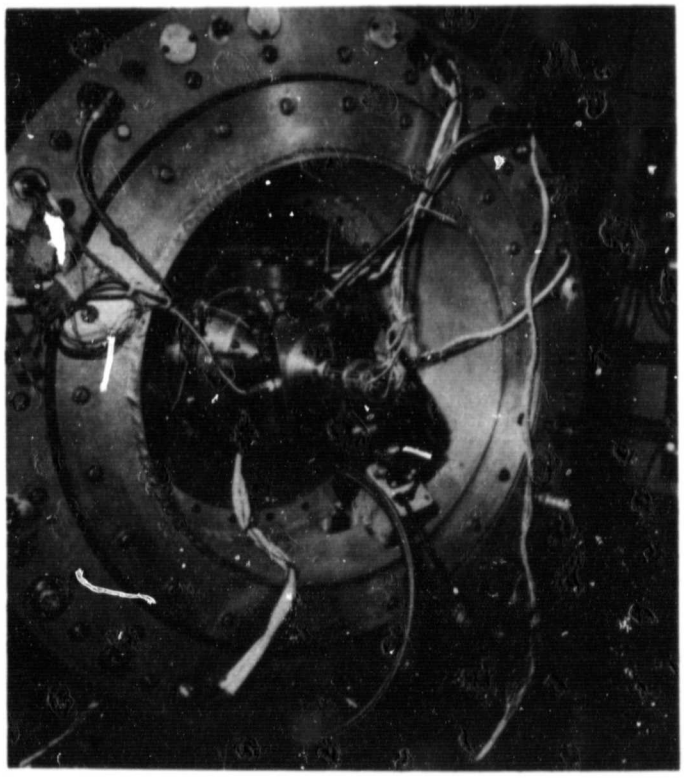

Figure 17. Compressor Test Rig with Slip Ring Assembly Installed in Test Cell.

Visual inspection revealed that the slip ring shaft was severed and the slip ring shaft bearing was failed; no other damage to the rig or aerodynamic hardware was noted.

This data, obtained during strain gauge testing, showed an excitation at 73,000 rpm (Figure 18) induced by a 4 per rev source (inlet distortion). The vibration was noted on five full blades at two different locations (Figure 19). The maximum strain level measured was less than $500\mu\epsilon$. This correlates to a maximum blade stress level of 26.3 ksi for the titanium impeller and 16.4 ksi for the aluminum impeller. Stress values for the aluminum impeller were ratioed by the modulus of elasticicity for the two materials. These values compare reasonably well with the predicted stress values (Reference 1). Maximum strain levels measured on the splitter blades were less than $150\mu\epsilon$.

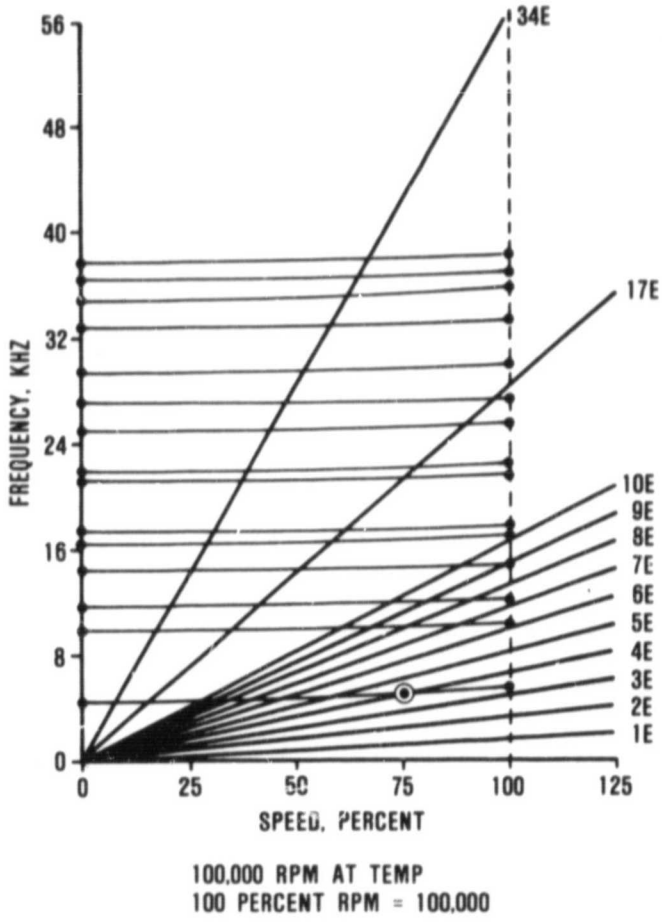

Figure 18. AGT101 Titanium Impeller Campbell Diagram, Excitation Source.

4.1.5 Compressor Aerodynamic Test Results

The compressor stage hardware (IGVs, impeller, and diffuser) was visually inspected following the impeller strain gauge slip ring failure. No damage was noted. The strain gauges were removed from the impeller and the test rig assembled for aerodynamic mapping.

Data were taken at corrected speeds of 50, 60, 70, and 80 percent for IGV settings of 0, +20, +40, +60, and +70 degrees. Impeller running clearance was maintained at 0.004 inch knee and 0.011- to 0.017-inch axial. Following initial mapping to 80,000 rpm, the test rig was accelerated to 90-percent corrected speed

LOCATION	BLADE	MEASURED STRAIN ($\mu\epsilon$)
1	2	311
1	6	229
1	8	493
2	3	224
?	9	291

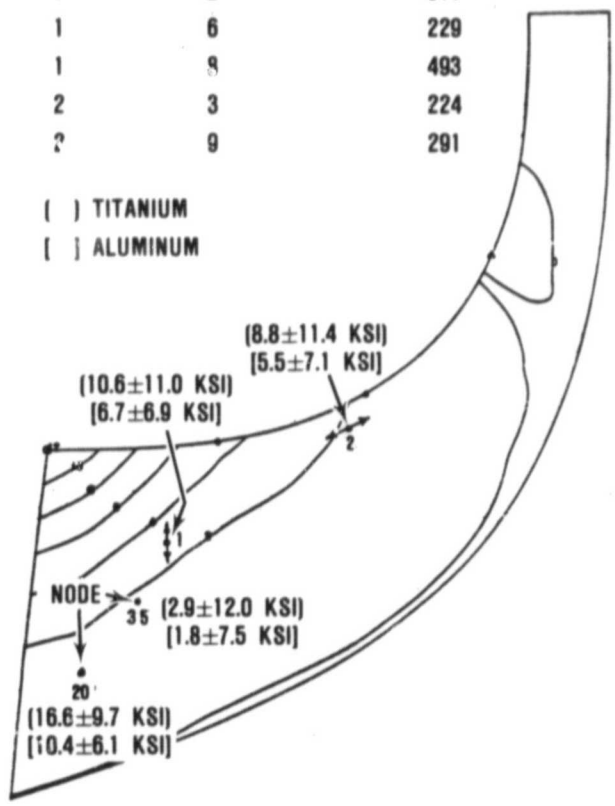

Figure 19. Strain Gauge Test Results.

(0-degree IGV) and data recorded. The test rig then was accelerated to 95-percent corrected speed. While setting the first data point (choke flow), an impeller rub occurred as shown in Figure 20. Clearances were readjusted and map ping of the 95- and 100-percent corrected speed condition was accomplished at 0-degree IGV setting. Additional data were taken at -20 degrees IGV setting for 50, 70, 90, and 100 percent design corrected speed.

Figures 21 through 25 present the aerodynamic performance data for the compressor stage. Figure 26 shows diffuser performance loss characteristics. Figure 27 shows the IGV flow and efficiency ratio compared with an existing Garrett design from which the AGT detail design was modeled. The impeller static pressure distribution as a function of meridional length is shown in Figure 28.

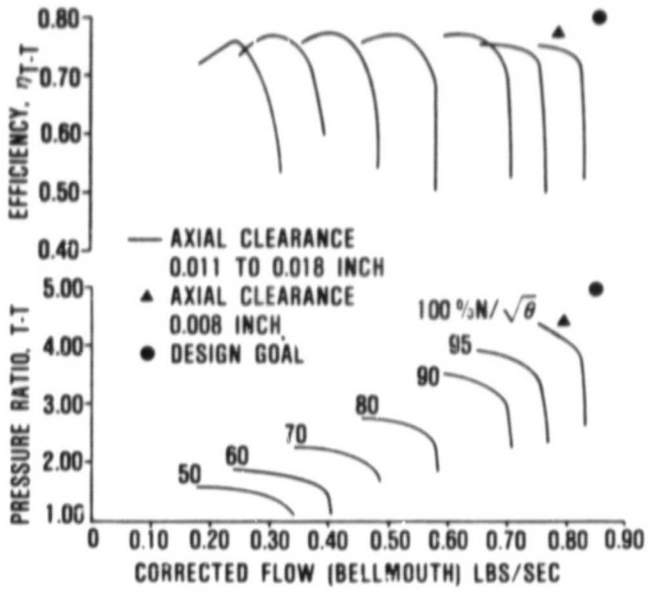

Figure 21. Baseline Compressor Test Results.

4.1.6 Discussion

The first compressor test showed very encouraging results. As shown in Figure 26, an excellent impeller/diffuser match was obtained. Peak stage efficiency at design speed was 78 percent compared with 79 percent predicted for the Mod I configuration. At all IGV settings, efficiency characteristics remained high

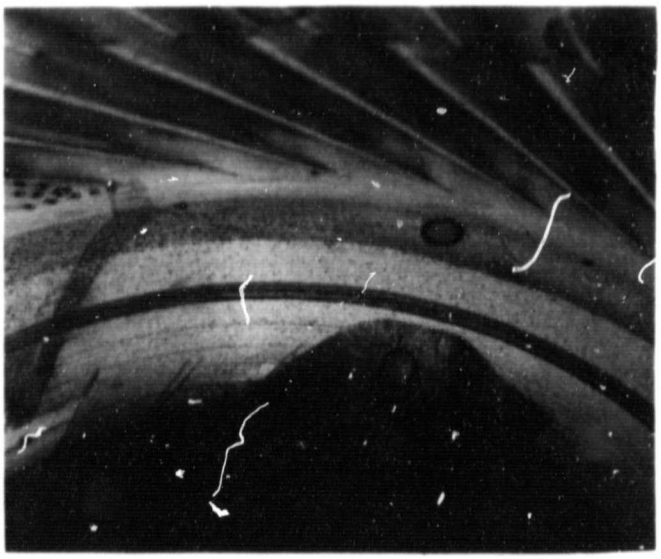

Figure 20. AGT101 Impeller Shroud Rub.

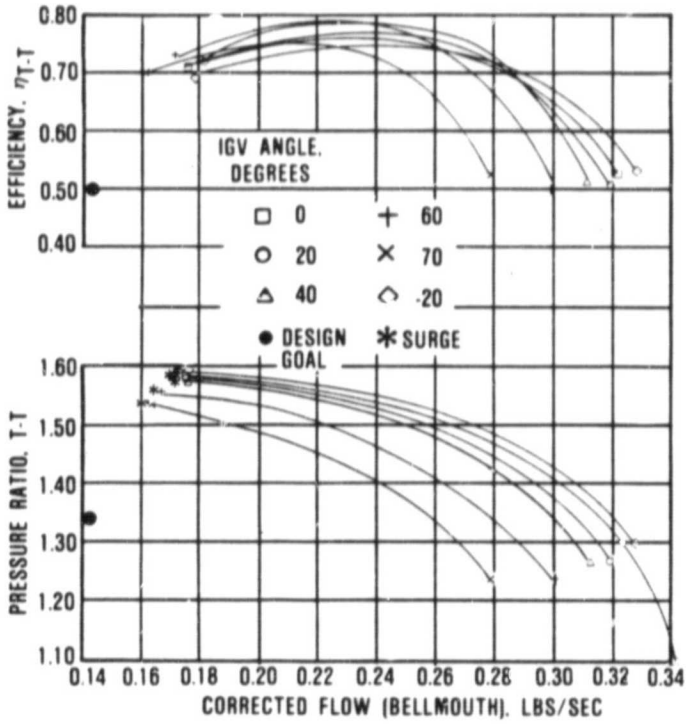

Figure 22. Compressor Test Results, 50-Percent Speed.

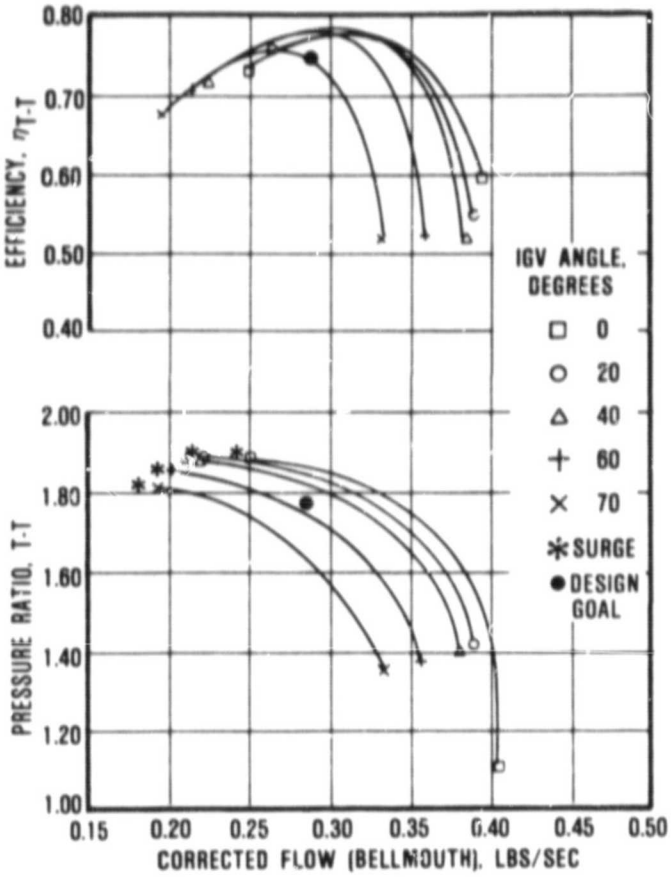

Figure 23. Compressor Test Results, 60-Percent Speed.

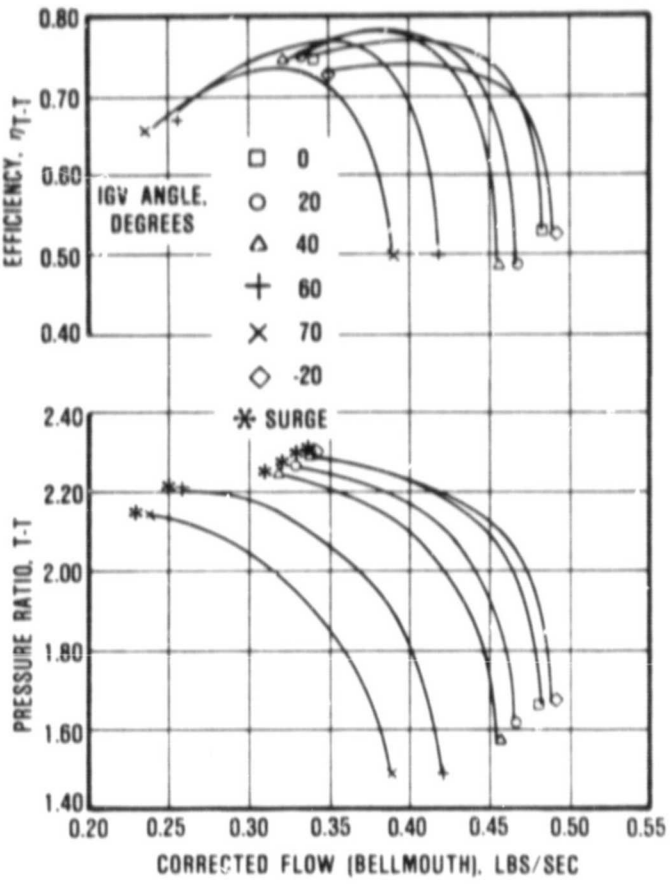

Figure 24. Compressor Test Results, 70-Percent Speed.

compared with 0-degrees IGV data. It is noted (Figure 21) that compressor flow and work input (pressure ratio) were below design by approximately 8 to 10 percent. Hardware discrepancies noted earlier and excessive axial clearance (0.008 inch tested compared with 0.003 inch design) account for a portion of these deficiencies; however, complete understanding of the responsible mechanism(s) is not evident at this time.

In an effort to better understand the tested compressor characteristics in relation to the overall engine/powertrain, the as-tested compressor map was input to the Mod II cycle, holding all other component technologies as predicted. Because of the aforementioned deficiencies of flow and pressure, a lower output horsepower resulted at maximum speed. However, as stated in References 1 and 2, maximum rated horsepower is not required over the CFDC. This cycle analysis shows that the AGT101 powertrain, with tested compressor, installed in a 3000-pound inertia weight vehicle achieved the same driveability characteristics and was within one mpg of the contract goal. This situation arises from the fact that less IGV closure is required to achieve cruise performance, which is where much of the CFDC time is consumed, as compared with the original prediction and therefore, although the current compressor is "small", the cruise/idle conditions are less off design than projected.

The IGV characteristics (Figure 27) are shown as normalized ratios of efficiency and pressure rise as a function of flow ratio. For comparative purposes, the Garrett Model

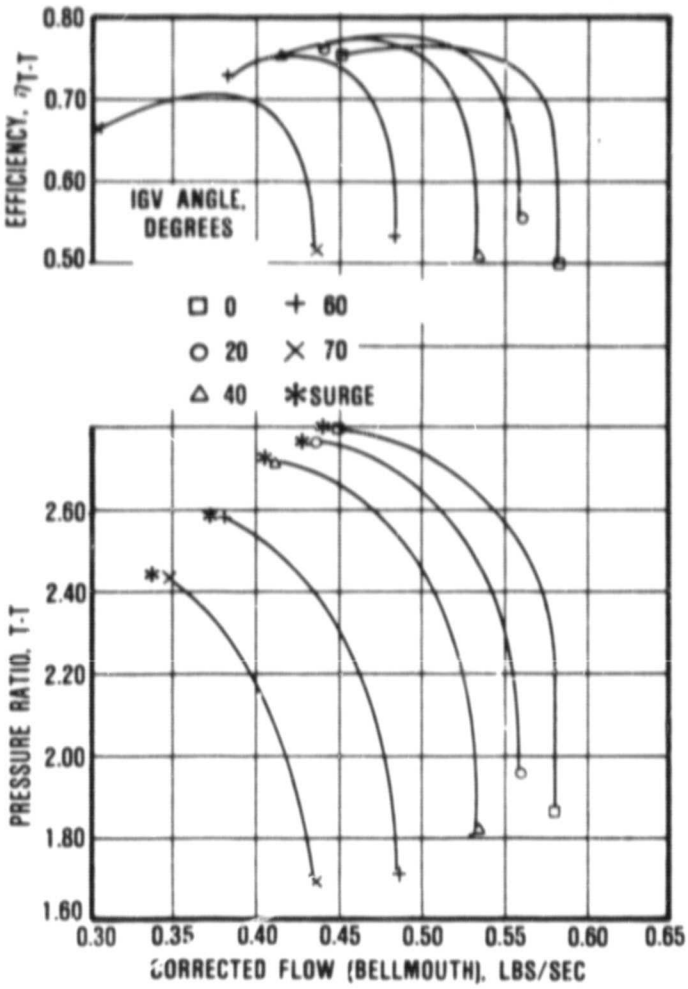

Figure 25. Compressor Test Results, 80-Percent Speed.

GTCP331-250 load compressor IGV characteristics are also displayed. Both systems utilize radially articulated IGVs and performance is very similar. However, original predictions (Reference 1), based on earlier Garrett IGV work, indicated the potential for a higher turndown ratio than is currently being achieved on the AGT. The differences between original predictions and test data are not wholly understood at this time; therefore, additional analysis and testing, as originally planned (see Section 4.1, herein), is required. Results of these exercises will be reported when restoration of the test program is accomplished.

The impeller shroud static pressure ratio versus meridional distance (Figure 28) is shown

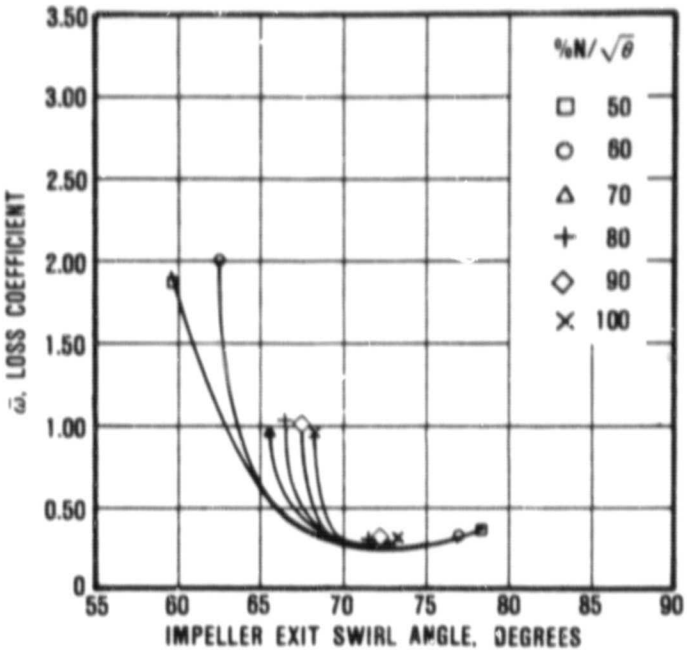

Figure 26. Compressor Diffuser Performance Loss Characteristics.

compared with design intent for peak stage efficiency. The higher static pressure near the inducer (relative to design) is a result of the lower flow achieved during test. Impeller exit static pressure differences are due to a combination of increased loss and aerodynamic blockage.

A second impeller, having additional edge-of-blade and tip radius stock, has been removed from parts storage and is being readied for test. Test No. 2 will be conducted with this impeller to recover the flow and pressure ratio. A minor change to the diffuser vane row 1 will be incorporated to match the modified impeller. Testing will be initiated with an impeller only (vaneless diffuser) test followed by a stage test during the next reporting period.

4.2 Turbine

Due to funding limitations, activities on the AGT101 cold turbine test program have been deferred. Mod I turbine testing has been completed and reported (Reference 3).

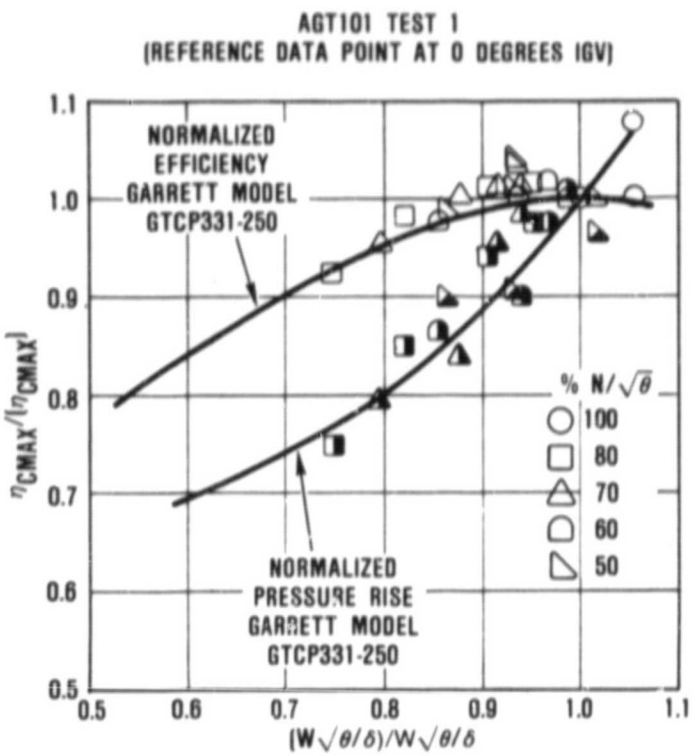

Figure 27. AGT101 Compressor Normalized IGV Characterisitics.

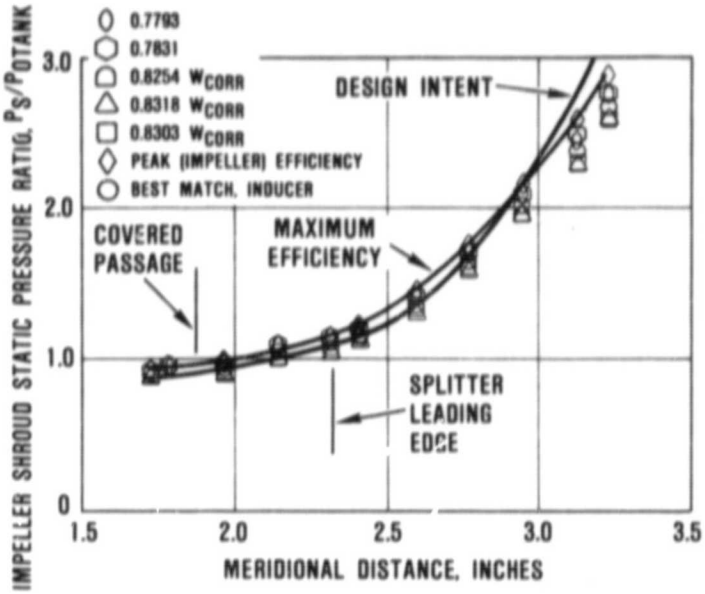

Figure 28. Compressor Impeller Meridional Static Pressure Distribution.

4.3 Combustion

Due to program redirection created by funding limitations, combustor testing was limited to the Mod I diffusion flame combustor (DFC) and reinitiation of various fuel nozzle designs for the Mod II RPD combustor. DFC test data was presented in Reference 3 with the exception of emissions test results which are presented below.

4.3.1 Diffusion Flame Combustor

DFC emission testing was conducted at simulated engine conditions with the inlet temperature held to a maximum of 1000°F. The combustion gas sample was obtained with a five element radial averaging probe. The probe was rotated through 160 degrees in 10 degree increments starting at 240 degrees from top dead center and rotated counterclockwise to 80 degrees. Chemicals measured were carbon dioxide (CO_2), carbon monoxide (CO), unburned hydrocarbons (HC), and oxides of nitrogen (NO_x).

The gas sampling scans were taken at the combustor exit and simulated turbine inlet for each of the three power points. For a given power point there was no difference in the emission levels for the two discharge planes measured, indicating that the combustion process was completed within the combustor. Also, there was virtually no variation in the circumferential direction denoting a uniform and symmetric combustion process over the sector scanned. Table 5 summarizes the emission test data. Although this combustor is not designed to meet program emission goals, the combustor did meet CO goals at all power points and HC goals at cruise and maximum

TABLE 5. EMISSION TEST DATA

Emission Index
Lbs/1000 Lbs of Fuel

Power Setting	NO_x	HC	CO	Combustor Efficiency (%)
Idle	6.1	8.8	26.9	98.60
Cruise	8.5	3.0	12.5	99.45
Max	12.6	0.2	2.7	99.92

power; the NO_x goals were not met at any power settings. Increasing the inlet temperature at idle and cruise power to actual engine conditions should further reduce HC and CO at these points with an attendant increase in NO_x.

4.3.2 Mod II Fuel Nozzle Development

The fuel nozzle development for the Mod II combustor consisted of improvement of the Delavan duplex fuel nozzle and the design of a module venturi nozzle. Spray testing of the initial duplex nozzle revealed poor atomization and streaking from each of the individual fuel spray orifices. The fuel discharges through six orifices in the secondary passage and through four orifices in the primary passage. The nozzle was reworked and an L-shaped prefilmer ring was added to improve the circumferential uniformity and eliminate the streaking problem.

Figure 29 shows a comparison of the original nozzle with two different configurations of the reworked nozzle with all fuel introduced through the secondary passages. Reworking improved the streaking and the atomizing characteristics although atomization was still coarser than desired. The reworked nozzle was also tested in the same two configurations with the fuel injected through the primary circuit only. Test results, shown in Figure 30, indicate that atomization was the same or slightly better than that of the secondary fuel injection.

A venturi nozzle was designed and fabricated from Lexan® to study the atomization and distribution characteristics. The venturi nozzle has the advantage of being easily fabricated from ceramic and has been used in a lean-burn system at NASA-Lewis. The nozzle was fabricated in a modular fashion in order to evaluate a number of different configurations. A nozzle cross sectional schematic is shown in Figure 31. Plans are to cold flow spray test the venturi nozzle and measure atomization and distribution for various configurations and flow conditions.

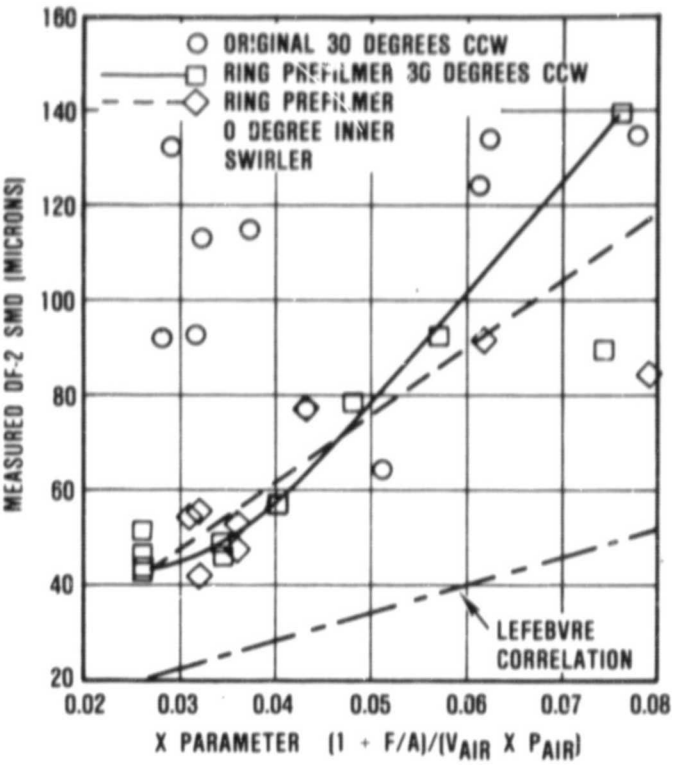

Figure 29. Droplet SMD, Reworked Duplex Fuel Nozzle, Secondary Fuel Only.

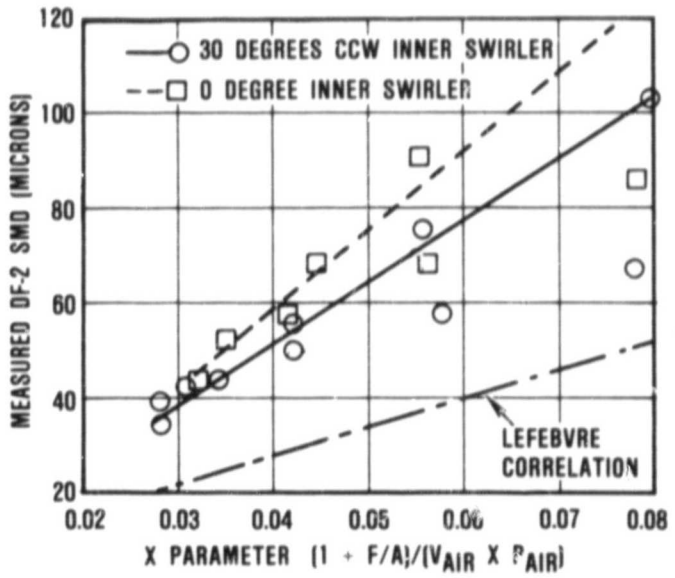

Figure 30. Droplet SMD, Reworked Duplex Fuel Nozzle, Primary Fuel Only.

4.4 Regenerator

4.4.1 Ford Regenerator Development

The main objective for the regenerator-seal, coating-wear rig testing was to determine the

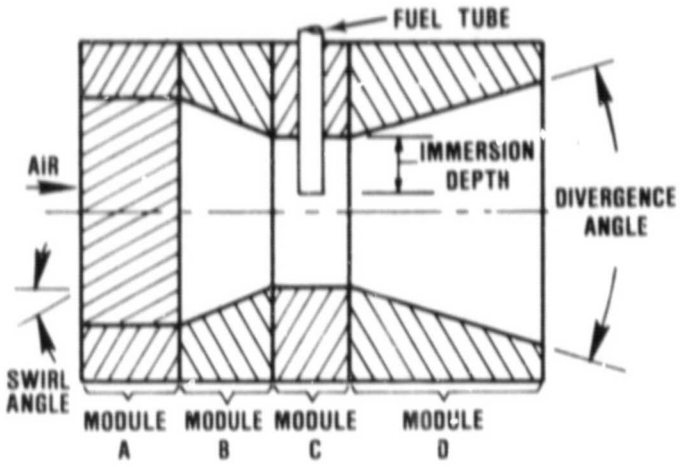

MODULE A
SWIRL ANGLE — 0, 15, 30 AND 45 DEGREES

MODULE B
CONVERGENCE — MATE WITH MODULE A AND C

MODULE C — CONSTANT

MODULE D
DIVERGENCE ANGLE — 15 AND 34.5 DEGREES

FUEL TUBE — 0.010 AND 0.069 INCH DISCHARGE ORIFICE
— DIFFERENT IMMERSION DEPTH

Figure 31. Venturi Fuel Nozzle Schematic Cross Section.

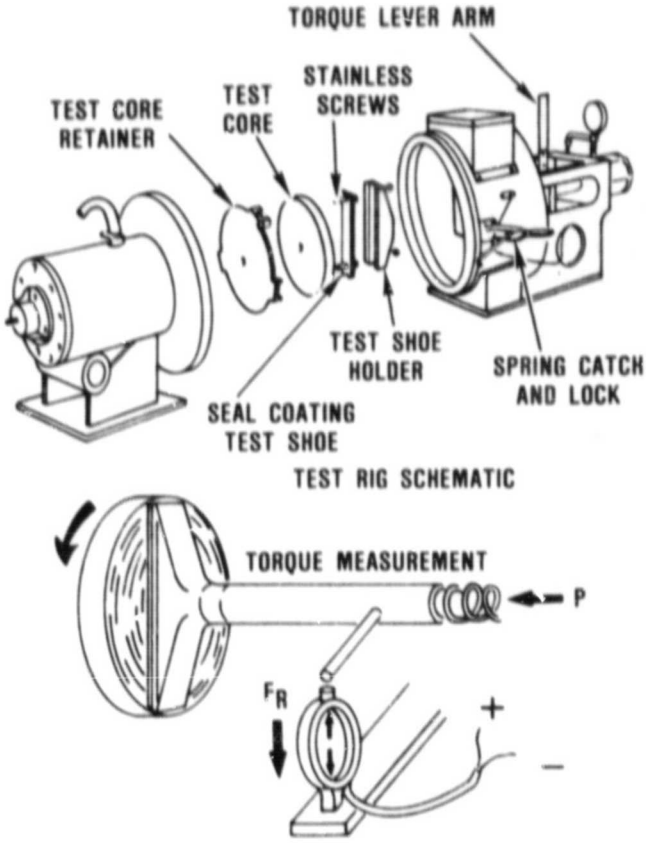

Figure 32. Regenerator Seal Coating Wear Test Rig.

upper temperature limit of the AGT engine hot (inboard) regenerator crossarm seal coating (I-112). In addition, the spraying capability of two new suppliers (Imperial and Jedco) was evaluated. A third objective was to determine the optimum process for producing the I-112 powder utilizing Ferro Corporation facilities.

For the AGT101 Mod II engine, the hot-side crossarm-seal coating must be capable of 2000°F regenerator gas inlet temperature operation.

To determine the upper temperature limit of the I-112 crossarm coating, the existing test rig (Figure 32) had to be revised to increase temperature capability from 1500 to 2000°F. The primary modification was replacement of the metal test shoe holder (Figure 31) with a ceramic holder.

The stationary test sample is loaded against the rotating test core by a compression spring. A lever arm, which is pinned to a center shaft, applies the torque reaction force against a calibrated load cell. By knowing the applied force (P), torque reaction force (F_R) and physical dimensions of the sample, the sliding coefficient of friction (f) can be determined. Periodic measurements of sample thickness determines the seal coating wear rate.

The design of an effective crossarm seal that has 2000°F temperature capability with acceptable friction and wear characteristics requires optimizations of the following parameters:

- Chemical composition and particle size distribution of the coating powder
- Spraying procedure for depositing the coating powders on the metal substrate

- o Interface coatings to accommodate the difference in thermal expansion between the I-112 coating and the metal substrate

- o Substrate serrations to form a mechanical bond attachment of the coating

A total of 14 samples, which accumulated over 2000 hours, were tested to evaluate the above parameters.

All of the I-112 powder evaluated has been provided by Ferro Corporation. In order to determine the optimum process for the I-112 powder using the equipment and facilities at Ferro Corp., three different batches of powder were processed. Preliminary evaluation of the I-112 powder is based on the wet chemical analysis of the composition and the particle size distribution. All three batches were within specification.

Prior to AGT Program initiation, all regenerator seal spraying was done by Alloy Tech. To promote competitive pricing, the need for qualifying additional spraying sources became imperative. Two additional suppliers (Jedco and Imperial) expressed interest in the AGT Program. Consequently, test specimens were procured for qualification purposes. The initial criteria for evaluating the spraying process is to maintain the same chemical composition after depositing the powder on the substrate. This can be evaluated by comparing the set chemical analysis of the coating before and after spraying. After several iterations, Jedco and Imperial demonstrated acceptable capability for spraying the I-112 powder.

The first nine samples tested were processed with the standard NiCr interface bond coating. After breaking in the coating at 800°F for approximately 20 hours, each sample was run at 1400°F for approximately 24 hours. To determine maximum temperature capability, the test temperature was increased in 50 or 100°F increments until the coating separated from the substrate. Maximum temperature without separation appeared to be limited to 1800 to 1850°F. Since separation appeared to occur at the NiCr layer, new interface bond coatings were investigated.

Samples sprayed with commercially available METCO 443, METCO 447, and GE Superalloy in place of NiCr were evaluated. To evaluate the effectiveness of the serrations, additional samples without serrations also were tested. A summation of the temperature capabilities of the various test combinations are listed in Table 6. Some improvement was evident with METCO 443 and METCO 447, which appeared to increase the temperature capability approximately 50 to 100°F. The GE superalloy appears to satisfy the 2000°F objective.

TABLE 6. TEST SAMPLE TEMPERATURE LIMIT

Interface Bond Coating	Maximum Temperature, °F	
	Without Serrations	With Serrations
NiCr (Standard)	1700-1750	1800-1850
METCO 443	1600-1650	1850-1900
METCO 447		1850-1900
GE Superalloy	1700-1750	2000+

The effectiveness of the deep serrations is clearly indicated in Table 6. Temperature capability appears to increase 100 to 300°F, compared with a non-serrated sample.

The initial set of AGT regenerator seals with the relocated crossarm diaphragms were assembled and evaluated in the static seal leakage rig. As expected, there was no leakage penalty associated with this design modification. Utilizing the static seal leakage rig, a thorough evaluation of regenerator seal assembly leakage was conducted during this period.

This procedure is imperative to reduce leakage to the program objective of 3.6 percent. Based on test results and observations, several design changes have been initiated. Die imperfections for the upper and lower peripheral diaphragms were corrected.

To apply additional seal loading at part-power engine conditions to reduce leakage, a new three-diaphragm system (Figure 33) was designed. Required dies for this design have

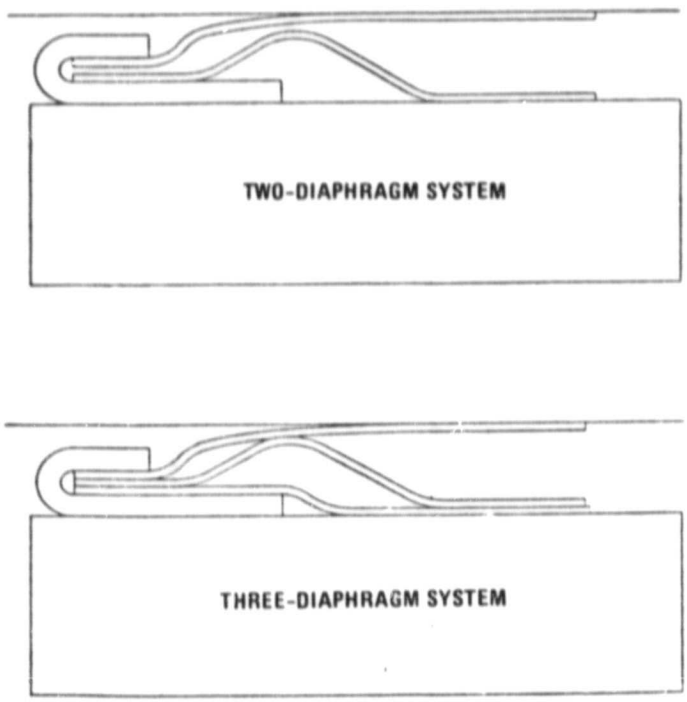

Figure 33. Revised Regenerator Seal Diaphragm Assembly.

been completed. Progress for fabricating seal assemblies of the new design was delayed during this period due to relocation of the Ford fabrication facility, loss of priority, and sickness of key personnel. Alternate sources were investigated. Jedco, Inc. in Grand Rapids, Michigan was deemed the most suitable due to previous experience from the Ford 707 seal package. Garrett also has initiated an in-house program to fabricate regenerator seal assemblies.

The original diaphragm dies, secondary diaphragms and five sets of coated rubbing shoes were delivered to Garrett during this period. Jedco has the dies for the new three-diaphragm system and are currently fabricating seal components that will be evaluated at Ford for process approval.

To evaluate a complete engine regenerator system (core plus two seal assemblies) in the static seal leakage rig at Ford, a new cover plate that will be available during the next period has been designed.

Due to the greater wall porosity of the NGK regenerator material, core leakage across the crossarm and through the inner and outer circumferences is higher when compared with the more dense Corning Glass material. NGK has developed a dense MAS coating that can be applied to the inner and outer circumferences. A matrix test sample with a thin layer of this coating was supplied by NGK for evaluation. Utilizing an existing test fixture, through-wall leakage as a function of pressure for the normal and coated matrix surfaces was evaluated. Based on this comparison, the high density coating appeared to reduce through-wall leakage approximately 80 percent.

Four full-size NGK cores have been shipped to Japan for coating of the outer and inner surfaces.

Installation of a new induction heater system, which is utilized in the regenerator ring gear bonding process, was initiated during this report period.

4.4.2 Garrett Regenerator Development

The regenerator hot test rig was assembled and installed in the test facility. The rig (Figure 34) was designed and fabricated to minimize extraneous leak paths (at seal locations) by eliminating all seals not required for unit assembly. Braze joints were utilized so that leakage from the HP side of the rig to the LP side can only occur across the static side of the regenerator seal, flipper seal and dynamic faces of the regenerator seals.

During rig Builds 1 and 2, minor assembly and laboratory problems precluded testing. Build 3 of the rig was completed and testing initiated. With the NGK core and first-generation Ford regenerator seals, static leak checks showed excessive leakage (≈25 percent of compressor inlet flow). The unit was disassembled and a series of vacuum leak tests were conducted. Several areas were noted as contributors with a significant leakage found in the NGK core. This core exhibited excessive throughwall porosity resulting in approximately 40 percent of the total cold leakage noted earlier. Subsequent testing of the Corning thin

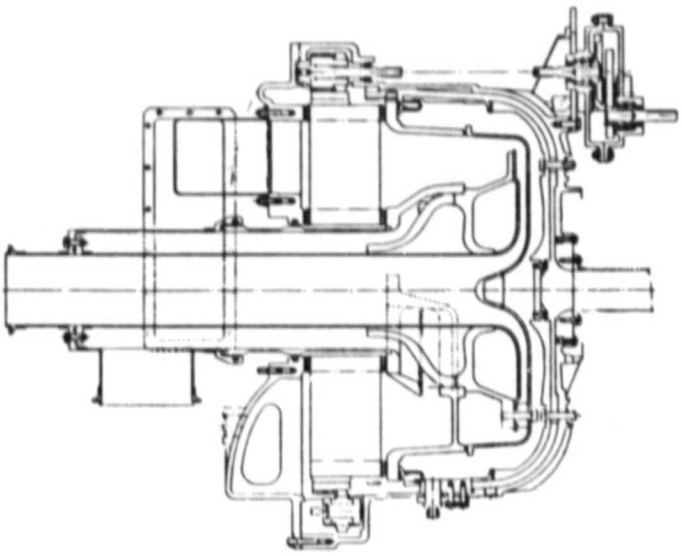

Figure 34. Hot Regenerator Rig Schematic.

wall cores exhibited negligible leakage. Modifications were incorporated to the test rig and the Corning core installed for Build 4.

Build 4 was completed and the unit installed in the test cell. Initial operation of the rig was conducted at ideal conditions (equivalent to 1600°F TIT) for approximately 4 hours to break in (or glaze) the seals prior to performance mapping.

Further testing was conducted at simulated engine conditions. Instrumentation was located upstream and downstream of the HP and LP core faces. Thermocouple rakes were located in equal area planes at five radial locations, spaced approximately 35 degrees apart.

Dynamic seal leakage was determined using a unique helium flow seeding technique depicted in Figure 35. Helium is injected and mixed at selected stations upstream of the HP inlet. Flow passing through the HP side of the core is then ducted overboard. Conditioned LP flow is then introduced to the slave burner to maintain proper LP and HP flow match. Fuel is introduced and combustion initiated. Regenerator seal leakage from the HP side (helium seeded flow) to the LP side (unseeded) can then be determined using a mass spectrometer to measure helium concentration levels at the LP exhaust. Leakage is measured accurately to approximately 0.2 percent of the HP inlet flow.

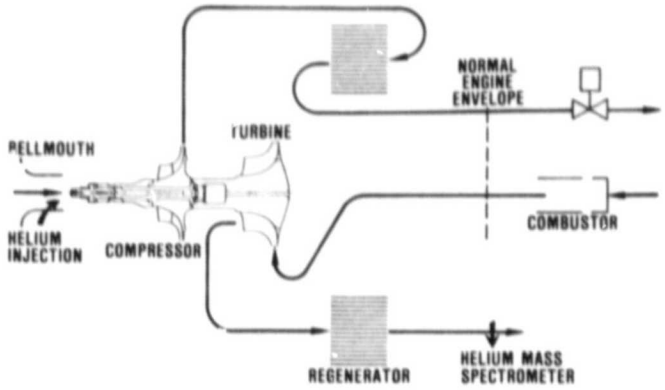

Figure 35. Regenerator Leakage.

4.4.2.1 Test Results

Due to requirements of the Mod I (1600°F) engine test program, testing was limited to an idle condition only. Additional testing will be conducted following engine testing.

At points near idle conditions, leakage was measured at 0.576 lb/min, approximately 5.2 percent of test compressor flow. Figure 36 shows the LP and HP core exhaust temperature profiles at the simulated idle condition. The tested temperature effectiveness of the HP side of the regenerator was 95.9 percent at idle conditions.

Figure 36 shows that the radial temperature gradients of the discharge gases at the carry-over points (170- and 350-degree arcs) are minimal indicating insignificant flow distortion effects.

4.4.2.2 Regenerator Technology Status

Table 7 compares the Mod I (1600°F) goals (idle reference cycle) with regenerator rig test results. The comparison shows that the Mod I 1600°F goals are feasible since they compare favorably in the first test configuration.

Interpath leakage, shown in Table 7, is about 30 percent higher than the goal at idle. Note that the idle leakage goal is a capillary and labyrinth flow prediction of idle leakage based on the 7.5 percent goal at full power.

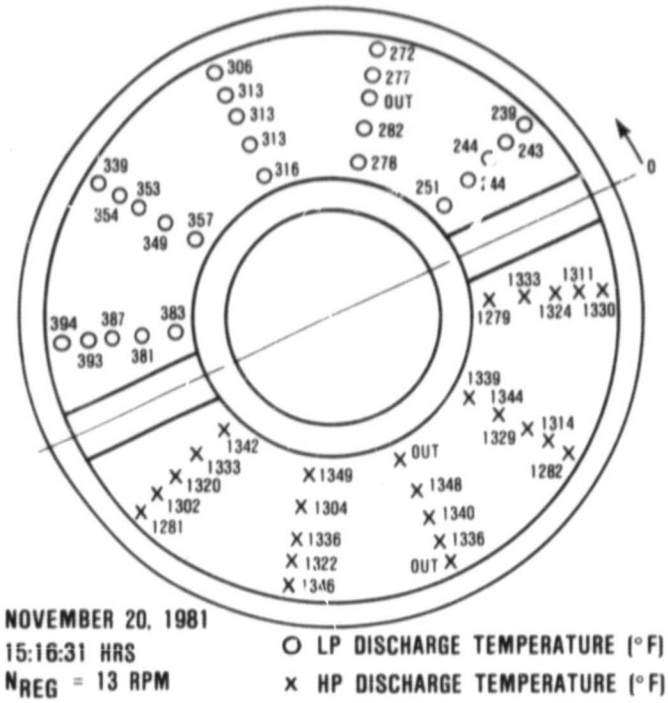

Figure 36. Steady State Regenerator Discharge Temperature Distributions.

Temperature effectiveness of the regenerator system is shown to be one percent lower than the goal. This deficiency may be solely the result of the additional interpath leakage.

Development of the Mod I regenerator system will continue in the areas of seal and core development. The Mod I (1600°F) design goals, as shown, appear to be readily achievable within the Mod I development time frame.

4.5 Gearbox/Transmission

All gearbox and transmission activities at Garrett and Ford (procurement and fabrication of hardware and test rigs) were deferred to a later time due to budget constraints. Existing hardware was placed in storage and outstanding hardware orders were cancelled, where applicable, to conserve project funds.

4.6 Ceramic Component Development

This section discusses progress on ceramic material characterization, ceramic component process development, and evaluation of ceramic components delivered to Garrett. Table 8 summarizes ceramic component sources, fabrication processes, and strength data measured for each material.

TABLE 7. REGENERATOR RIG TEST RESULTS

	Mod I (1600°F) Predicted	Regenerator Rig Test Test Results
Regenerator HP Inlet Pressure (psig)	6.14	5.42
HP Side Inlet Flow (lb/min)	10.07	11.08
LP Side Inlet Flow (lb/min)	9.88	11.13
HP Inlet Temperature (°F)	158	165
LP Inlet Temperature (°F)	1451	1375
LP Exhaust Temperature (°F)	239	314
HP Exhaust Temperature (°F)	1411	1325
HP Temperature Effectiveness	0.969	0.959
Interpath Leakage (lb/min)	0.431	0.576

4.6.1 Carborundum Ultra-fine Grain Reaction Sintered SiC

As a rotor candidate material, test bars of KX-02 isopressed ultrafine grained reaction sintered SiC were evaluated at room temperature and 2000°F. All test bars were machined to a 0.125 by 0.25 inch cross section and were 4-point flexure tested using a 1.5 inch outer and a 0.75 inch inner span. The material was tested in the as-machined condition as well as after a

TABLE 8. AGT101 COMPONENT AND MATERIAL SUMMARY

Supplier	Material	Process	Condition	Qualification Bar							Ceramic Component						
				Room Temperature			Elevated Temperature				Room Temperature			Elevated Temperature			
				σ_θ[4]	M	Population	σ_θ[4]	M	°F	Population	σ_θ[4]	M	Population	σ_θ[4]	M	°F	Population
ACC																	
Inner Diffuser	RBSN (RBN104)	Slip Cast	As-Fired	49.7	4.5	30	52.1	10.1	2200	10	--	--	--	--	--	--	--
Outer Diffuser Turbine Shroud			Longitudinally Ground	53.2	5.5	10					46.3	5.3	27	--	--	--	--
ACC																	
Stator	RBSN (RBN124)	Injection Molded	As-Fired[1]	40.1	4.8	19	44.5	8.4	2200	23	--	--	--	--	--	--	--
ACC																	
Rotor	Sintered Si_3N_4 (SNN 502)	Slip Cast	Longitudinally[2] Ground	--	--	--	--	--	--	--	60.7[3]	18.5	24	--	--	--	--
	Sintered Si_3N_4 (SNN 522)	Injection Molded	As-Fired	89.2	8.9	30	66.1	11.1	2000	30	--	--	--	--	--	--	--
Carborundum																	
Turbine Shroud, Stator	Sintered α-SiC	Injection Molded	As-Fired	48.6	9.5	30	45.0	5.0	2500	10	--	--	--	--	--	--	--
Combustor Baffle	Sintered α-SiC	Slip Cast	Longitudinally Ground	49.4	5.8	30	41.4	6.7	2500	10	--	--	--	--	--	--	--
Transition Duct, Regen Shield, Back-shroud	Sintered α-Sic	Isopressed	Longitudinally Ground	57.7	7.7	30	56.2	11.9	2500	10	--	--	--	--	--	--	--
Ford																	
Rotor	SRBSN (RM-2)	Slip Cast	Longitudinally Ground	109.3	19.8	6	73.1	16.4	2200	6	--	--	--	--	--	--	--
Stator	RBSN	Injection Molded	As-Fired	43.1	9.2	39	45.8	7.7	2200	10	--	--	--	--	--	--	--
NGK																	
Backshroud, Transition Duct	Sintered Si_3N_4 (SN-50)	Isopressed	Longitudinally Ground	87.6	10.5	10	47.1	13.6	2000	7	--	--	--	--	--	--	--

All test bars 0.250 x 0.125 inch cross section unless noted. Bars tested in 4-point flexure, 1.50 inch outer span and 0.75 inch inner span. Cross head speed, 0.02 inch/minute

(1) Test bar cross section 0.31 x 0.15 inch

(2) Test bar cross section 0.2 x 0.1 inch

(3) 95 percent dense

(4) Characteristic strength, ksi

2000°F 2-hour oxidizing treatment. Results are summarized in Table 9. Fracture surfaces were examined both visually (40x) and by SEM and indicated predominantly surface-initiated fractures. Although only a limited number of test bars were tested, these results indicate that a considerable strength improvement was attained through the oxidation treatment.

The microstructure of KX-02 is shown in Figure 37 in both the as-polished and etched condition. The size of SiC grains contained within the silicon matrix are 1 to 2 microns. The microstructure is uniform and homogeneous.

4.6.2 Cyclic Oxidation Testing of Ford RM-2 Si_3N_4

Ford RM-2 sintered reaction-bonded Si_3N_4 is one of the major material candidates for the radial rotor. To evaluate the stability of this material under dynamic, cyclic oxidation conditions, as-machined test bars were exposed in the NASA/Garrett cyclic durability facility (Reference 4) for 100 and 350 hours.

The NASA/Garrett durability test facility is schematically shown in Figure 38. It consists of a high velocity oil burner, a furnace-type enclosure, a specimen drive and actuation system, cycle and temperature controls, and an

TABLE 9. WEIBULL PARAMETERS FOR FLEXURAL TESTS OF ISOPRESSED ULTRAFINE GRAIN SILICONIZED SiC (KX-02)

Material Condition	Temperature (°F)	Characteristic Strength, σ_θ (ksi)	Weibull Modulus	Population
As-machined	72	50.6	2.8	12
As-machined	2000	97.9	4.3	7
Oxidized 2200°F/2 hrs	72	71.4	25.6	6
Oxidized 2200°F/2 hrs	2000	112.2	7.7	4

Test Bar Cross Section: 0.125 x 0.25 inch
Four-Point Flexure
Outer Span: 1.5 inches Inner Span: 0.75 inch
Cross Head Speed: 0.02 inch/minute
Test Bars Machined in Longitudinal Direction

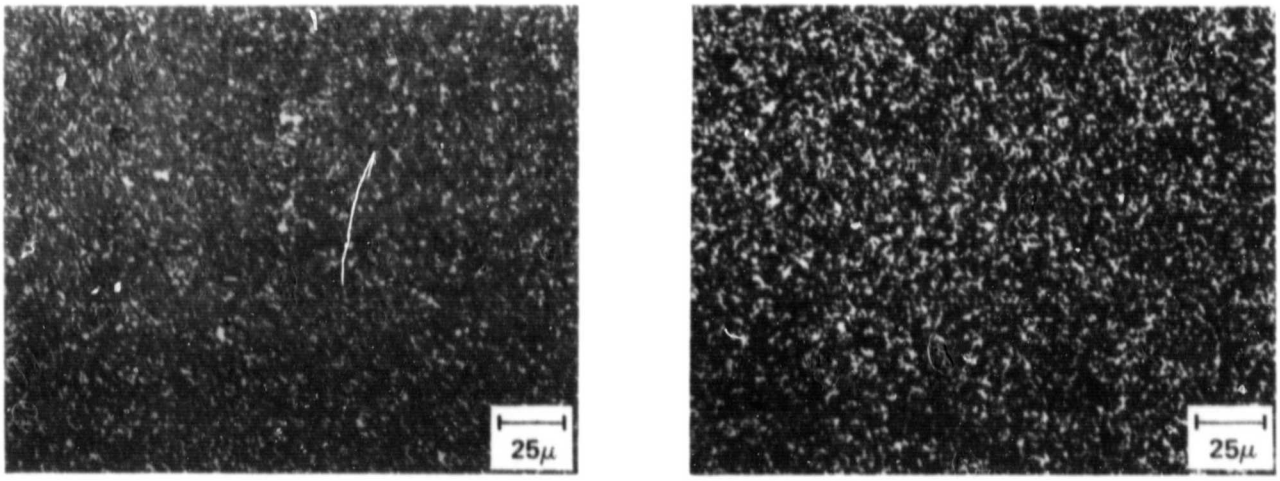

Figure 37. As-Polished and Etched Microstructure of Carborundum Ultrafine Grain RSSIC (KX-02).

air-cooled specimen holder. For the current tests, diesel referee grade fuel MIL-F-46162B(ME) was used.

The test specimens were 0.125 x 0.250 x 4 inch bars supported in an air-cooled specimen holder (shown in Figure 39). The specimen holder rotated continuously so that all the specimens were similarly exposed.

Thermal cycling was accomplished by translating the specimen holder in and out of the furnace enclosure through a specimen port. At the conclusion of the cyclic exposures, the ceramic specimens were removed from the holder and strength tested in quarter point bending (outer span 1.5 inches, inner span: 0.75 inch). Typically, two fractures could be obtained on each test bar, one in the outer third

of the bar where the exposure temperature was maximum (2200°F in these tests) and one near the specimen holder where the temperature was somewhat lower (estimated at 1500 to 2000°F, depending on the distance of the fracture from the top of the specimen holder).

The cyclic durability facility provides exposure conditions much closer to those of a gas turbine operating environment than can be achieved by oxidation exposure in a static furnace atmosphere.

Important characteristics of the durability testing include the following:

- Repeated, rapid thermal cycling from the peak temperature to below the cristobalite polymorphic transformation temperature*
- Exposure of the specimen to a high velocity combustion environment
- Exposure of the test specimens to a thermal gradient over the length of the specimen which allows detection of oxidation of corrosion anomalies over a broad temperature range
- Use of a specimen configuration that allows correlation of oxidation effects with strength and microstructure

The RM-2 material was exposed in the durability rig to a peak material temperature of 2200°F using a cycle consisting of 11 minutes at temperature with a 30-second airblast quench

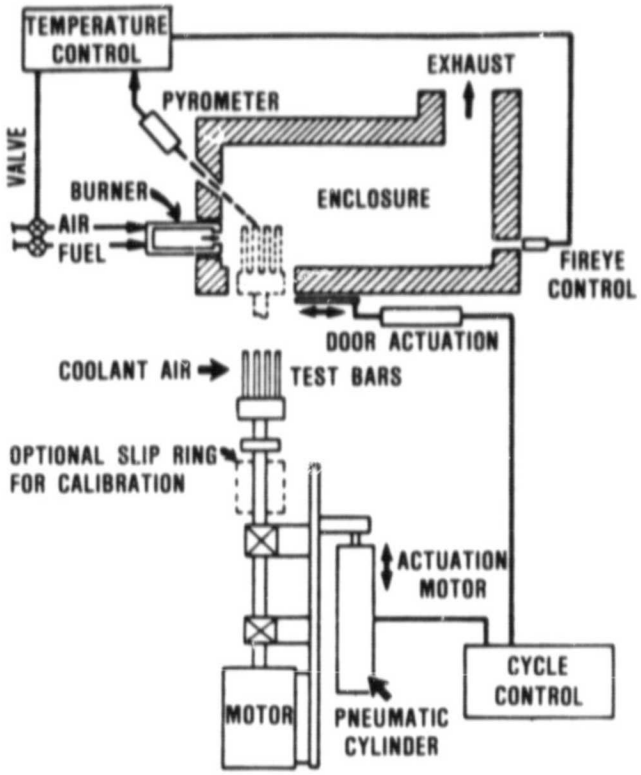

Figure 38. NASA/Garrett Cyclic Durability Test Facility.

(to below 400°F). Sixteen Ford RM-2 test bars were cyclically exposed to 2200°F for 100 hours. Eight bars were removed from the specimen holder and replaced with filler bars. The bars exposed for 100 hours were visually inspected, weighed, measured for dimensional changes and broken in four-point flexure at both room temperature and 2200°F. The remaining eight bars were tested for an additional 250 hours. These bars also were visually inspected, weighed, measured for dimensional changes and flexure tested at room temperature.

The flexure strength test results are summarized in Table 10. The average strength of as-machined unexposed (baseline) test bars was 107 ksi at room temperature and 71 ksi at 2200°F. The room temperature strength in the 2200°F exposure region of the test bars showed a slight (but probably not statistically significant) decrease to 97 and 104 ksi respectively

*Si_3N_4 and SiC form a thin SiO_2 surface layer which protects the underlying material from oxidation. The SiO_2 typically crystallizes to form cristobalite. Cristobalite undergoes a reversible polymorphic transformation at about 450°F, which results in a 3 percent dimensional change. This can crack the surface layer providing a potential path for accelerated oxidation during the next high temperature cycle. The cracks also can act as surface defects which reduce the room temperature strength of the material.

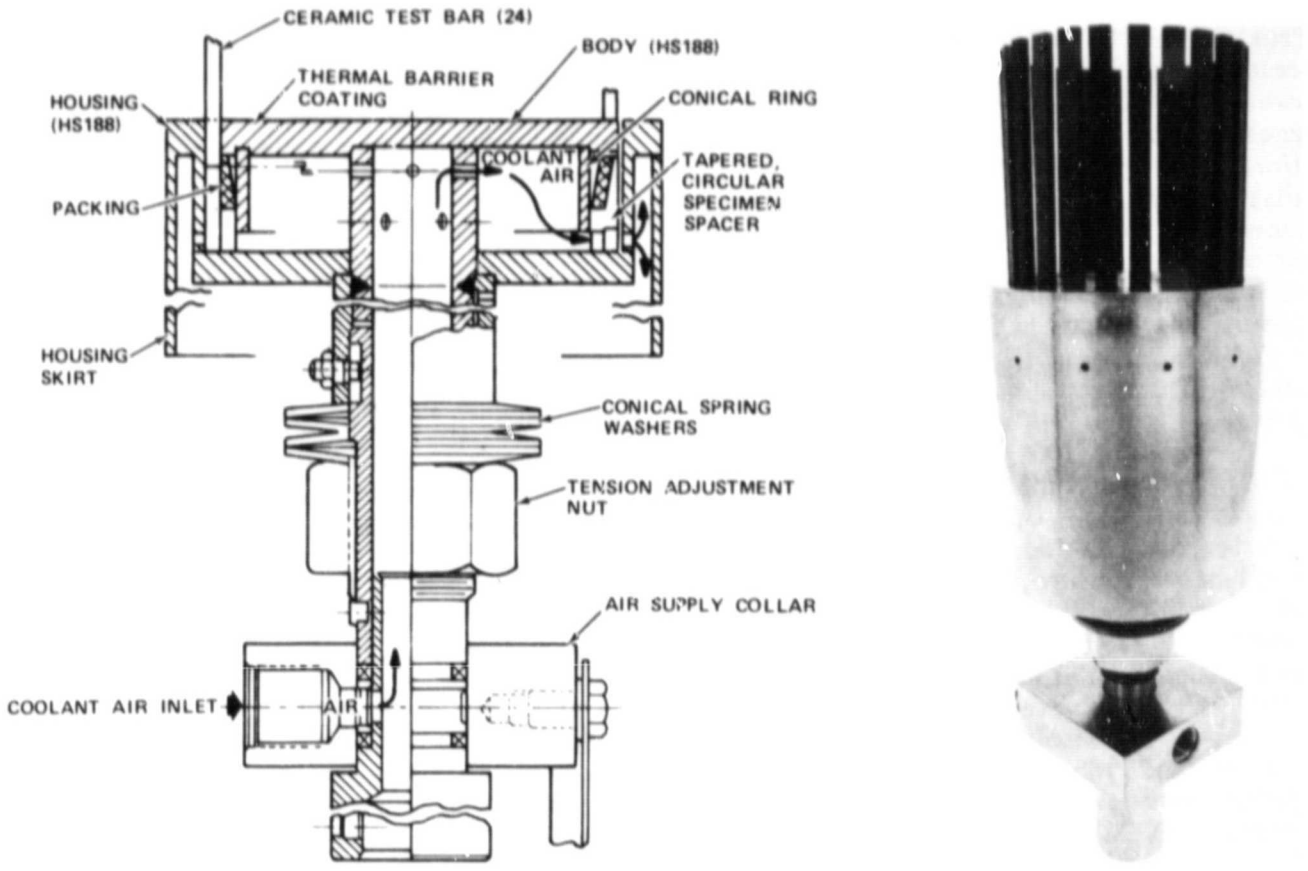

Figure 39. NASA/Garrett Air-Cooled Ceramic Test Bar Holder.

TABLE 10. FORD RM-2 SRBSN - CYCLIC EXPOSURE TESTING

Test	Flexure Test - Bar Location	Number of Test Bars	Flexure Test Temperature (°F)	Mean Strength (ksi)	Standard Deviation (ksi)	Weibull Slope	Characteristic Strength, σ_θ (ksi)
Baseline Strength (As-Machined)	--	6	72	106.7	5.6	19.8	109.3
		6	2200	71.0	4.4	16.4	73.1
100 Hours Cyclic Exposure to 2200°F	In 2200°F Area	4	72	97.3	7.3	--	--
		4	2200	79.3	4.1	--	--
	≈1500-2000°F Area	4	72	80.2	5.9	--	--
		3	2200	80.2	9.3	--	--
350 Hours Cyclic Exposure to 2200°F	In 2200°F Area	8	72	103.8	9.0	10.9	108.4
	≈1500-2000°F Area	8	72	91.2	13.0	7.4	96.9

All test bars tested in 4 point flexure with 1.5 inch outer span and 0.75 inner span.

Test bar cross sections were 0.250 by 0.125 inches. Cross lead speed was 0.02 inches/min.

for the 100- and 350-hour exposures. The 2200°F strengths for the 100-hour test increased to 80 ksi. These data indicate excellent stability for the Ford RM-2 material. However, visual inspection of the test bars suggested that the level of oxidation was not uniform over the length of the test bars (i.e., oxidation appeared greater in the lower temperature region of the bars between the area of burner impingement and the top of the cooled specimen holder). Typical bars after exposure are shown in Figure 40. The end to the right containing the specimen number was inserted into the holder during the durability exposure.

Room temperature strengths of the lower temperature regions of the test bars were only 80 ksi for the 100-hour exposure and 91 ksi for the 350-hour exposure, which were significantly lower than either the baseline material or that exposed to 2200°F. However, the 2200°F strength also was 80 ksi, which was comparable to the 2200°F exposed material and greater than that of the baseline material. In an effort to understand the differences, the fracture surfaces were examined by scanning electron microscopy (SEM). The results are illustrated in Figure 41. The material exposed to 2200°F had a thin oxide scale about 0.0006 inch thick. The material exposed to the lower temperature had a discolored region about 0.006 inch thick. This region was different from the typical surface oxide layer formed on Si_3N_4. There were no bubbles or signs of glass formation.

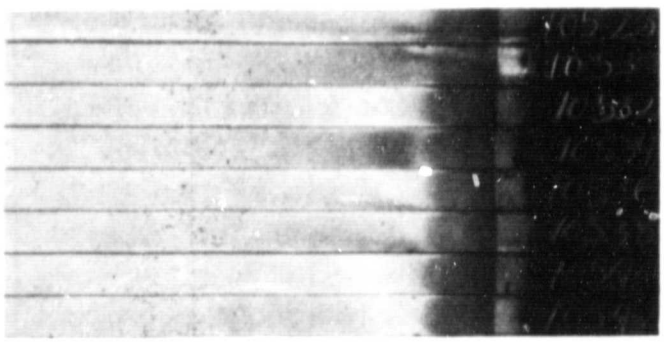

Figure 40. Ford RM-2 SRBSN After 350 Hours/2200°F Cyclic Durability Testing.

The original microstructure was still visible, but had a diffuse appearance when compared with the sharp microstructure in the specimen interior. These regions are compared at higher magnification in Figure 42. The fracture path in the surface layer appears to be more intragranular, which would account for the lower strength.

The oxidation behavior of this lot of RM-2 specimens is of concern. Effort to understand the nature and source of this behavior is continuing. The following section reports the results of a gradient furnace test conducted to determine the temperature range of the oxidation sensitivity. Stress rupture tests are in progress at the most sensitive temperatures and will be reported in the next semiannual progress report.

4.6.3 Gradient Furnace Testing of Rotor Materials

A gradient furnace test was conducted on ACC SNN-522 sintered Si_3N_4 and Ford RM-2 sintered reaction bonded Si_3N_4 to evaluate oxidation behavior over a broad temperature range. The gradient furnace consists of a refractory brick-lined box furnace with the heating elements arranged such that a controlled temperature gradient is present from the front of the furnace to the back. Figure 43 illustrates the test bar arrangement and temperature gradient for the 245-hour exposure that was conducted.

The graph in Figure 43 summarizes strength and oxidation results for the two materials. The SNN-522 developed a very thin oxide scale which had no adverse effect on strength. The strength of SNN-522 was controlled by material defects which were present in the material prior to oxidation exposure. Test data indicates that no anomalous oxidation behavior is occurring for this material.

The Ford RM-2 Si_3N_4 showed a variation in oxidation behavior as a function of temperature. Below 1400°F and above 2100°F the oxide layer was very thin. For intermediate temperatures the oxide layer was similar to that seen

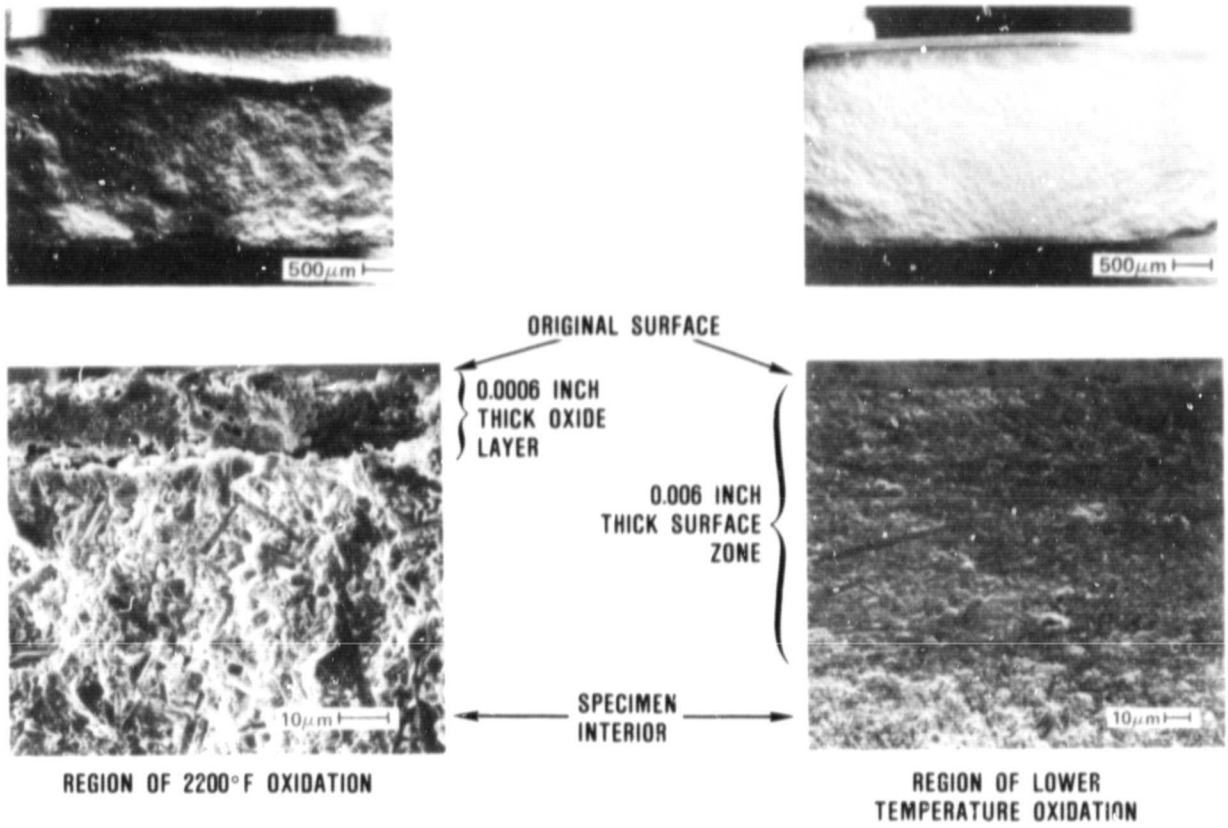

Figure 41. SEM Photomicrographs Showing Fracture Surfaces of 2200°F and Temperature Regions of RM-2 Bars Exposed 100 Hours in the Durability Rig.

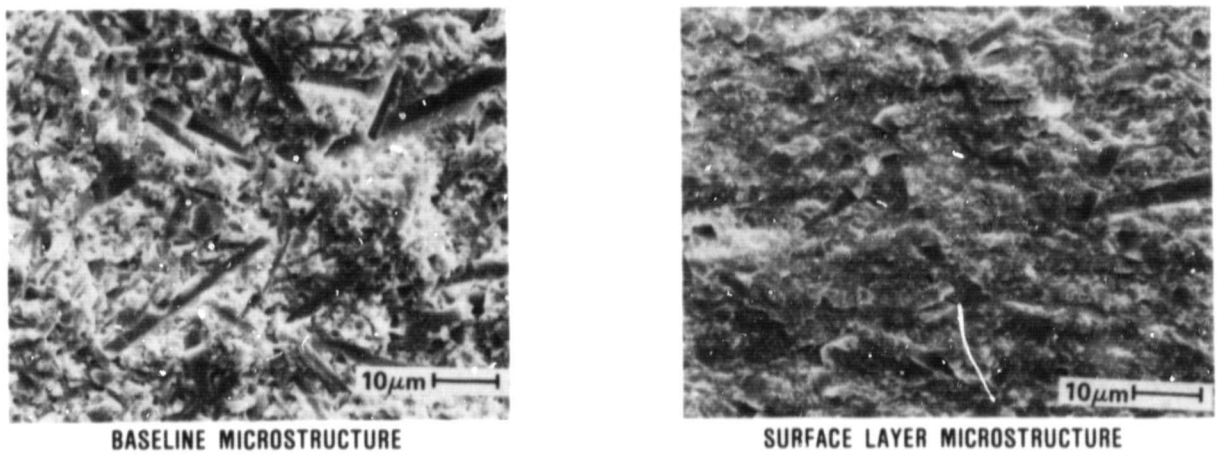

Figure 42. SEM Photomicrographs Showing Fracture Surface of Low Temperature Regions of RM-2 Bars Exposed 100 Hours in the Durability Rig.

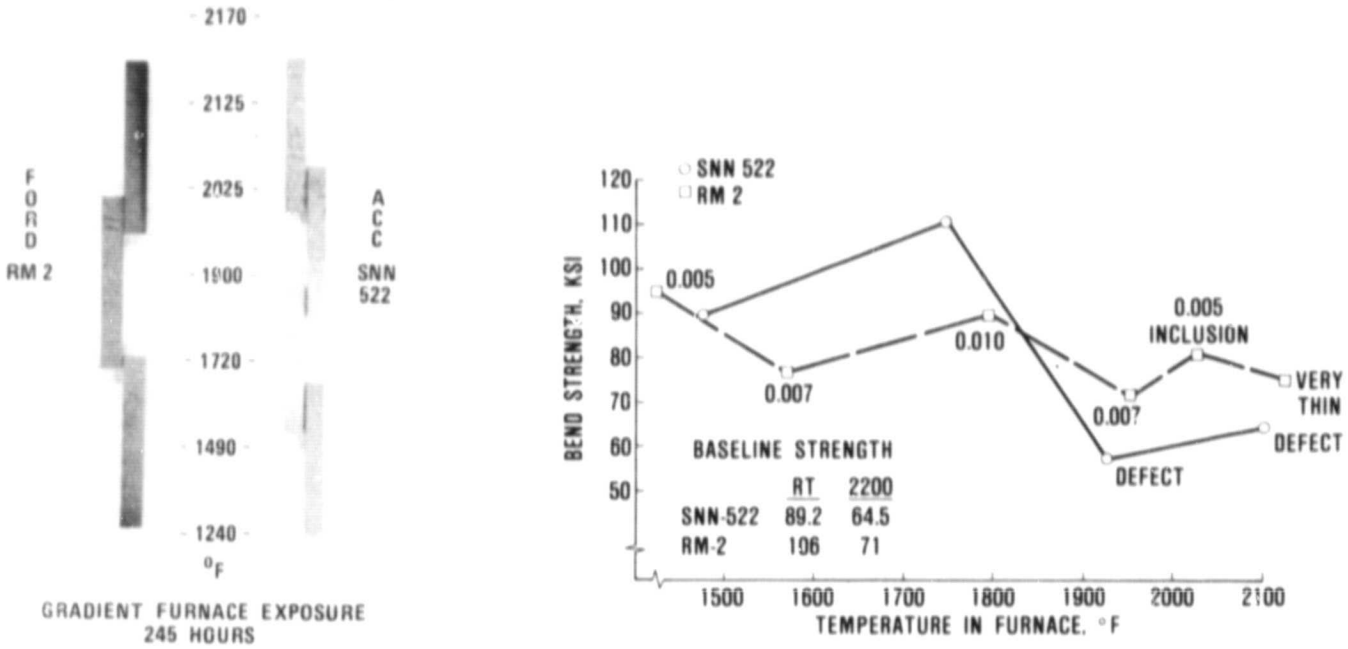

Figure 43. Gradient Furnace Test Results.

during the durability testing and ranged in thickness up to about 0.010 inch. The greatest thickness occurred at about 1800°F. The room temperature strength measured after exposure averaged about 80 ksi.

The RM-2 material has been reported by Ford to contain 8 percent Y_2O_3. Some prior hot-pressed Si_3N_4 materials containing a similar content of Y_2O_3 have very good stability at high temperature but severe degradation at intermediate temperatures (References 4 through 7). The cause was identified as oxidation of specific Si-Y-N-O compositions that were present on the grain boundaries. At high temperature, a SiO_2 layer was quickly formed on the material surface, protecting against oxidation of these grain boundary phases; however, at intermediate temperatures in the 1400 to 1800°F range, a protective SiO_2 surface layer did not have time to form before oxidation began along the grain boundaries. The unstable quaternary phase is reported to substantially increase in volume during oxidation, which would likely cause localized cracking and accelerate penetration.

Oxidation of the RM-2 material is much less severe than reported for these prior materials and may not even be due to the same mechanisms. For instance, intergranular fracture is expected if grain boundary degradation is occurring, but the fracture through the surface layer appears more intragrannular. Ford is conducting careful x-ray diffraction studies in an effort to identify the oxidation mechanism for RM-2. Ford and Garrett also are conducting stress rupture tests at 1800°F to determine if the oxidation will influence near-term use of the RM-2 material for rotor testing.

4.6.4 Stress Rupture Testing of Rotor Materials

Stress rupture (SR) testing of both Ford and ACC provided rotor materials is being performed to assure that these materials will meet the life requirements under the most severe stress conditions. Rotor analysis indicates that the most severe stress rupture conditions occur during steady state maximum power as tabulated in Table 11. This table indicates the

TABLE 11. POTENTIAL STRESS RUPTURE LIFE LIMITING CONDITIONS FOR THE AGT ROTOR

	Rotor Location	
	Blade	Hub
Maximum Stress Condition* (ksi at °F)	20 at 2000	27 at 2000
Maximum Temperature Condition* (ksi at °F)	5 at 2150	25 at 2050
S/R Testing: 2050°F at 30 ksi for hub and blades 2150°F at 5 ksi for blades		

*Steady state, maximum power

stress and temperature predictions at the maximum stress and maximum temperature conditions for both the blade area and hub region. The table also illustrates that SR testing at two temperature and stress states will satisfy all four conditions (i.e., testing at 2050°F and 30 ksi will define SR limits for the hub and blades and testing at or above 2150°F and 5 ksi will complete the SR limitations for the blades).

Initial testing under these conditions has been completed for both ACC SNN-522 and Ford RM-2 rotor materials and is summarized in Figures 44 and 45. The four-point flexure strength of specimens surviving the SR tests are included in these figures. Deformations due to creep are also noted.

All testing (SR and fast fracture) was performed in four-point flexure using a 1.5-inch outer span and a 0.75-inch inner span. All test bars were 0.250 x 0.125 inch in cross section. A cross head speed of 0.2 inch per minute was used.

Results for the Ford RM-2 material at both test conditions clearly indicate the adequacy of this material under these SR conditions.

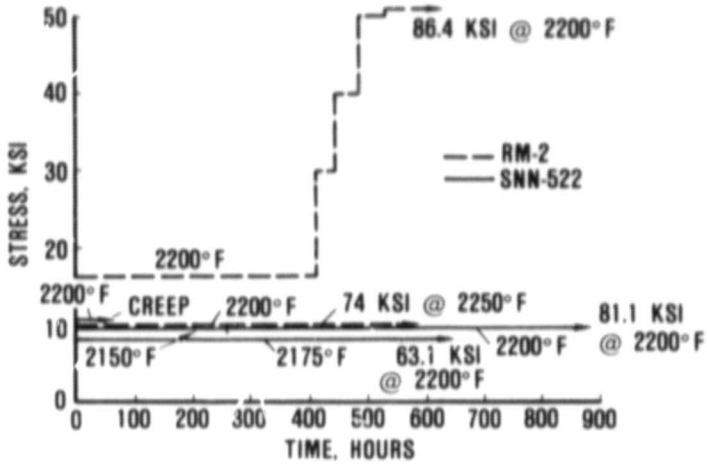

Figure 44. Stress Rupture Testing for Blade Life.

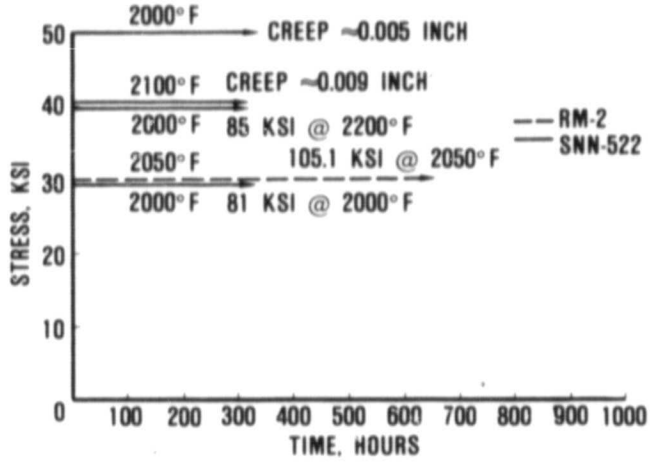

Figure 45. Stress Rupture Testing for Hub and Blade Life.

Results for the ACC SNN-522 indicate the adequacy of the material for rotor use and that creep occurs at conditions only slightly more severe than rotor conditions.

Additional testing is being performed to confirm these results and to evaluate these materials at intermediate temperatures.

4.6.5 Thermal Shock Testing of Stator Vanes

A torch thermal shock test was successfully used in prior programs (References 8 through

10) to screen design iterations and to qualify stator vanes for rig and engine testing. The Garrett thermal shock rig has been modified to evaluate the initial stator vanes received from ACC and Carborundum under the AGT program.

Figure 46 shows the time-temperature curves estimated by analysis for the AGT101 stator vanes under a normal engine start and a worst-case engine start. The top curve in each graph is the most severe and represents the center of the trailing edge. The objective of the experimental effort was to duplicate the worst-case trailing edge heating curve for RBSN and sintered α-SiC vanes with the Garrett thermal shock test rig.

The general thermal shock test arrangement. It consists of two castable alumina stator vane holders (each designed to hold three stator vanes), one or more oxyacetylene torches, two airblast cooling tubes, a timer-actuated slide table and a small-focal-spot infrared pyrometer*. The following procedure is used during a typical test:

1) The vane holder with three sample vanes is positioned on the slide table with an oxyacetylene torch aimed tangentially on each side of the center vane.

2) The pyrometer is focused on a 1/4-inch diameter region at the center of the trailing edge of the center vane in the 3-vane fixture.

3) The slide table is actuated so that the vane is not is the path of the torches.

4) The torches are lit and adjusted.

*Ircon Series 300L Infrared Radiation Thermometer.

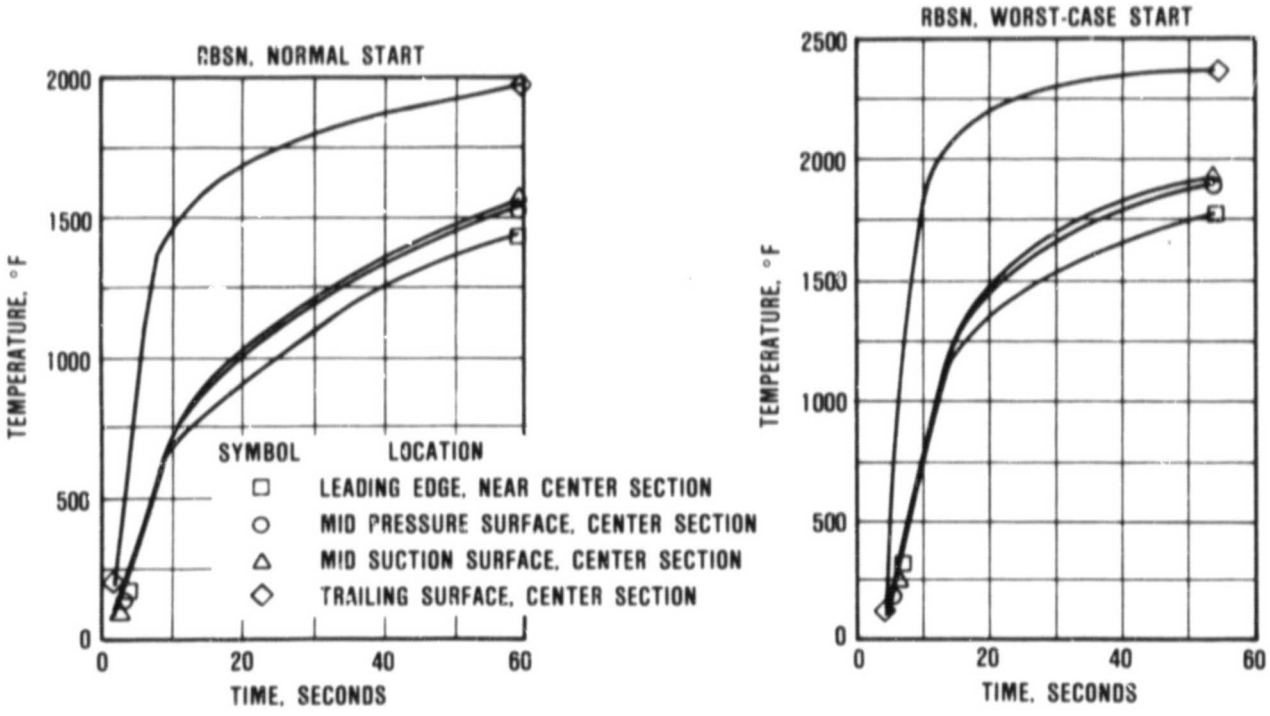

Figure 46. Transient Temperature Response for RBSN for a Normal and a Worst-Case Engine Start.

5) The slide table is actuated so the vane is returned to the path of the torches and pyrometer.

6) The temperature output of the pyrometer is recorded as a function of time.

7) The test is repeated and the torches readjusted as required until a temperature response curve comparable to the condition-selected for Figure 46 is achieved.

8) The sample vanes are then replaced with test vanes and cyclic thermal shock test conducted, recording the thermal reponse each time to assure that the test conditions have not changed.

A number of iterations were required to identify the setup and torch conditions that simulate the analytically-predicted thermal response of the stator vane trailing edge in the engine. Initial attempts with one torch did not produce a realistic temperature profile on the vane or an acceptable thermal response curve. The use of two torches yielded the response curves shown in Figure 47. Cycle A was defined to simulate the worst-case start, and Cycle B the normal start.

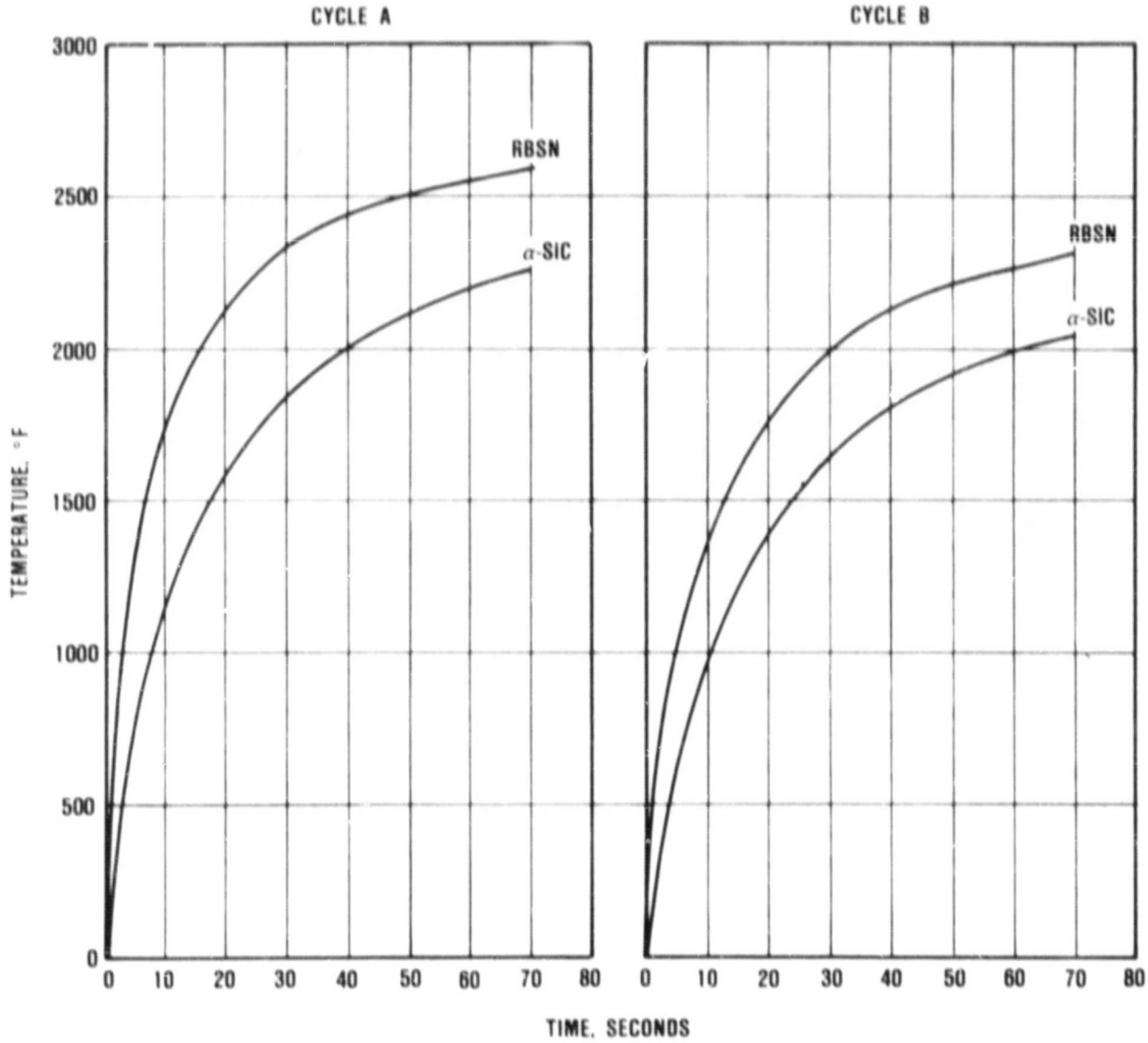

Figure 47. Transient Temperature Response for ACC RBSN and Carborundum SA Stator Vanes, Worst-Case and Normal Start Conditions.

Table 12 compares the temperature-time response of Cycles A and B with predicted response in the engine. The slope of the Cycle A curve appears to be lower than that of the worst-case start-up to 20 seconds, but is higher from 30 to 60 seconds. However, the temperatures recorded by the pyrometer represent an average over the 1/4-inch area, whereas the analytical prediction is essentially for the peak temperature right at the center of the trailing edge. Therefore, the peak temperature during the thermal shock test likely is higher than recorded by the pyrometer, and Cycle A is probably more severe than the worst-case start. Similar reasoning can be applied to Cycle B to show that it is equivalent to or slightly more severe than the predicted normal start transient.

The thermal response for both RBSN (ACC RBN 124) and α-SiC (Carborundum SA) are shown in Figure 47. In every test the α-SiC heated up more slowly and uniformly than the RBSN and reached a lower steady-state temperature. This is probably due to the higher thermal conductivity of the α-SiC.

Initial thermal shock testing has been conducted on reject vanes from ACC and Carborundum. The ACC vanes were rejected due to voids in the leading edge; the Carborundum vanes were rejected due to dimensional problems. All of these vanes were from the first batches made by ACC and Carborundum and were tested in the as-sintered condition with no final machining. The objective was to identify potential design or material deficiencies as early as possible.

Figure 48 shows RBSN stator vanes in the test rig and after testing. Some vanes survived both Cycles A and B, indicating that the design and material properties for the AGT101 engine are acceptable. Other vanes failed at processing defects, some at the large voids that had been detected by radiography and some at the mold line at the radius between the trailing edge and the platform. The mold line failure mechanism requires more study to determine if subsurface material defects are responsible or if it is just a geometrical stress concentration effect. The latter would be easily resolved by the hand finish final machining operation, which will occur for engine test stator vanes. The former would require processing improvement and possibly injection molding tool modification.

Figure 49 shows Carborundum α-SiC vanes in the thermal shock rig and after testing. For illustrative purposes, the top of the specimen holder has been removed and only one torch is

TABLE 12. COMPARISON OF THERMAL RESPONSE FOR THERMAL SHOCK CYCLES A AND B WITH ANALYTICAL PREDICTIONS FOR AGT101 STATOR ENGINE TRANSIENTS

Thermal Conditions	Temperature/Time Response				
	10 sec	20 sec	30 sec	45 sec	60 sec
Analysis for Normal start	1500	1670	1800	1900	2000
Thermal Shock Rig Cycle B	1350	1770	2000	2170	2260
Analysis for Worst-Case Start	1860	2240	2300	2330	2360
Thermal Shock Rig Cycle A	1800	2150	2340	2480	2550

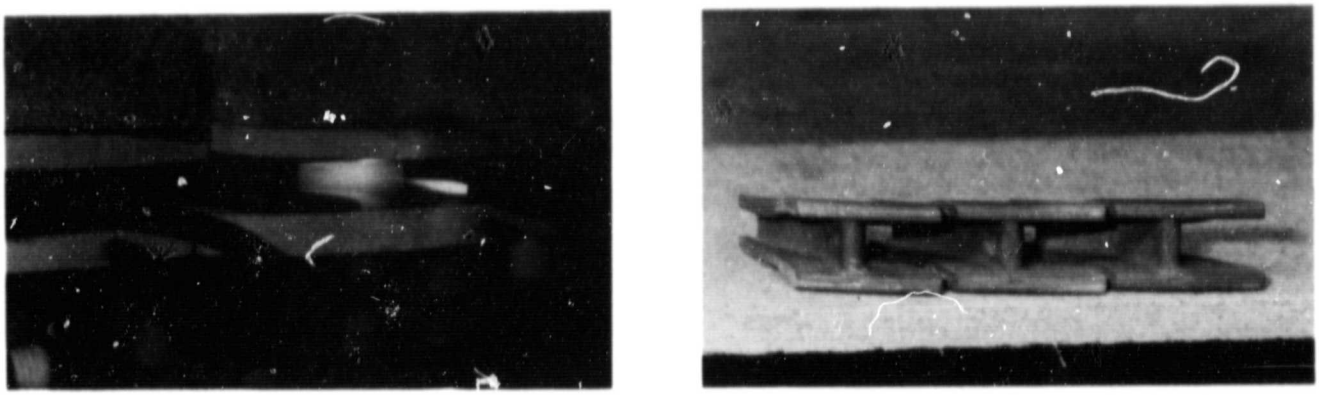

Figure 48. ACC RBSN Stator Vanes in the Thermal Shock Test Rig (Left) and After Testing (Right).

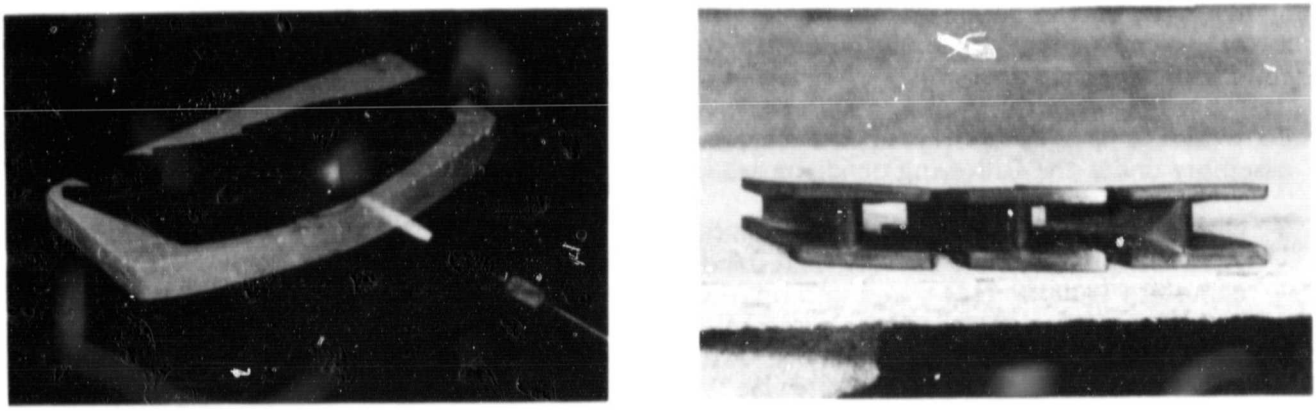

Figure 49. Carborundum α-SiC Stator Vanes in the Thermal Shock Test Rig (Left) and After Testing (Right).

in place. The results with α-SiC were similar to those for RBSN. Some vanes survived both Cycles A and B, indicating that the design and material properties are acceptable for the AGT101 engine. As was the case for RBSN, some SiC vanes fractured at the trailing edge mold line at the radius between the trailing edge and platform. This is being further investigated and is not expected to be a difficult problem to resolve.

4.7 Ceramic Structures - Component Development

Efforts during this reporting period concentrated on continuance of thermal screening rig fabrication, structures rig fabrication, and additional mechanical screening tests on selected components.

4.7.1 Thermal Screening Test Rigs

Two thermal screening test rigs were designed and fabrication initiated. These rigs were designed to simulate transient temperature conditions as a result of engine start up and were based on stress analyses wherein peak stresses occur during this first 2 to 3 minutes after engine light-off. The test rigs, shown in Figures 50 and 51, are low pressure rigs intended to subject the ceramic parts to combustor discharge temperatures up to 2100°F for short periods of time.

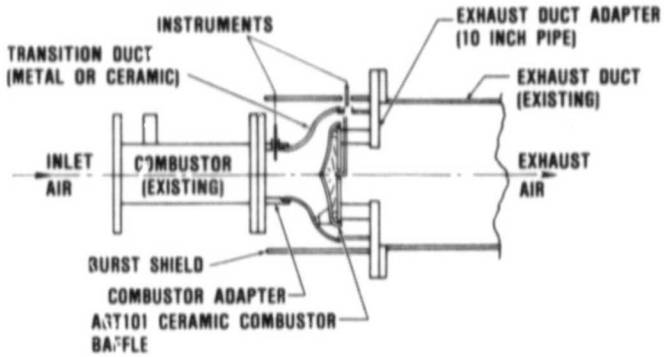

Figure 50. AGT101 Ceramic Combustor Baffle/Transition Duct Thermal Screening Rig.

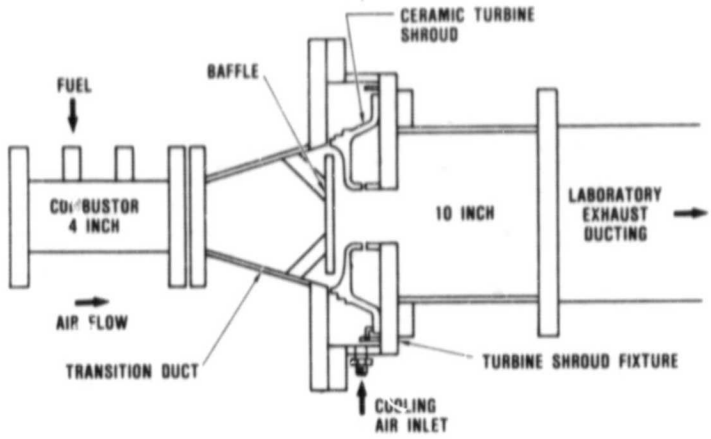

Figure 51. AGT101 Turbine Shroud Thermal Screening Rig.

4.7.2 Ceramic Structures Rig

The ceramic structures rig is a high temperature test bed for the complete set of ceramic structural components. The purposes of the ceramic structures rig are:

a) To evaluate the durability of the ceramic assembly under the following conditions:

   - o Normal engine start conditions for the AGT101 Mod I (1600°F TIT) and Mod I complete (2000°F TIT)
   - o Steady state engine conditions for Mod I and Mod I complete at idle and cruise

b) To evaluate ceramic interface compatibility under Mod I and Mod II conditions at idle and cruise.

c) To evaluate the ceramic turbine shroud support/alignment system under Mod I and Mod I complete start, cruise, and idle conditions.

d) To demonstrate the ceramic assembly durability for ten normal start cycles for the AGT Mod I and Mod I complete conditions.

The ceramic structures rig is shown on Figure 52. This rig has separate hot (LP) and cold (HP) airflow paths featuring ceramic engine components. The rig also incorporates a rotating ceramic regenerator and static deswirl (in place of the turbine rotor).

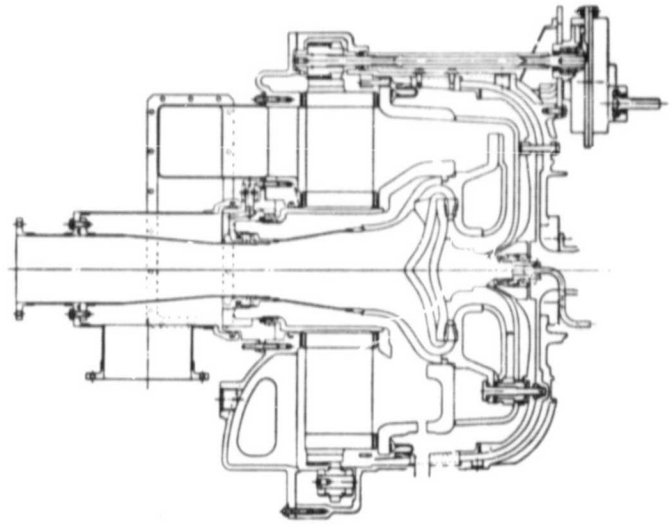

Figure 52. 2000°F Structures Rig.

Air, as hot as 2000°F, enters the structures rig through the spring duct, and then diffuses through the ceramic transition duct; thus heating the combustor baffle, turbine shroud, piston rings, segmented turbine stators, turbine backshroud, inner and outer turbine diffusers, and LP side of the flow separator housing. The air then passes through the regenerator.

The cold, HP air enters the rig at temperatures up to 200°F, flows along the compressor backshroud and compressor housing, turns in the exhaust cover, and is heated through the regenerator. The air then flows over the HP

side of the flow separator housing, around the transition duct, through the regenerator shield, and out of the rig.

One unique feature of the ceramic structures rig is the turbine shroud support/alignment system. This design, shown in Figure 53, features an eccentric sleeve for shroud alignment and a system of crowned spacers and washers. The advantage of this design lies in the ability to allow relative growth of the turbine shroud with respect to the compressor backshroud while maintaining alignment of the turbine shroud and allowing only rolling contact between interfaces.

4.8 Rotor Dynamics

Testing continued on the rotor dynamics test rig, Figure 54. Effort during this reporting period concentrated on developing the following components and parameters:

- Rotating components and group balance requirements
- Rotating assembly interfaces, pilots and curvics
- Rotating assembly tie rod and shaft stretch
- High speed pinion gear
- High speed pinion/thrust bearing
- Pinion/thrust bearing hydraulic mount geometry

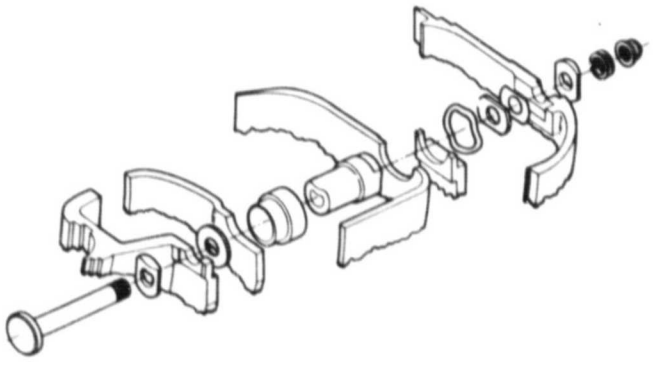

Figure 53. AGT101 Turbine Shroud Support/Alignment System.

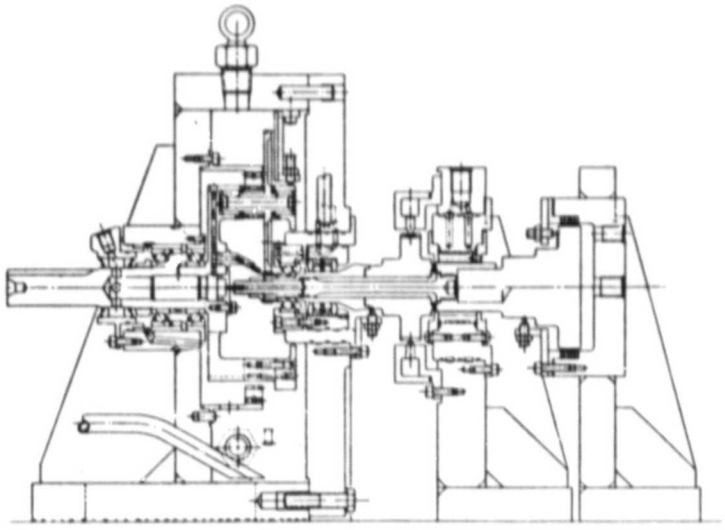

Figure 54. Rotor Dynamics Test Rig.

- Compressor ring seal (dual carbon element) clearance
- Foil bearing, backing springs, and carrier

The rotor dynamics test program experimentally developed a satisfactory Mod I rotating assembly. The following paragraphs discuss this development. Table 13 presents a summary of the development testing.

4.8.1 Rotating Group Assembly

Small, closely toleranced, lightweight, high-speed components comprise the rotating assembly. In order to achieve smooth operation, normal balancing techniques were deemed inadequate for the AGT. Garrett balance technicians utilized an updated force balance procedure wherein the unbalance force and vector were determined for each rotating component. Then, during group assembly, the amount of unbalance and vector were systematically opposed for adjacent components such that the resulting group unbalance was repeatable and within blueprint requirements.

Runout checks, as shown in Figure 55, were taken before and after each build to develop a history and to establish guidelines for power section assembly. During rotating group assembly, close attention was paid to component

TABLE 13. SUMMARY OF SELECTED COMPONENTS AND PARAMETERS

Item	Configuration or Parameter	Comments
Gearbox Planetary Gear Train	o Fixed carrier o Rotating ring gear o Tapered roller bearings, output shaft o Assembly P/N 3609246-1	o Lowest subsynchronous on-rotating assembly
Foil Bearings, Springs, and Carrier	o 6 mil foils o Material - CRES302/spring temper o Teflon S coating (1 mil) o Spring P/N 3608014-4 o 10 mil sway space o Foil P/N 3608103-3 and carrier P/N 3826212-1	o MOD I configuration only o Coated Inco 750X foils for Mod I complete
High Speed Pinion	o P/N 3822083-1 o Per assembly P/N 3801035-1	o Detail design and installation acceptable
Thrust Bearing	o P/N 3822082-2 o Suppliers - Split ball - FAG - Barden	o Mechanical integrity acceptable for all suppliers o Drawing revision recommended to improve dimensional control of length of flat on OD
Hydraulic Mount and Supply Pressure	o P/N PAP 253310-1 or PAP 253467-6 o Diametral clearance - 4.7 mils o Length of land, 0.330 to 0.355 inch (Dim L) o 0.030 inch diameter (Nom) drain o 3 each, 0.124 to 0.129 inch diameter supply passages o Mount supply pressure 55-65 psig	o Either configuration acceptable for operation to 100,000 rpm
Compressor Ring Seal	o P/N 3826200-1 o Diametral clearance with Compressor Shaft P/N 3822085-2 of 1.3 to 1.5 mils	o Diametral clearance of 1.4 to 1.6 mils provides less carbon wear
Ring Seal Buffer Pressure	o 25 PSIG	
Lubrication System	o Gearbox Lubrication for P/N 3609246-1 o Inner Race Lubrication of Thrust Bearing	
Rotating Assembly Interfaces - Pilots - Curvics	o See Assembly P/N 3801035-1 - Turbine Rotor P/N 3842044-4 - Compressor Rotor P/N 3608335-2 - Compressor Shaft P/N 3822085-2 - Tie Rod P/N 3842039-6	o All interfaces acceptable
Tie Rod	o P/N 3842039-4 or -6 o Load 5000 pounds with Compressor Rotor P/N 3822086-1 (Aluminum) o Load 7000 pounds with Compressor Rotor P/N 3608335-2 (Titanium)	o Five confirmed cases -1 and -2 tie rod (0.260 to 0.265 inch diameter) runnout increased from 0.0005 inch maximum allowed to 0.0015 to 0.0035 inch o Two -4 or -6 tie rods (0.308 to 0.313 inch diameter) no problem

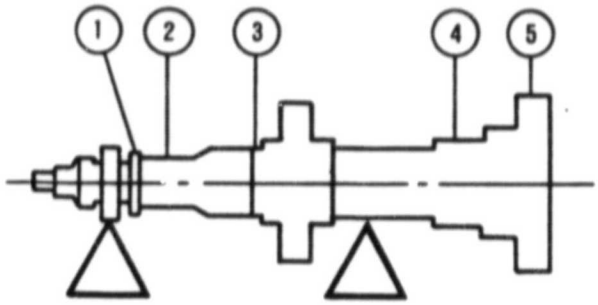

STATION	RUNOUT, INCHES	
	MEASURED	LIMIT
1	0.00015	0.0002
2	0.00005	0.0003
3	0.00015	0.0006
4	0.00025	0.0006
5	0.0004	0.001

Figure 55. AGT101 Rotor Dynamics Runout Check.

interfaces, pilots, and curvic coupling cleanliness. Tiebolt stretch was verified and later varied during different builds to ascertain the influence of coupling force on the rotating group. As noted in Table 12, a tie rod diameter of 0.260 to 0.265 inch yielded unacceptable runouts whereas the 0.308 to 0.313 inch diameter tie rod was acceptable.

4.8.2 Hydraulic Mount

The stiffness characteristics of the thrust bearing hydraulic mount greatly influences the critical speed response of the rotating group. If stiffness values for the mount increase, the first, second, and third critical speed mode shapes change and occur at higher rpm or excitation frequencies. Conversely, as stiffness decreases, critical speeds are reduced with the potential of the third mode (bending) occurring within the engine operating range.

Considerable time and effort were devoted to thrust bearing hydraulic mount optimization as shown in Table 14. Numerous variations of diametral clearance and mount land length were evaluated. These efforts were required to determine the mount stiffness and damping characteristics and asociated effect on rotor dynamics.

Variations in the diametral clearance and land length affect stiffness and damping as related by the following equations:

$$\text{Stiffness} = K = 2\mu\omega(L/C)^3 \, \epsilon/(1-\epsilon 2)^2$$

and

$$\text{Damping} = \pi\mu R/2 \, (L/C)^3 \, 1/(1-\epsilon 2)^{1.5}$$

where:

L = Length of mount (inch)
C = Radial clearance (inch)
ϵ = Eccentricity ratio
ω = Speed (rpm)
μ = Viscosity
R = Radius (inch)

4.8.3 Dynamic Behavior

As stated in Reference 1, the calculated critical speeds for the AGT101 are 5,850, 38,260 and 135,200 rpm for the first three modes of excitation. Figure 56, graphically displays the critical speed responses as a function of ball bearing stiffness. Note the relative changes in critical speed response as stiffness increases. Since numerous test runs have been accomplished with differing bearing mount configurations, two representative examples have been chosen to show the effects of mount configuration.

Figure 57 represents the typical rotor dynamics for a "tight" mount and Figure 58 shows the characteristics of a satisfactory configuration. In both cases, the gearbox was coupled to the rotating group.

During development testing, a 0.001-inch peak-to-peak amplitude was established as an upper limit for initial testing. This limit was specifically chosen to assure safe, stable operation during engine testing.

TABLE 14. HARDWARE CONFIGURATIONS TESTED (HYDRAULIC MOUNTS)

P/N	Diametral Clearance (MILs)	Land Length	0.030 Inch Diameter Drain Hole
3608291-3	8	0.410	Yes
PAP225376-3	8	0.375	No
PAP225376-2	7	0.375	No
	7	0.375	Yes
PAP225376-1	6	0.375	Yes
PAP253467-8	5.1(1)	0.355	Yes
PAP253467-5	5.1	0.250	No
PAP253467-5	5.1	0.250	Yes
3608291-1	4.7	0.375	Yes
PAP253467-6	4.7(1)	0.355	Yes
PAP253310-1	4.7(1)	0.330	Yes
PAP253467-3	4.7	0.250	No
PAP253467-3	4.7(1)	0.250	Yes
PAP253467-4	4.7	0.150	No
PAP253467-7	4.1	0.355	Yes
Unknown	2.8	0.375	Yes
PAP253467-1	2.8	0.250	No
PAP253467-2	2.8	0.150	No
PAP253467-2	2.8	0.150	Yes
PAP225376-3	3.8 (8 MIL mount with shims)(2)	0.375	No
PAP225376-2	2.8 (7 MIL + shims)(2)	0.375	No
PAP225376-1	1.8 (6 MIL + shims)(2)	0.375	No

(1) Tested with one, then three oil passages to the mount

(2) Shim 0.0021-inch thick

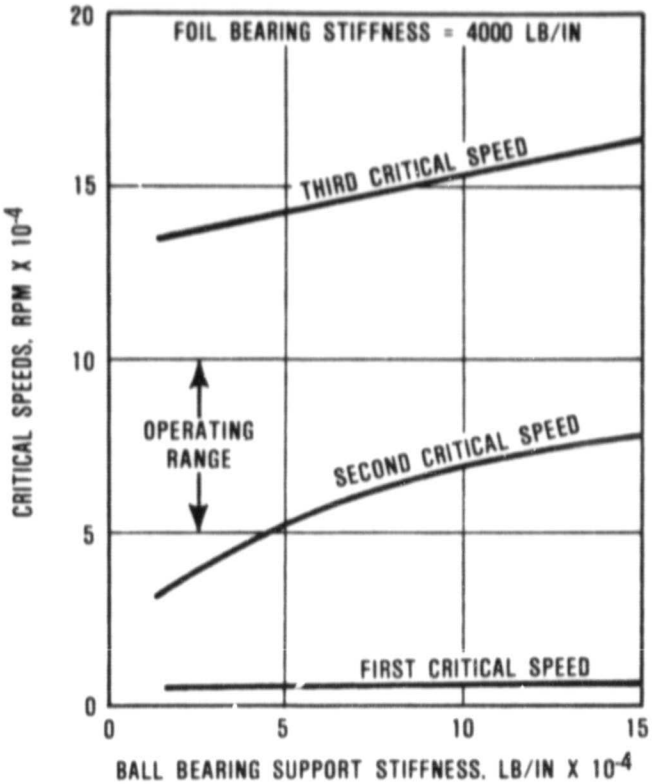

Figure 56. AGT Engine Critical Speeds Versus Ball Bearing Stiffness.

As shown in Figure 57, dynamic behavior of the rotating group is excited at the turbine end by subsynchronous excitaton from the gearbox, while excitation at the forward bearing (hydraulic mount) is entirely synchronous. Note the rapid climb in excitation near the 70,000 rpm speed. This corresponds very closely to the analytically predicted second critical with a ball bearing stiffness of 90,000 lbs/inch (Figure 56).

Dynamic behavior of the rotating group with the selected mount geometry is depicted in Figure 58. Testing indicates that acceptable behavior is achieved by allowing the ball bearing end of the rotor to displace with the subsynchronous excitation from the gearbox. When this condition is allowed to occur, the subsynchronous response at the turbine end is minimized. Further, the "softer" mount lowers the second critical as compared with the stiffer mount configuration (Figure 56).

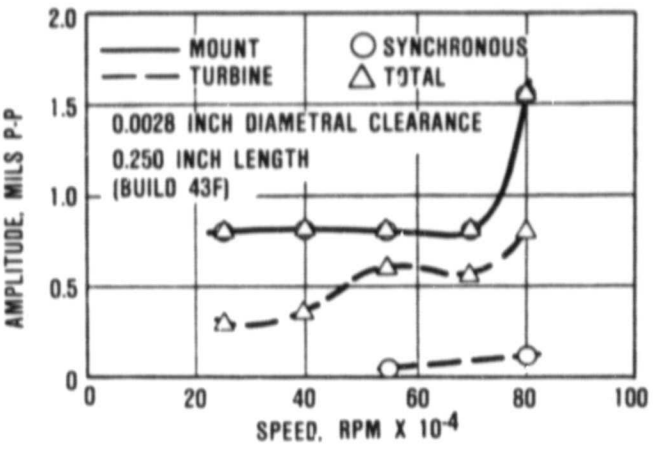

Figure 57. Dynamic Behavior with "Tight" or "Pinched" Hydraulic Mount.

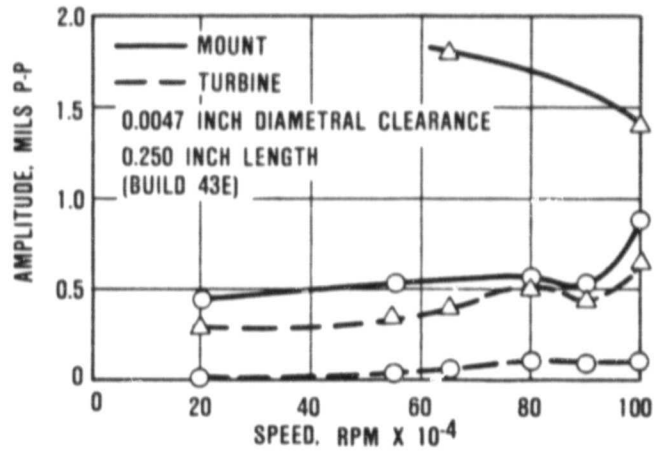

Figure 58. Dynamic Behavior with Satisfactory Hydraulic Mount.

Numerous runs have now been achieved both with and without the gearbox coupled and smooth, stable, repeatable operation has been achieved to full speed. The geometries and assembly procedures developed as a result of tests have been incorporated in the engine. Testing is now transitioning to hot foil bearing testing.

4.9 AGT101 Controls

This reporting period ended with the successful integration and engine test of most elements of the control system hardware. The electronic control unit (ECU) was the sole major component remaining to be added to the engine test setup. All known controls problems have been resolved, and all required hardware was on hand for the regenerator seal break-in and the first series of engine runs.

To conserve resources for resolution of problems during engine development, all nonessential controls work was completed or deferred, with the intent to concentrate whatever time and effort might be required for engine test support.

4.9.1 Systems Integration and Analysis

The AGT101 transient computer model was adapted and finalized to the present Mod I engine configuration. Control system development, evaluation, and fine tuning were accomplished based on that model, and results of this analysis effort were incorporated in the ECU digital control software. Detailed verification and checkout of all areas of ECU operation were completed.

4.9.2 Fuel System

Assembly of the pilot combustor control was completed. Preliminary testing indicated that required drive current for the electrically driven pumping unit was much higher than expected. However, further investigation was deferred to conserve resources, and the pilot combustor control hardware was consolidated, boxed up, and stored until a liquid-fueled pilot combustor controller is required for engine development.

A complete mockup of the engine fuel control system was assembled, checked out, calibrated, and evaluated prior to installation on the engine. This system included the dc fuel boost pump, inlet filter, dc motor driven high pressure fluid power design piston pump, Servotronics metering valve, pressurizing valve, high pressure relief valve, control solenoids, and all related fuel and air assist tubing.

A final verification of the fuel system mockup was accomplished via installation in the combustion test cell and operation with the Mod I atomizer and combustor. Interfacing, operation, and performance were successfully accomplished. A significant result of this test was the confirmation that the 180 cycle per second fuel pulsation frequency, out of the RPD piston pump, did not cause any detectable combustor instability.

The prototype fuel control system was installed and operated on the engine during regenerator seal break-in and engine testing.

A test of pulse width modulated (PWM) control of the fuel metering valve also was completed at the end of the reporting period. Repeatability, hysteresis, and linearity were all observed to be improved over the existing proportional fuel control signal. Frequency response testing also showed some improvements in the critical low flow area. These results indicate that an engine test of PWM control should be accomplished to provide additional data on which to decide whether to convert to PWM.

4.9.3 Electrical Accessories

The high temperature Platnell thermocouples were received, and calibration runs on four of them were performed in the Standards Laboratory. Points at 800, 1300, 1700, and 2000°F were checked, and calibration curves were prepared.

A speed sensor test rig was fabricated and used for evaluation of the eddy current speed sensors and for fine tuning the electronic speed signal conditioning circuitry. Problems with signal attenuation, due to long wire length from the sensor to the electronics, were resolved by conditioning the signal at the engine and transmitting the conditioned signal to the ECU.

4.9.4 Electronic Control Unit

Fabrication, programming, and final checkout of the first two ECUs was completed, including modifications to the speed signal conditioning circuitry dictated by the results of the speed sensor rig testing.

Working documentation of the control software also was completed.

Areas of additional work to be accomplished on the ECU (which are not required prior to integration with the engine) include development of:

- Control software to handle turbine inlet and combustor flame temperature calculations
- Improved fault enunciation capabilities
- Improved diagnostic hardware and software

APPENDIX A

FORD MOTOR COMPANY
ADVANCED GAS TURBINE (AGT) POWERTRAIN SYSTEM DEVELOPMENT PROGRAM
FOURTH AGT SEMIANNUAL TECHNICAL PROGRESS REPORT

1. TASK 2.3 - CERAMIC ROTOR - FORD

1.1 Material Development and Characterization

In References 2 and 3, data has been presented on the first generation Sintered Reaction Bonded Si_3N_4 (SRBSN) material, designated RM-1. The initial strength and 1832°F oxidation behavior of this material appeared suitable for rotors, however subsequent testing revealed two problems. (1) The billet-to-billet, run-to-run variation in strength was excessive. Characteristic strengths varied from a low of 74 ksi to a high of 107 ksi. (2) A more serious problem was the 1292°F oxidation behavior, where strength reductions of up to 89 percent were experienced after 700 hours of exposure.

This behavior led to further development which resulted in a second generation SRBSN material called RM-2. This material contains 8 percent Y_2O_3, as did RM-1; however, process improvements have resulted in improved properties.

The properties of RM-2 SRBSN are shown in Table 15. The data summarizes the extensive characterization work conducted at Ford during the course of this development program. Material characterization, which is continuing, proved to be extremely useful in developing an understanding of the SRBSN process and the effect of process changes.

The density of RM-2 ranged from 3.26 g/cm^3 (98 percent TD) to 3.33 g/cm^3 (99.9 percent TD). The strength was measured at both room temperature and 2192°F. The room temperature strength data shown in Table 14 is a compilation of 60 samples machined from 10 billets, resulting from 6 sintering runs. The characteristic strength of 107.6 ksi and the Weibull modulus value of 21.1 therefore represents the run-to-run, billet-to-billet variations normally expected.

The microstructure of RM-2 is shown in SEM fracture surface micrographs (Figure 59). The structure is composed of interlocking elongated needle shaped grains of β-Si_3N_4. The fracture surfaces exhibit both transgranular and intergranular fractures. Some grains fractured transgranularly with one half of the grain being pulled from the matrix, leaving behind an indentation in the matrix. This type of fracture behavior should indicate a material with a high fracture toughness.

The 2192°F strength data was generated from 10 samples machined from 1 billet. The 91.7 ksi value, which is 85.3 percent of the room temperature value, corresponds to the strength of an 8-percent Y_2O_3/Si_3N_4 composition at 2192°F obtained during previous work (Reference 2).

Preliminary MOR strength tests were conducted at varying strain rates at 2192°F to investigate the possibility of slow crack growth occurring in this material. The results indicated no strain rate dependence implying that slow crack growth is not a problem, at least at 2192°F. This work will be extended to confirm these preliminary results.

The thermal expansion coefficients (1.78 to 1.94 x 10^{-6}/°F) are slightly higher than encountered in reaction bonded or hot-pressed Si_3N_4(MgO doped), due to the effect of the Y_2O_3 addition.

The oxidation behavior of RM-2 was studied over the temperature range of 1292 to 2552°F. Figure 60 shows the average weight gain for exposures in a static air atmosphere. The data

TABLE 15. PROPERTIES OF RM-2 SRBSN

COMPOSITION	8-percent Y_2O_3/Si_3N_4		
DENSITY	3.26 to 3.33 g/cm^3 (98 to 99.9 percent TD)		
STRENGTH	Char NOD MOR	"m"	N
Room Temperature	107.6 ksi	21.1	60
2192°F	91.7 ksi	15.4	60

THERMAL EXPANSION COEFFICIENTS

1472°F	1.78×10^{-6}/°F
1832°F	1.83×10^{-6}/°F
2192°F	1.94×10^{-6}/°F

STRENGTH CHANGE AFTER STATIC OXIDATION

Temperature	Exposure Time, hours	Strength Change, Percent
1292°F	300	+3.6
	700	0
1832°F	300	-11.7
	700	-14.8
2192°F	300	-6.7
2552°F	300	-7.9

STEP-STRESS RUPTURE

Temperature	Stress, ksi	Time, hours	
2192°F	65.2	310	
	73.4	24	
	81.6	24	
	89.7	4	NO FAILURE

THERMAL SHOCK RESISTANCE

Temperature	Cycles	Strength Change, Percent
1832°F	100	-8.3
	1000	-6.8
2192°F	100	-2.0
	1000	+7.9

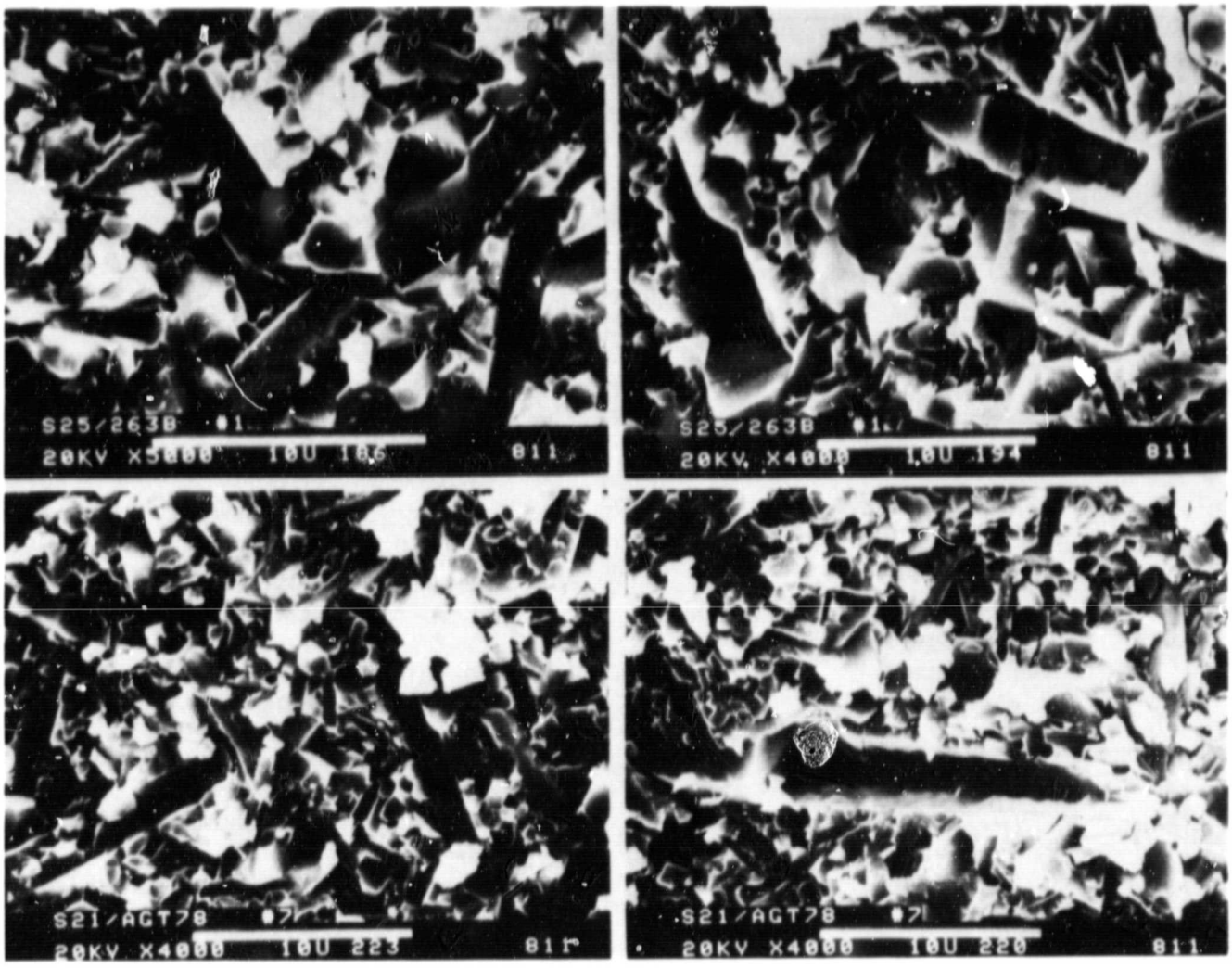

Figure 59. Microstructure of RM-2 SRBSN.

shows low weight gains for 1292, 2192 and 2552°F exposures but a higher weight gain for the 1832°F exposure. This is characteristic of Y_2O_3 doped Si_3N_4, but after about 100 hours of exposure, the material stops gaining weight indicating any oxidation reactions have reached equilibrium.

However, the final test of a material should not be its weight gain behavior alone, but should include strength data as a function of exposure time. This data has been generated for RM-2 and is summarized in Table 15 as percent strength change after 300 and 700 hours exposure at temperature. This data is plotted in Figure 61 in terms of absolute strength. One observes that the strength loss after the 1832°F exposure is greater than at other temperatures. However the 700-hour strength is only slightly lower than the 300-hour strength, indicating that the degradation mechanism has stabilized as did the weight gain. The strength level after 700 hours at 1832°F is still 92 ksi, which should provide a safe strength margin for the AGT rotor.

The stress rupture characteristics were evaluated, in a preliminary manner, using a step

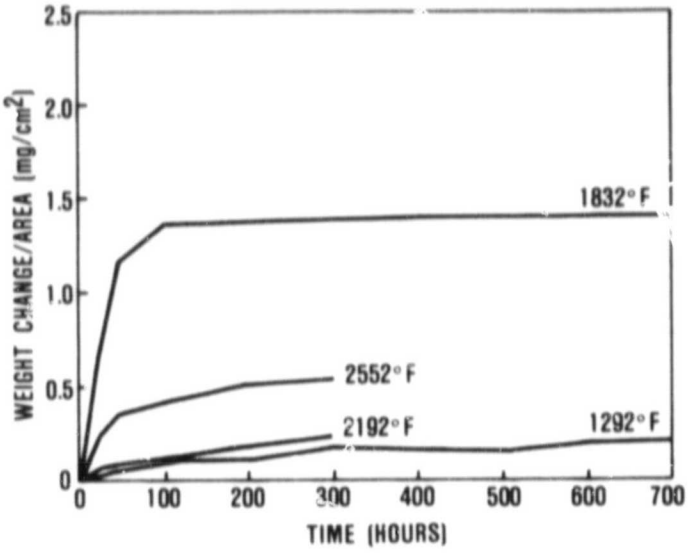

Figure 60. Oxidation Weight Gain of RM-2 Versus Time at Several Test Temperatures.

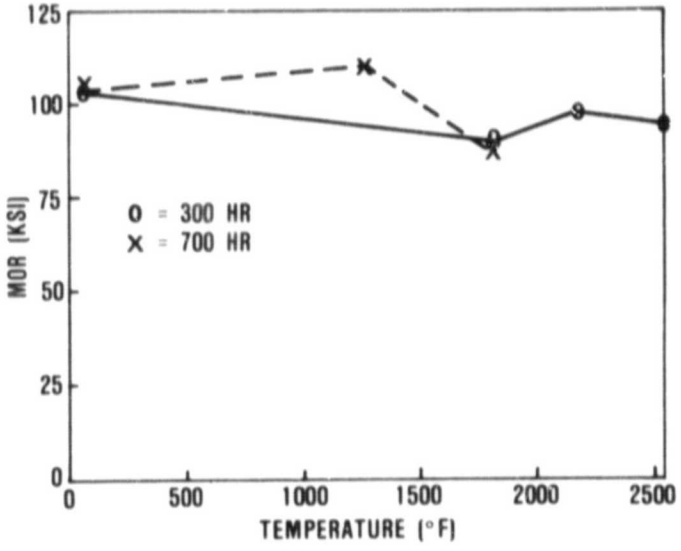

Figure 61. Strength of RM-2 SRBSN After Oxidation.

stress test at 2192°F. The data is summarized in Table 15 and plotted in Figure 62. The RM-2 material was loaded to stresses between 65 and 89.7 ksi for 362 hours. The sample was

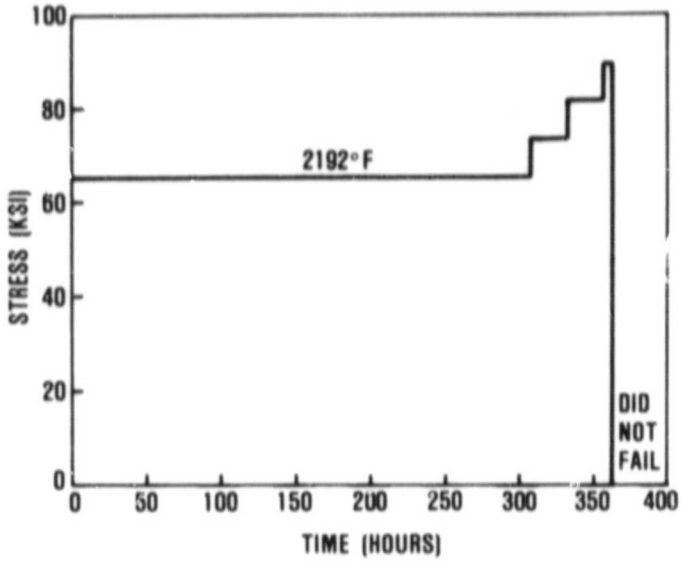

Figure 62. Step-Stress Rupture Test of RM-2 SRBSN at 2192°F.

unloaded without failure. This test indicates that the material strength at this temperature is stable for long times and does not appear to exhibit a time dependent fracture behavior (i.e. slow crack growth). Further work is planned to better define the stress rupture characteristics of RM-2.

RM-2 also was tested to determine its thermal shock resistance using Ford's Thermal Shock Test Rig. This rig provides automated and rapid cyclic heating and cooling of MOR test bars. The bars are heated using an oxy-gas flame and cooled by compressed air jets. The heating curves as measured by an optical pyrometer are shown in Figure 63. The cooling rates were estimated to be at least 248°F/second. Samples were run for 100 and 1000 cycles at both 1832 and 2192°F part temperature. The strength change data is summarized in Table 15 and shows no serious degradation due to thermal cycling.

This characterization work performed thus far on RM-2 indicates that it is a strong material, capable of withstanding long exposures at a variety of temperatures with little effect on properties. The characterization effort, while not complete, indicates that RM-2

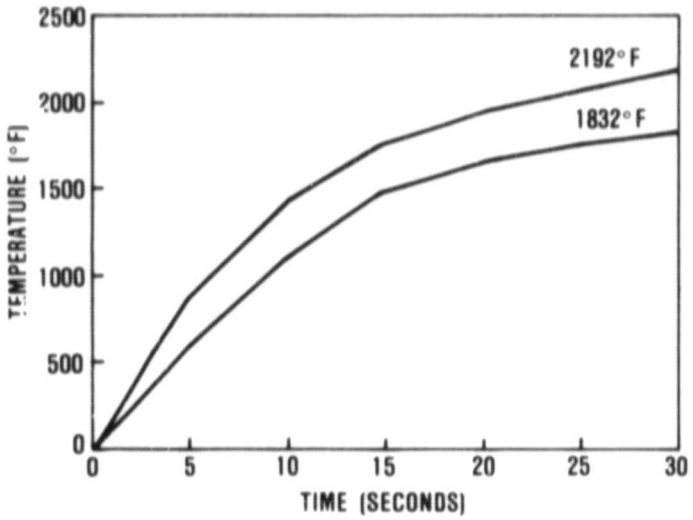

Figure 63. Heating Curves of Test Samples of RM-2 SRBSN During Thermal Shock Testing.

is a suitable material, at least for initial testing, for the AGT Turbine Rotor.

1.2 Bladed Rotor Testing

One early bladed rotor (S/N 5) shown in Figure 64, which had a low bulk density (3.10 g/cm^3) as well as visual defects in the blades, especially in the blade tip area, was cold spin tested. The results are summarized in Table 16. This rotor was subjected to multiple spin tests, with blade tip failures occurring at 78,800, 95,900 and 106,700 rpm. Following each blade failure or shutdown, the rotor was inspected and rebalanced, if necessary, before retesting. The rotor was finally tested to 115,100 rpm with no further incident. Figure 65 shows the rotor after testing was completed. A portion of the blade tip opposite each failed blade was removed for rebalancing.

Failure analysis showed that the failures occurred at the junction of the blade and the backface, a region that was machined following sintering. The actual rotor configuration deviated from design in this area, as shown schematically in Figure 66. It is probable that the failures were a result of the notch effect resulting from this machining deviation rather than obvious material deficiencies, since no material defects were observed on the fracture surfaces.

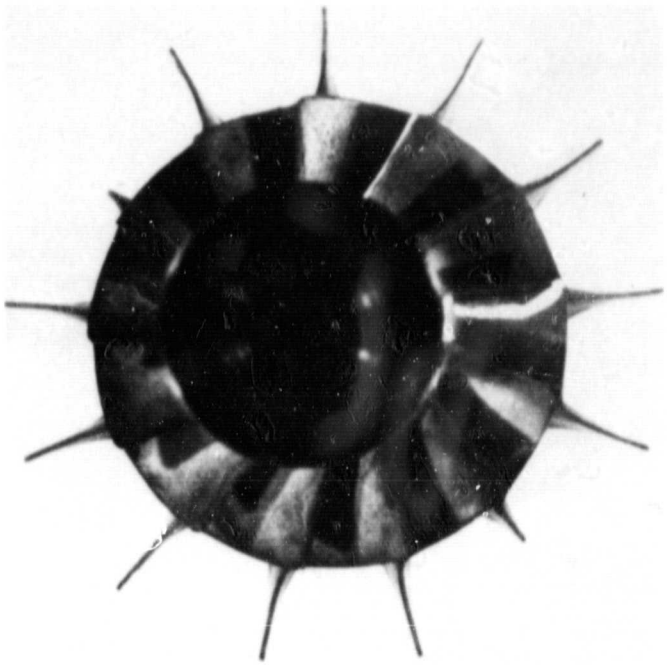

Figure 64. Bladed Rotor S/N 5 Prior to Spin Testing.

TABLE 16. BLADED ROTOR SPIN TEST RESULTS

Rotor S/N	Sintered Density (g/cm^3)	Spin Test Speed (rpm)	Comment
5	3.10	78,800	Lost blade tip "B"
		95,900	Lost blade tip "C"
		106,760	Lost blade tip "K"
		115,100	No failure

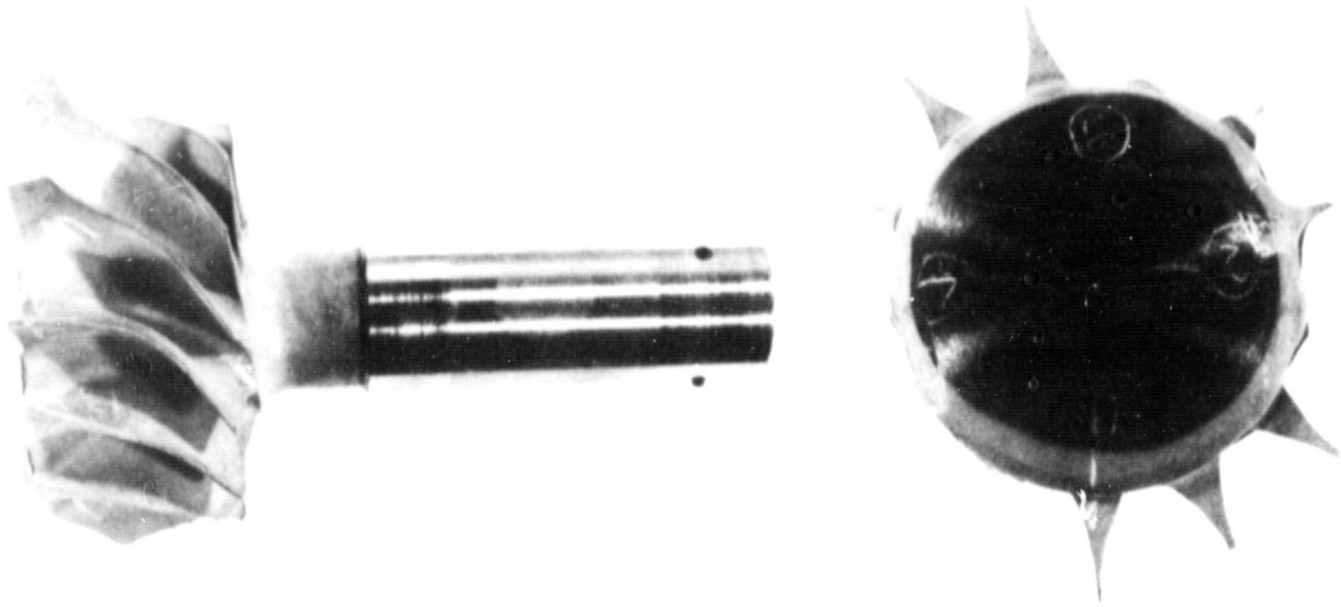

Figure 65. Bladed Rotor S/N 5 After Final Spin Testing to 115,100 rpm.

While improvements in the blade tip quality and overall blade resolution are required, these tests demonstrate that rotors produced using sintered reaction bonded Si_3N_4 can survive the speeds required for the AGT101 gas turbine rotor.

1.3 Properties of Bladed Rotors

A bladed rotor (S/N 9) with a density of 3.29 g/cm^3 was sectioned into test samples, with the location of the bars being recorded. The results, summarized in Figure 67, show the blades and the hub region had densities approaching 100 percent TD, while the neck and the shaft regions had successively lower densities, due primarily to gradients encountered in the casting process. The strength of the hub material ranged between 105 and 115 ksi, with lower strengths in the neck and shaft region.

These data show that the properties of RM-2 can be obtained in the highly stressed regions of bladed rotors. The low density and strength in the neck and shaft regions is a concern, although the stresses in these regions are relatively low.

1.4 Bladed Rotor Fabrication

Following initial fabrication of AGT bladed rotors with blade support in the backface region, problems were encountered in the fabrication of net shape components. These problems were poor tip definition, generally poor blade resolution, and cracks at the blade roots and in the hub region.

The tip definition and blade resolution problems were improved by using a rotational casting technique that forces slip into the mold cavity due to centrifugal force.

Blade root cracking appears to be improved by modifications in the wax mold removal technique. The hub cracking problem appears to be improved by more careful removal of the plaster mold base. A stringent program also will be instituted to assure that plaster molds are properly maintained and retired from service when degradation begins to appear.

2. TASK 2.7 - STATOR

The tooling to injection mold monolithic stators was completed and shipped to Ford

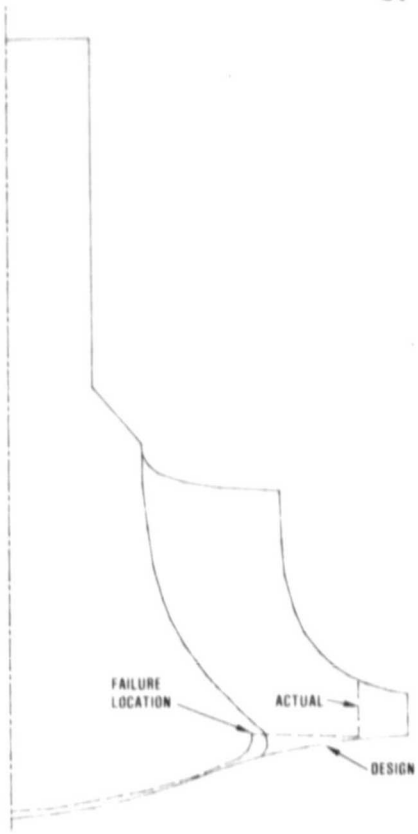

Figure 66. Schematic Representation of Machining Notch Believed to Cause Blade Failures of Bladed Rotor S/N 5.

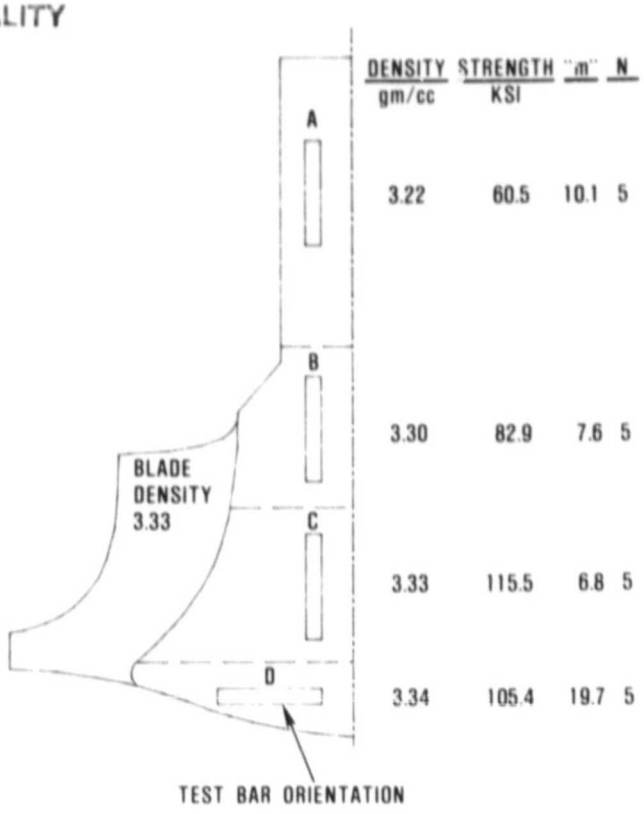

Figure 67. Properties of Test Samples Cut from Bladed Rotor S/N 9 at Several Locations.

during this reporting period. However, during shipment, 12 of the 19 outer inserts which form the major portion of the airfoils were broken. The cause of the breakage was an interference condition between the inner and outer inserts with the tool in the closed position.

The outer inserts were redesigned to eliminate the interference and a complete set of new outer inserts fabricated. The inner inserts were reworked at the interfaces to the outer inserts and the tool reassembled.

The tool was installed on the vertical Tempcraft molding machine and checked out. A water leak in the heating/cooling circuit in the bottom half of the tool prevented heating of this half, therefore a lower density material (2.5 g/cm^3 nitrided density) having higher flow in a cold tool than the 2.7 g/cm^3 material originally planned for stator molding was used for initial molding trials. Complete filling of the die cavity was achieved. However, it was noted that at least one crack was produced in the solid shroud during ejection and removal of the molded stator from the die. The tool was reworked to increase the ejector stroke and to eliminate the axial drag on the inner surface of the solid shroud during ejection. During this rework the vendor also repaired the water leak; the tool has been reinstalled and molding trials initiated.

With proper heat in the tool, complete cavity fill was achieved with the 2.7 g/cm^3 material. Figure 68 shows a group of stators molded during these initial trials. Evaluation of

Figure 68. Integral AGT Stators as Injection Molded.

molding parameters is in progress to improve component quality.

3. TASK 2.7 - FLOW SEPARATOR HOUSING

3.1 Component Fabrication and Evaluation

Four flow separator housings were delivered by Corning during this reporting period. Of this group, S/N 12 and S/N 14 were dimensionally inspected and non-destructively evaluated (NDE). NDE results indicated some reduction in the number of voids in S/N 14 versus S/N 12 reflecting recent process changes at Corning. However, additional process modifications will be required to fabricate a high quality flow separator housing. Both S/N 12 and S/N 14 have been sent to Garrett for engine and rig testing.

Housing S/N 17 is the most recent housing delivered by Corning. NDE of this component also revealed voids in what are considered non-critical areas. Overall, the quality of S/N 17 was judged to be approximately the same as S/N 14.

Housing S/N 15 was visually inspected and judged to be unacceptable. This component had a crack-like defect at the joint of the cross-arm and outer shell on the low pressure side of the housing. Rejection was based on previous operating experience with the 820 gas turbine inner housing where more than 70 percent of the failures occurred in a similar area before design changes and casting improvements were made.

APPENDIX B

AIRESEARCH CASTING COMPANY (ACC)
ADVANCED GAS TURBINE (AGT) POWERTRAIN SYSTEM DEVELOPMENT PROGRAM
FOURTH AGT SEMIANNUAL TECHNICAL
PROGRESS REPORT

1. SUMMARY

Fabrication of the simulated rotor was superseded by development of bladed rotor fabrication processes. Several patterns and several mold approaches were evaluated with processing ultimately limited to one pattern type with two mold approaches, both of which yield satisfactory castings. With forming capability demonstrated, material development has become more active. Studies, to date, are showing the effect of specific variables on final properties and reproducibility. Completion of these studies will result in improvements over what already has been successfully spun to 115-percent speed.

Sufficient quantities of all ceramic structures requested were delivered. Design changes in turbine shroud and inner diffuser were quickly implemented. Processing and evaluation continue to assure backup components and reliable processes. A summary of all delivered items is listed in Table 17.

2. ROTOR - MATERIALS AND FABRICATION DEVELOPMENT

2.1 Injection Molding Process

Efforts to produce the simulated rotor by the injection molding process were suspended pending process improvements developed in alternate programs including an AiResearch Casting Company funded IR&D program to screen potential binder compositions. Improvements in binder strength and dimensional stability have been shown and binder removal, from thick sections, is being evaluated. Injection molding efforts to produce the AGT rotor have remained on hold to concentrate on furthering the success of the slip casting process.

2.2 Slip Casting Process

Simulated Rotor

Casting efforts of the simulated rotor were completed in June 1981. Fabrication process development, using several bladed configurations discussed below, continued. Bladeless rotors on hand were processed through drying and sintering cycles.

Bladed Rotor

Bladed rotors were fabricated using molds from three different pattern sizes and/or types. Efforts using rubber patterns based on an actual metal rotor continued until a metal pattern (matrix) was obtained with allowance for 14.5 percent sintering shrinkage. As part of the scale-up evaluation, and to evaluate an alternate approach, wax patterns (with 10 percent shrinkage allowance) also were utilized. Scale-up for 14.5 percent shrinkage was successful. All castings, by the close of this reporting period, were aimed at producing parts of the size suitable for engine application.

Three mold concepts were evaluated:

1) An all plaster mold using plaster inserts between the blades

2) An organic shell mold, to form the blades, joined to a plaster base to form the hub dome

3) An "inverted" organic shell mold, to form the blades and hub, joined to a plaster base to form the rotor shaft.

The all plaster mold concept resulted in part cracking, while both organic shell techniques have produced castings free of voids and

TABLE 17. DELIVERIES THROUGH DECEMBER 1981

Component	Green for Machining	Densified for Test Development	Densified for Test Evaluation
Simulated Rotor			7
Bladed Rotor		3	
Shaft Specimen		2	5
Stator		53(1)	56
Shroud	9(2)	3(2)	0
Inner Diffuser		2(2)	2
Outer Diffuser		1	2

(1) Product of parametric study
(2) Shipped prior to design changes: shroud (10/81) and inner diffuser (8/81)

cracks. Uniform density has been measured in castings from each process (data are presented in Table 18). Avoiding air entrapment during mold fill is easiest when using the inverted casting technique, but filling techniques developed for upright casting are now regularly successful.

Casting in the upright position requires 50 percent less time than inverted casting. Both techniques are being evaluated further to determine the better approach.

Organic shell mold fabrication from rubber patterns, and water soluble wax patterns, was demonstrated. The development effort was primarily performed using rubber patterns.

Several shell mold materials were evaluated with varying degrees of success. A paraffin

TABLE 18. DENSITY UNIFORMITY IN SNN503 AGT BLADED ROTORS

Sample Location	Casting Position	
	Upright	Inverted
Shaft end	3.11	3.15
Shaft/hub	3.13	3.14
Hub	3.12	3.14
Dome	3.11	3.14
Blade	3.12	3.14

based material, optimized for wax patterns, initially was used for mold fabrication with rubber patterns. It appeared useful but was opaque and did not coat the blade edges well. Ethyl cellulose and butyrate based dip seal materials provided transparent molds, helpful in visualizing entrapped air, and excellent edge coating but were not dimensionally reproducible. A translucent mold material was developed, similar to the original material, with improved edge coating capability. This improved shell mold material is being used in continued process development.

Once the shell mold is formed, the rubber pattern is simply pulled from the mold cavity. It was found necessary to reinforce the mold during this process. Initially, molten water soluble wax was poured into a container and allowed to solidify around the mold. This resulted in mold distortion. The improved procedure involves building up the reinforcing material in layers.

Molds formed around water soluble wax patterns can be more complex in shape and need no reinforcement during pattern removal. The patterns available, however, were characterized by injection mold parting lines which are difficult to remove from the pattern. Since these patterns were designed only for 10 percent shrinkage, the process was not optimized.

Two potential spin testable bladed rotors, Figure 69, were shipped to Garrett. Figure 70 shows a closeup of the rotor blading. Hand finishing may be sufficient to remove known surface flaws in each part. Additional inspection will be performed at Garrett. Additional castings are being prepared.

Shaft Specimens

Shaft attachment development specimens are being fabricated by a slip casting process similar to the rotor process. Shaft processing has included a thermal presintering process to allow for machining a straight cylinder from a tapered slug. A tapered mold was required to prevent centerline shrinkage in the long cylinder. Five shaft specimens are in process for shipment in January.

Material Development

The simulated rotor has demonstrated sufficient strength to allow spin testing at 15 percent overspeed at Garrett. Test bars machined from the center of simulated rotors have shown a range of strengths with only limited excess strength. With successful demonstration of bladed rotor fabrication, emphasis shifted to study process variations that may lead to improved properties and reproducibility.

Casting density measured on many samples showed a range of 2 to 2.2 g/cm^3. It was felt that this could be controlled within a much tighter range by adjustments in deflocculant, electrolytes, and slippage. A factorial experiment evaluating each of these variables at two levels was designed by studying results in slip properties and green and sintered densities. A second iteration was performed to verify results.

Results of these experiments showed that small variations in these parameters did not have significant effect in the final (sintered) density. Variations in green density did occur but no direct relationship between green and sintered was found. Optimum viscosity was observed with slip formulations previously standardized. These results indicate that evaluation of other parameters are necessary.

Powder preparation procedures are now being evaluated for impact on slip properties and green and sintered density. To provide good casting properties using the desired mix of Y_2O_3, Al_2O_3, and Si_3N_4, the powders have been mixed together, calcined (heated in air), and then remilled prior to forming the slip. In experiments currently underway, heating temperature and remilling conditions are being explored. Increased milling time and wet milling (milling slurry rather than powder) are expected to produce an improved microstructure.

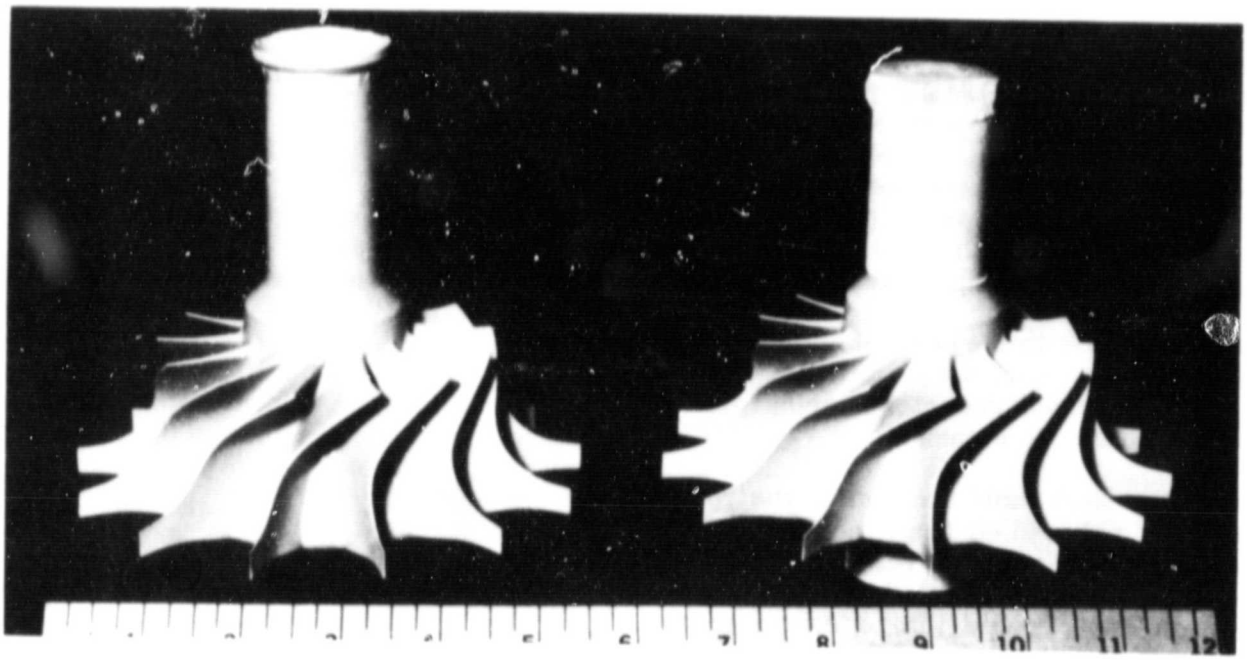

Figure 69. ACC SNN Bladed Turbine Rotors.

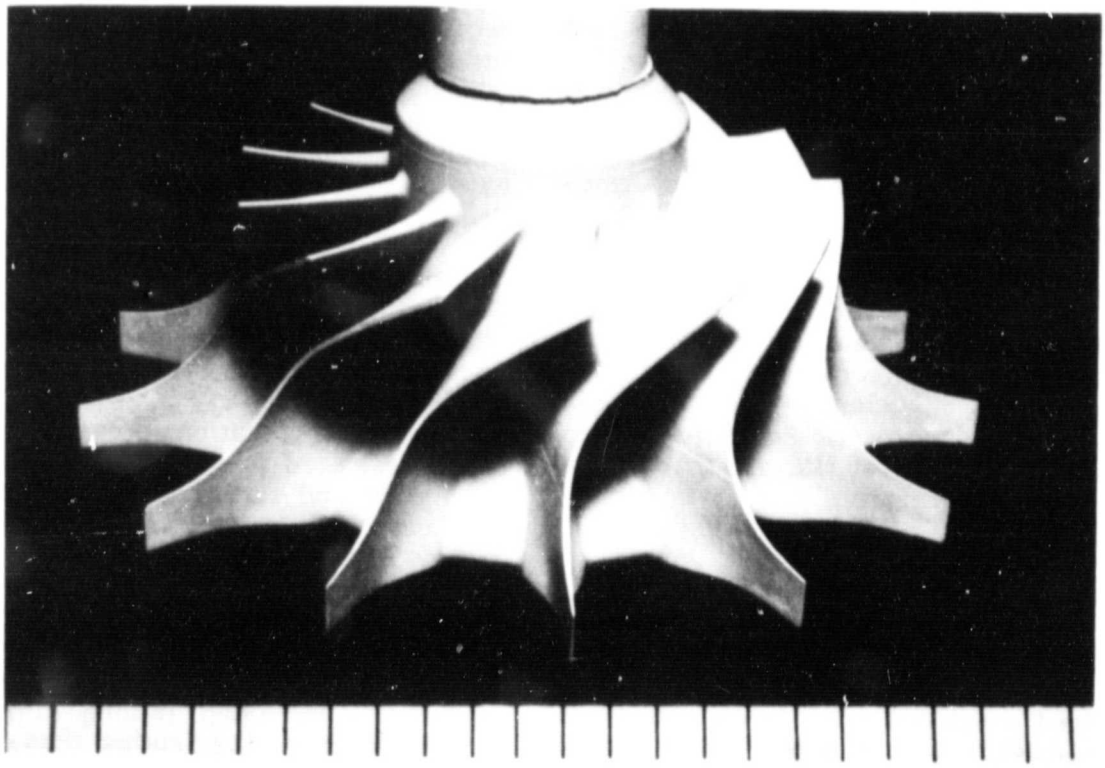

Figure 70. Blade Detail, ACC SNN Turbine Rotor.

TABLE 19. POWDER PREPARATION VARIATION

Slip No	Process Condition			Viscosity	Gelation	Casting Rate*
	Temp °F	Mill Time	Mill Type			
1	2012	6 hrs	Wet	65	Little	14
2	2192	6 hrs	Wet	80	Little	10
3	2012	24 hrs	Dry	35	None	10
4	2192	24 hrs	Dry	70	None	8
5	2012	6 hrs	Dry	105	None	11
6	2192	6 hrs	Dry	115	None	10

*Casting rate based on relative thickness in a 3 hour casting

obtained will be evaluated for additional significance and recommended follow-on studies.

A deairing experiment also was performed. Initially, various levels of vacuum were used to expand and remove air bubbles from the slip prior to casting. Sintered samples from the various levels all revealed spherical type bubbles up to 200 microns in diameter. Hexanol, a conventional defoaming aid, was added with little obvious effect. Efforts will continue in this area with emphasis in other chemical additives and improved slip handling techniques.

Drying parameters for castings have been demonstrated to be extremely significant. A microprocessor controlled humidity chamber was scheduled for use to improve and reproduce parameters for drying. Delays were encountered in obtaining all necessary hardware and the chamber now is in final assembly. All drying is currently being performed at conservative rates at room temperature.

Sintering

Sintered density variations have been evident in rotor and shaft castings. Furnace reproducibility has been demonstrated using identical dry-pressed disks in many sequential cycles. Density for these disks is generally 3.20 ±0.02 g/cm^3. One furnace cycle was performed with 18 test samples distributed throughout the furnace in central and extreme (top, bottom, front, back and side) positions. These samples again showed ±0.02 g/cm^3 deviation. Density variations of 0.10 g/cm^3 are more likely to result from identifiable process variations than subtle sintering variations.

3. CERAMIC STRUCTURES

3.1 Injection Molding Process

Turbine Stator

The turbine stator is the only AGT component being produced by injection molding

at ACC. Fifty-six stator vanes, Figure 71, were processed through nitriding, inspected, and shipped as potential hardware for engine testing. All of these were of AirCeram RBN-124, a recent upgrade in injection molded RBSN. Forty-eight additional samples were sent for machining, assembly and testing evaluation at Garrett.

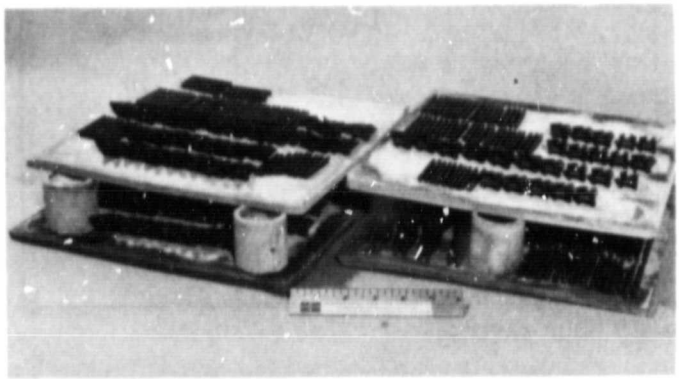

Figure 71. ACC RBN-124 Stator Vanes as Molded.

3.2 Slip Casting Process

Turbine Shroud

Twelve pre-nitrided turbine shrouds were shipped for machining and three have been processed through nitriding and shipped. Figure 72 shows a turbine shroud prior to machining. The nitrided components do not reflect the most recent design changes incorporated by Garrett. Four castings, S/Ns 150 and 174 through 176, recently shipped for machining did incorporate the latest changes. After machining, two were returned for nitriding.

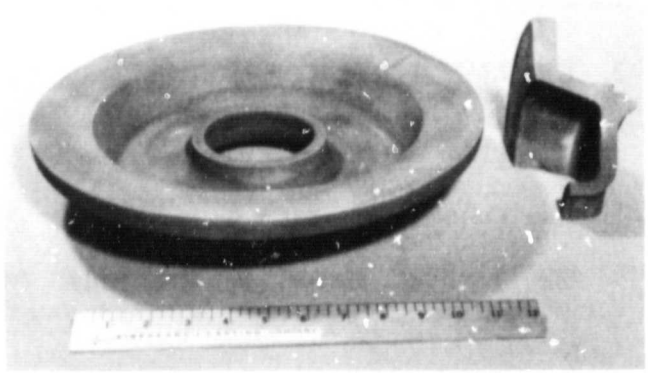

Figure 72. Turbine Shroud as Cast.

Design changes have resulted in mold forming tool modifications only where stock could be removed. Individual plaster molds are cut to yield additional changes. This process results in some variation between molds but deviation is within the machining allowance for this part. Tighter tolerances or increased shipments would indicate permanent tool modifications.

With the tool now qualified, additional parametric studies are being initiated to assure best possible hardware delivery. These studies will include injection parameters using potential improved binders as well as developing binder removal approaches.

Turbine Inner Diffuser

Three inner diffusers, free of known flaws, were nitrided and shipped. Two of these, S/Ns 172 and 173, Figure 73, reflected the most recent design changes. Representative test bar strength was 41 ksi with component weight gains of 60.7 and 59.2 percent.

Engine design changes allowed elimination of three lugs previously required in engine building. Removing these lugs reduced casting difficulty by eliminating the extreme thickness differences between the lug and the remainder of the casting. The lug was difficult to cast to completion. Also, the changing geometry created a stress riser increasing the probability of the occurrence of drying cracks. This design change marks a significant improvement in the fabricability of this component.

Turbine Outer Diffuser

Two nitrided outer diffusers, Figure 73, were shipped to Garrett for final grinding.

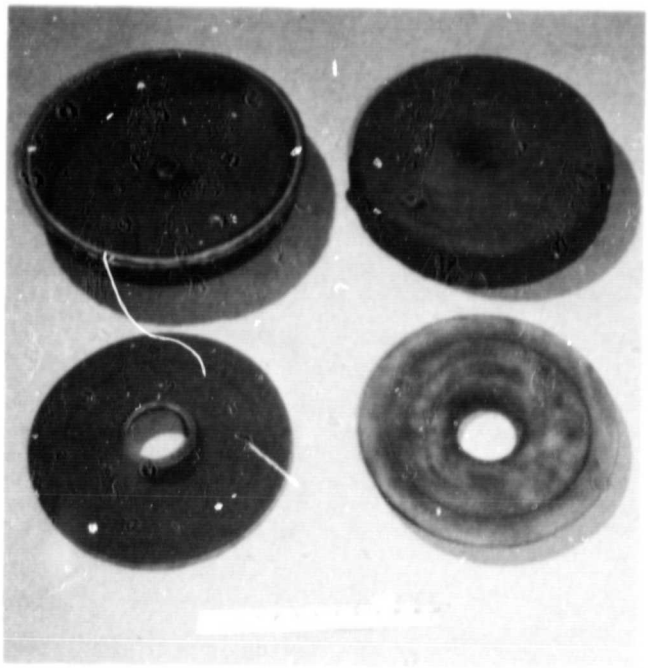

Figure 73. Inner and Outer Diffuser Housings.

These are S/Ns 145 and 146 with data as follows:

- Nitriding weight gain = 60.6 and 60.5 percent
- Density = 2.79 g/cm^3 for both
- Average strength = 48 ksi for both

Additional casting of this component was deferred pending final evaluation by Garrett.

APPENDIX C

THE CARBORUNDUM COMPANY
(UNIQUE WORK)
ADVANCED GAS TURBINE (AGT) POWERTRAIN SYSTEM DEVELOPMENT PROGRAM
FOURTH AGT SEMIANNUAL TECHNICAL PROGRESS REPORT

1. BACKGROUND

This report summarizes the work carried out by the Carborundum Company during the period from July 1, 1981 to December 31, 1981 for the Garrett Turbine Engine Company on the Advanced Gas Turbine Powertrain System Development Program authorized under NASA Contract DEN3-167 and sponsored by the Department of Energy (DOE).

As a major subcontractor to the program, Carborundum is required to develop silicon carbide components for the AGT hot flow path.

Injection molding, slip casting, and green machining were the fabrication processes selected to produce hardware for the program.

Ceramic fabrication technology has been successfully demonstrated to produce complex shapes economically with precision on small items such as backshrouds, stator, vanes, duct spacers, and large components such as turbine shrouds, combustor baffles and transition ducts. At the beginning of the program, injection molded components were limited to approximately 1 inch thick maximum cross sections. Technical progress now has significantly extended cross section capabilities so that large and complex components can be successfully produced to net shape with minimal grinding required. The development of two new SiC materials designated Hexoloy^{TM} KX-01 and Hexoloy^{TM} KX-02 represented significant strength improvements, which when optimized will apply to a variety of components including the rotor.

Activities during this period addressed properties optimization of the new Hexoloys^{TM} for the rotor and also the optimization of fabrication processes for the static structures.

2. ROTOR MATERIALS DEVELOPMENT

The approach to rotor development was to investigate several materials and fabrication techniques, which were to be narrowed down until a combination having a high probability of success could be identified. Injection molding using a binder system capable of being removed from thick sections has been selected as the process to produce the bladed rotor. The material having properties required for performance also have been identified as Hexoloy^{TM} KX-02.

The Hexoloy^{TM} KX-02 is an ultrafine grain RBSiC material modified to enhance fabricability and/or properties. The property improvement of injection molded test bars achieved during the reporting period is exhibited by the increase from MOR values of 53.7 ksi and 105.6 ksi at room temperature and 2192°F, respectively, for samples produced by one process system to MOR values of 79.6 ksi and 144.3 ksi at room temperature and 2192°F, respectively, utilizing an alternative process, Table 20. It also was demonstrated that good material properties can be obtained using alternate fabrication techniques such as cold pressing and isostatic pressing. These results are shown in Table 21.

Overall results indicate material and fabrication methodology exists that have the potential to produce a bladed rotor. However, because of funding constraints, no additional material development work nor fabrication effort is planned for rotor components.

TABLE 20. FOUR-POINT BEND TEST RESULTS INJECTION MOLDED HEXOLOY™ KX-02.

Original Procedure Characteristic Strength, ksi		New Method of Incorporating Additive Characteristic Strength, ksi	
77°F 0.75 inch Top Span	2192°F 0.50 inch Top Span	77°F 0.75 inch Top Span	2192°F 0.50 inch Top Span
55.29	77.92	59.82	171.20
65.33	110.40	84.80	104.40
55.17	93.75	75.51	140.70
56.99	115.10	91.32	148.50
55.19	108.30	94.65	108.20
75.80	101.60	77.04	184.10
46.53	121.30	73.70	136.10
54.06	113.30		186.60
37.14	106.80		119.00
35.14	107.10		
Mean: 53.66	Mean: 105.60	Mean: 79.56	Mean: 144.30
SD 12.07	SD 12.26	SD 11.82	SD 31.08
NOTE: Test Bar Size = 0.1 inch x 0.2 inch x 2 inches Cross Head Speed = 0.02 inch/minute			

TABLE 21. FOUR-POINT BEND TEST RESULTS HEXOLOY™ KX-02.

Cold Pressed Characteristic Strength, ksi		Isopressed Characteristic Strength, ksi	
77°F 0.75 inch Top Span	2192°F 0.50 inch Top Span	77°F 0.75 inch Top Span	2192°F 0.50 inch Top Span
85.35	134.5	91.38	134.80
108.30	152.5	91.34	128.40
56.68	157.0	87.23	131.30
59.03	111.9	89.95	134.50
90.04	158.9	80.07	111.70
92.63	161.9	94.99	128.00
65.52	147.1	101.00	122.00
65.83	142.4	87.39	125.70
	182.1	104.30	122.70
		101.90	107.90
Mean: 77.92	Mean: 149.81	Mean: 92.96	Mean: 124.50
S.D. 18.71	S.D. 19.57	S.D. 7.61	S.D. 8.94
NOTE: Test Bar Size = 0.1 inch x 0.2 inch x 2 inches Cross Head Speed = 0.02 inch/minute			

3. STATIC STRUCTURES

3.1 Turbine Stator

The injection molding process was selected for fabrication development of the stator assembly in Hexoloy™SA, a sintered alpha silicon carbide material. During this reporting period, the injection molding process was further refined to produce stator segments to near net shape. Fabrication development consisted of identifying molding parameters to produce visually good parts. Acceptance criteria for further processing included:

- o Complete fill at the airfoil trailing edge
- o Absence of surface irregularities such as blisters, sinks and burn marks
- o Absence of flow lines in regions that were to be unground

A group of 97 stator segments, which were processed through sintering, is shown in Figure 74.

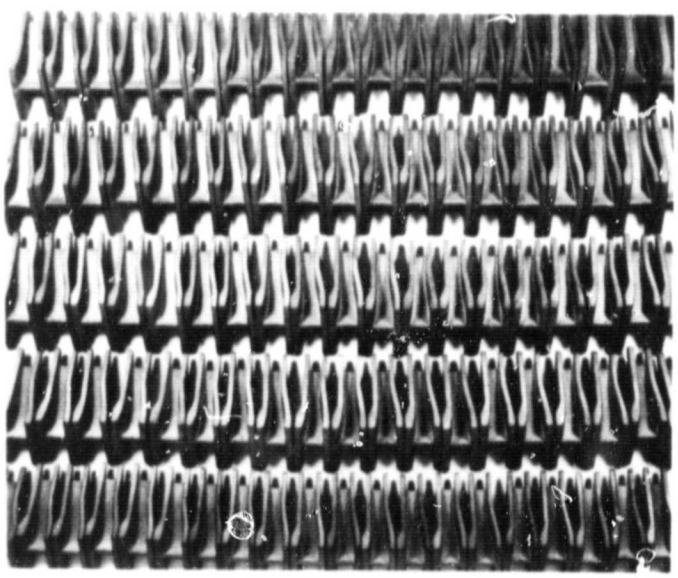

Figure 74. SiC Injection Molded Stator Segments.

Anisotropic shrinkage is normally observed when sintering complex injection molded shapes. It also was observed in the sintered alpha silicon carbide stator segments. While the airfoil size and shape was correct as shown in Figure 75, the shroud platforms were smaller than required for finish grinding. Compositional adjustments to provide platforms with a minimum of 0.010 inch grinding stock resulted in airfoils whose chord lengths were approximately 0.050 inch longer than print specifications.

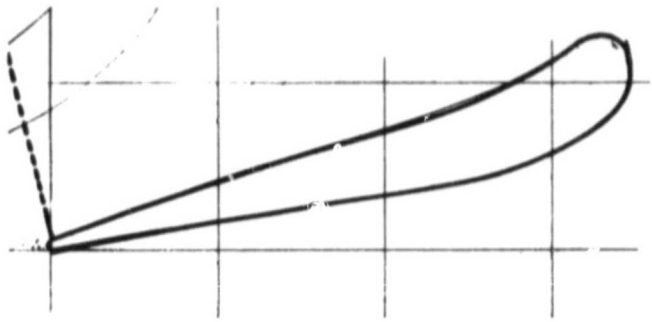

Figure 75. Turbine Stator, Airfoil Profile.

The option to rework the tool was exercised and the shroud platforms were enlarged to provide the necessary grinding stock. Molding activity was resumed and approximately 200 segments were produced for subsequent processing.

Grinding methodology is being developed utilizing the undersize sintered segments. An example of an unground set of 19 segments is shown in Figure 76, and an example of a ground and as-fired segment is shown in Figure 77.

3.2 Turbine Shroud

Since the turbine shroud has a variable wall and precise contours, injection molding was selected to produce the part in Hexoloy™SA. The finished part weighs approximately 10 pounds and represents the largest single piece ever injection molded in this material. During this reporting period, the injection molding process was further refined to produce a turbine shroud for evaluation. Molding and sintering parameters, which resulted in a crack-free part, were established.

Figure 76. Stator Assembly Before Machining.

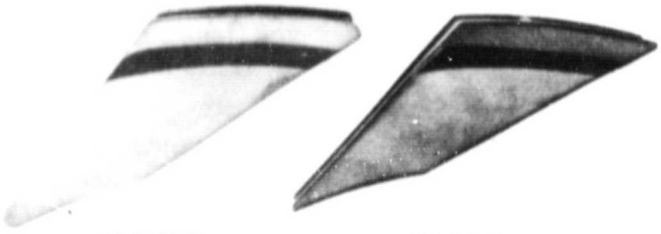

Figure 77. Sintered Stator Segments.

Molding was carried out on a 1000-ton reciprocating screw machine equipped with microprocessor controls. A total of 43 parts were molded using a matrix of conditions. The key variables were material temperature, injection velocity, and cooling times.

Sintering variations were limited to the type of fixtures used to maintain dimensional integrity. An example of a sintered and molded turbine shroud is shown in Figure 78. Measurements taken on the sintered shroud indicated that the part was undersize by approximately 1 to 1.5 percent on the diameters. The tool was changed to produce a larger part and, at Garrett request, several design changes were incorporated for improved functionality.

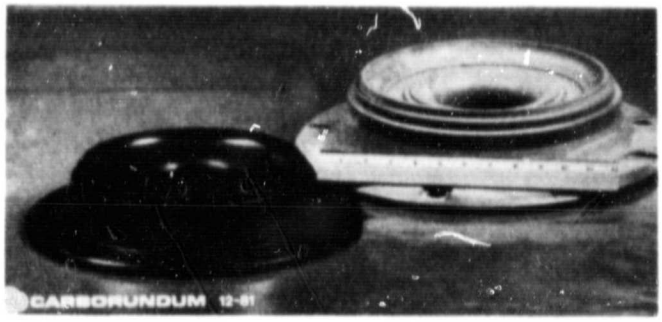

Figure 78. Sintered and Molded Turbine Shroud.

Additional molding compound was prepared and a molding run is scheduled on the same 1000-ton injection press during the next reporting period.

3.3 Combustor Baffle

Slip casting was selected as the fabrication method appropriate for producing the combustor baffle in Hexoloy™SA. Slip compositions were developed which were capable of producing the 0.4-inch wall thickness required on the part. During this period, the slip casting development emphasized process improvements yielding crack-free baffles after sintering.

The casting procedure was optimized to provide a wall thickness in excess of 0.4 inch to allow sufficient stock for machining and grinding. Several slip compositions were evaluated using a simulated combustor baffle shape. The slip composition selected for the part consisted of a bimodal grain distribution of submicron and -1000 mesh alpha silicon carbide. In addition to providing excellent casting characteristics, it had good dry strengths for green machining which is necessary to develop a uniform contour

on the drain side of the casting. An example of a sintered simulated baffle is shown in Figure 79. However, limitations in final grinding to produce the OD radius and the airfoil shape on the struts necessitated a change in the fabrication approach.

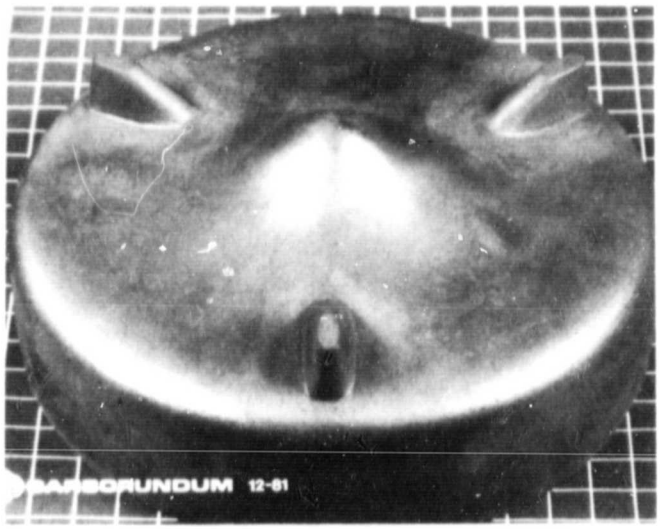

Figure 79. Sintered Simulated Combustor Baffle.

A new approach was adopted to produce the OD and the struts to net shape. The initial castings show the feasibility of this approach. The first cast and dried part is shown in Figure 80.

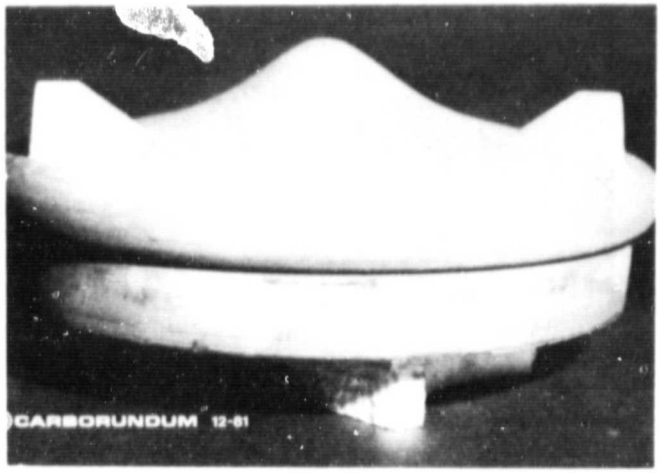

Figure 80. Cast Combustor Baffle With As-Cast Airfoil Struts and OD Radius.

To conserve material and to minimize machining, the outside contour was developed by isostatically pressing around a formed core, which is shown in Figure 81. The pressed blanks ready for green machining are shown in Figure 82. A lathe equipped with Computer Numerical Control (CNC) was used to develop the OD contour and CNC milling was used to produce the pocket and adjacent projection detail.

Sintering fixtures to maintain shape integrity were designed and fabricated for the part and grinding parameters were developed to produce contact surfaces to dimensional specifications.

3.4 Transition Duct

At the outset of the program, slip casting was the fabrication method selected to produce the transition duct. However, this technique was limited to producing the correct external contour only. The critical contour, which determines the gas flow path, could only be achieved by green machining. Therefore a decision was reached to produce the entire part by machining to net shape. During this period, the process of green machining an isopressed billet was emphasized to produce the transition duct.

3.5 Turbine Backshroud

The turbine backshroud is being developed by green machining isopressed blanks followed by grinding after sintering. Six items were delivered for dimensional evaluation during this reporting period. Results of the evaluation revealed that the contour facing the rotor, as machined to the data point profile, was not within print tolerances and a remake of the part was initiated.

Figure 81. Formed Core for Pressing Transition Duct.

The first six articles were produced on a lathe equipped with a template tracer attachment. The template was developed from coordinate data having 12 points/inch. The remake is scheduled to be produced on a CNC lathe using 50 points/inch for improved accuracy. The new coordinate data was used to generate a program for the CNC lathe. Billets have been produced for machining stock and a special fixture to prevent distortion during sintering was designed and fabricated.

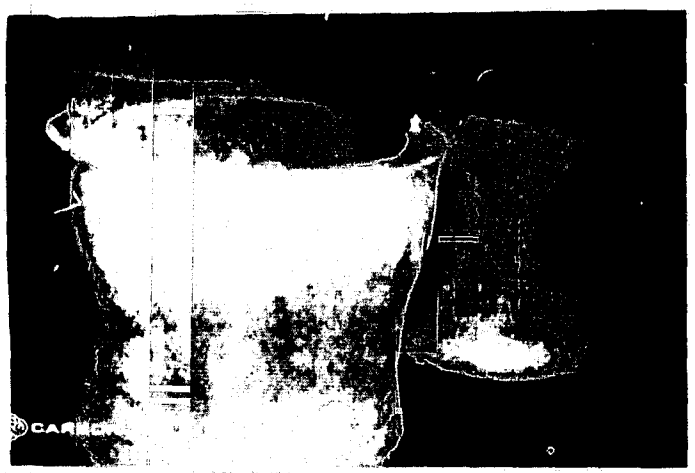

Figure 82. Isopressed Blanks for Transition Duct.

APPENDIX D

LIST OF SYMBOLS, ABBREVIATIONS AND ACRONYMS

Acronym	Definition
ACC	AiResearch Casting Company
AGT	advanced gas turbine
AGT101	the AGT model being developed by Garrett/Ford
Al_2O_3	aluminum oxide
AS	aluminum silicate
°C	degrees Celsius
C_L	clearance probes
CFDC	Combined Federal Driving Cycle
CNC	computer numerical control
CO	carbon monoxide
CO_2	carbon dioxide
DFC	diffusion flame combustor
DOE	U.S. Department of Energy
ECU	electronic control unit
EPA	Environmental Protection Agency
°F	degrees Fahrenheit
Ford 707	an industrial gas turbine engine by Ford
FY	fiscal year
GE	General Electric Company
HC	hydrocarbon
Hexoloy™ KX01	Carborundum material, SiC
Hexoloy™ KX02	Carborundum material, SiC
Hexoloy™ SA	Carborundum material, SiC
HP	high pressure regenerator inlet (cold side)
Hz	Hertz (frequency)
ID	inner diameter
IGV	inlet guide vane (compressor)
IR&D	internal research and development
I-112	regenerator seal coating material

LIST OF SYMBOLS, ABBREVIATIONS AND ACRONYMS (Contd)

Acronym	Definition
JP-4	jet propulsion fuel Number 4
ksi	thousand pounds per square inch
lb/min	pounds per minute airflow
LP	low pressure regenerator inlet (hot side)
"m"	Weibull modulus
MAS	magnesium aluminum silicate
METCO 443	flame spray coating
METCO 447	flame spray coating
MgO	magnesium oxide
Mod I	first development engine
Mod II	second generation ceramic engine
MOR	modulus of rupture
N	population, number of samples
NASA	National Aeronautics and Space Administration
NGK	NGK-Locke, Inc.
NiCr	nickel chrome
NO_x	oxides of nitrogen
OD	outer diameter
P/N	part number
P_S	static pressure
psia	pounds pressure per square inch, absolute
psid	pounds pressure per square inch, differential
psig	pounds pressure per square inch, gauge
P_T	total pressure
PWM	pulse width modulated
RBN 104	ACC RBSN material
RBN 124	ACC RBSN material
RBSiC	reaction bonded silicon carbide
RBSN	reaction bonded silicon nitride

LIST OF SYMBOLS, ABBREVIATIONS AND ACRONYMS (Contd)

Acronym	Definition
RM-1	Ford rotor material, first generation
RM-2	Ford rotor material, second generation
RPD	reference powertrain design
rpm	revolutions per minute
RSSiC	reaction sintered silicon carbide
SEM	scanning electron microscopy
SiC	silicon carbide
SiO_2	silicon oxide
Si_3N_4	silicon Nitride
SMD	sauter mean diameter
S/N	serial number
SNN 522	ACC sintered silicon nitride
SN-50	NGK silicon nitride material
S/R	stress rupture
SRBSN	sintered RBSN
TC	thermocouple
TD	theoretical density
TIT	turbine inlet temperature
T_T	total temperature
T-T	total-to-total
Y_2O_3	yttrium oxide
α-SiC	Carborundum material, Hexoloy™
β	beta
θ	temperature/temperature standard
$\mu\epsilon$	micro strain
σ	pressure/pressure standard
σ_A	characteristic strength

REFERENCES

1. Garrett Turbine Engine Company, "Advanced Gas Turbine (AGT) Powertrain System Development for Automotive Applications", Semiannual Progress Report Number 1 (October 1979 through June 1980), Report No. NASA CR-165175, November 1980, Contract No. DEN3-167.

2. Garrett Turbine Engine Company, "Advanced Gas Turbine (AGT) Powertrain System Development for Automotive Applications", Semiannual Progress Report Number 2. (July 1980 through December 1980), Report No. NASA CR-165329, June 1981, Contract No. DEN3-167.

3. Garrett Turbine Engine Company, "Advanced Gas Turbine (AGT) Powertrain System Development for Automotive Applications", Semiannual Progress Report Number 3 (January 1981 through June 1981), Report No. NASA CR-167901, December 1981, Contract No. DEN3-167.

4. W. D. Carruthers, D. W. Richerson and K. W. Benn, 3500-Hour Durability Testing of Commercial Ceramic Materials, NASA CR-159785, July 1980.

5. F. F. Lange, S. C. Singhal and R. C. Kuznicki, "Phase Relations and Stability Studies in the Si_3N_4-SiO_2-Y_2O_3 Pseudoternary System", J. Amer. Ceram. Soc., 60, 249 (1977).

6. H. Knoch and G. E. Gazza, "Effect of Carbon Impurity on the Thermal Degradation of an Si_3N_4-Y_2O_3 Ceramic", J. Amer. Ceram. Soc., 62 [11-12], 634-35 (1979).

7. N. J. Tighe, K. Kurodo, T. E. Mitchell and A. H. Heuer, "In Sitre Oxidation of Y_2O_3-doped Si_3N_4", NBS IR 80-2075, August 1980.

8. C. F. Johnson and D. L. Hartsock, "Thermal Response of Ceramic Turbine Stators" in Ceramics for High Performance Applications" edited by J.J. Burke, A.E. Gorum and R.N. Katz, Brook Hill Publishing Co., Chestnut Hill, Mass. (1974).

9. L. P. Wynn, D. J. Tree, T. M. Yonushonis and R. A. Solomon, "Proof Testing of Ceramic Components", in DARPA/NAVSEA Ceramic Gas Turbine Demonstration Engine Program Review, MCIC Report MCIC-78-36 (1978).

10. K. M. Johansen, L. J. Lindberg and P. M. Ardans, Ceramic Components for Turbine Engines, 8th Quarterly Technical Report, Garrett Report No. 21-2794(10), prepared under AFML/APL Contract F33615-77-C-5171, pp. 63-72 (June 5, 1980).